

Diss. ETH Nr. 13862

# **ENGINE THERMOMANAGEMENT FOR FUEL CONSUMPTION REDUCTION**

A dissertation submitted to the  
SWISS FEDERAL INSTITUTE OF TECHNOLOGY  
ZURICH

for the degree of  
Doctor of Technical Sciences

presented by  
ELENA CORTONA KANNE

Laurea di Dottore in Ingegneria Meccanica, Politecnico di Torino  
born 28.4.1970

accepted on the recommendation of  
Prof. Dr. L. Guzzella, examiner  
Prof. Dr. Ch. Bader, co-examiner

2000

Seite Leer /  
Blank leaf

“Facts are better  
than dreams.”

Winston Churchill

Seite Leer /  
Blank leaf

## ACKNOWLEDGMENTS

This dissertation was written while I was with the Engine Systems Lab at the Institute of Energy Technology of the ETH in Zürich. I wish to thank my advisor, Prof. Dr. Lino Guzzella for his support and for making this research work possible.

Furthermore I would like to thank Prof. Dr. Ch. Bader for accepting to be my co-examiner and for the improvements he suggested.

A special thank you goes to Dr. Chris Onder who always encouraged and motivated me and without whose help this work would hardly have been accomplished. I also thank him for being an honest discussion partner.

I immensely appreciated the fellowship and the support of the entire staff of the Engine Systems Lab. I thank them for the great time we had together and for morally sustaining me during the difficult times. In this context I would like to acknowledge Dr. Alois Amstutz. I am grateful to the office colleagues of many years, Patrik Soltic and Rolf Pfiffner, for the good atmosphere and the excellent team work. I would like to assure my gratitude to Brigitte Rohrbach for her patience and competence while correcting my dissertation text.

Finally, my thanks go to my husband Ulf for encouraging me during these years. His daily support made this dissertation possible in the first place. Thanks.

Seite Leer /  
Blank leaf

# CONTENTS

<b>Acknowledgments</b>	<b>v</b>
<b>Abstract</b>	<b>xi</b>
<b>Zusammenfassung</b>	<b>xiii</b>
<b>Notations</b>	<b>xv</b>
<b>1 Introduction</b>	<b>1</b>
1.1 Methods for the reduction of fuel consumption	2
1.2 Importance of heat transfer	7
1.2.1 Engine energy balance	8
1.2.2 Other benefits	11
1.3 Methods for improving engine thermomanagement	12
1.4 Objectives of the thesis	13
1.5 Main results and new contributions	14
<b>2 Modeling for Engine Thermomanagement</b>	<b>17</b>
2.1 Main components of the cooling circuit and their models	18
2.1.1 Cooling pump	18
2.1.2 Conventional thermostat	18
2.1.3 Electrically operated bypass valve	22
2.2 System modeling	24
2.2.1 Engine internal cooling circuit	26
2.2.2 Engine external cooling circuit	35
2.2.3 Parameters used for modeling	38

2.3	Model validation	42
2.4	Conclusion	43
<b>3</b>	<b>Controller Design</b>	<b>45</b>
3.1	Control specifications	46
3.2	Definition of the minimal coolant mass flow	46
3.3	Model linearization	49
3.4	Feedforward controller	50
3.4.1	Reduction to a SIMO system	51
3.4.2	Approximation of the delays	54
3.4.3	Controller design	56
3.4.4	Model-based estimator	58
3.4.5	Simulation results	59
3.4.6	Measurements	63
3.5	Feedback controller	66
3.5.1	System reduction	66
3.5.2	Control strategy	67
3.5.3	Controller design	69
3.6	Feedforward and feedback controllers	75
3.7	Conclusions	79
<b>4</b>	<b>Experimental Setup</b>	<b>81</b>
4.1	Test bench configuration	81
4.2	Engine	83
4.3	Cooling system components	84
4.4	Emulation of vehicle and powertrain	86
4.4.1	Vehicle	87
4.4.2	Powertrain	87
4.4.3	Results	89



<b>5</b>	<b>Engine Thermomanagement Benefits</b>	<b>95</b>
5.1	Test bench settings	95
5.2	Engine cold start under stationary operating conditions	96
5.2.1	Coolant temperature	97
5.2.2	Oil temperature	99
5.2.3	Fuel consumption	100
5.2.4	Water pump energy demand	106
5.3	MVEG-A test cycle	108
5.4	Error estimation	113
<b>6</b>	<b>Conclusions and Outlook</b>	<b>115</b>
	<b>Appendix A</b>	
	<b>Emulation Parameters</b>	<b>119</b>
	<b>Appendix B</b>	
	<b>Thermal Model of the Engine</b>	<b>123</b>
	<b>Appendix C</b>	
	<b>Error Estimation</b>	<b>127</b>
	<b>References</b>	<b>137</b>
	<b>Curriculum Vitae</b>	<b>147</b>

Seite Leer /  
Blank leaf

## ABSTRACT

This thesis analyses the possibility of reducing vehicle fuel consumption by improving engine thermomanagement. It proposes a solution for advanced temperature control. In conventional applications, combustion engine cooling systems are designed to guarantee sufficient heat removal at full load. The cooling pump is belt-driven by the combustion engine crankshaft, resulting in a direct coupling of engine and cooling pump speed. It is dimensioned such that it can guarantee adequate performances over the whole engine speed range. This causes an excessive flow of cooling fluid at part-load conditions and at engine cold start. This negatively affects the engine efficiency and, as a consequence, the overall fuel consumption. Moreover, state-of-the-art cooling systems allow the control of the coolant temperature only by expansion thermostats (usually solid-to-liquid phase wax actuators). The resulting cooling temperature does not permit to optimise engine efficiency.

In this work an active control of the coolant flow as well as of the coolant temperature has been realized using an electrical cooling pump and an electrically driven valve which controls the flow distribution between the radiator and its bypass. For this purpose the whole cooling system has been modelled. Model based feedforward and feedback controls of coolant temperature and flow have been designed and tested.

The improvements obtained with the proposed configuration in terms of fuel consumption reduction have been measured on a dynamic test bench. Both engine cold start under stationary engine operation and the European Driving Cycle MVEG-A in case of engine cold start have been tested. The fuel consumption reductions achieved vary between 2.8% and 4.5% depending on the engine operating conditions. Compared to vehicle mass reduction or internal engine improvements engine thermomanagement is a simple and flexible solution which should be taken into account for its low realization costs.

Seite Leer /  
Blank leaf

## ZUSAMMENFASSUNG

Die vorliegende Arbeit befasst sich mit der Optimierung des Thermomanagements von Verbrennungsmotoren mit dem Ziel einer Verbrauchsreduktion. In konventionellen Anwendungen wird die Kühlmittelpumpe mittels eines Riemenantriebes direkt vom Motor angetrieben. Das Kühlsystem muss gewährleisten, dass auch unter extremen thermischen Bedingungen (Vollast bei Nenndrehzahl) genügend Wärme abgeführt werden kann. Durch die direkte Kopplung von Motor- und Pumpendrehzahl über den Riemenantrieb ist die Kühlleistung beim Teillastbetrieb mehrfach überdimensioniert. Dadurch wird der Motorwirkungsgrad verschlechtert, was eine Erhöhung des Brennstoffverbrauchs verursacht. Die konventionelle Regelung der Kühlmitteltemperatur wird mittels eines Thermostats ("expansion-element wax actuator") realisiert. Der Öffnungsgrad des Thermostats regelt den Kühlmittelstrom durch den Kühler und damit die vom System abzuführende Wärmemenge. Die resultierende Kühlmitteltemperatur ist für normale Betriebsbedingungen (z. B. im MVEG-A Test-Zyklus) in allgemein nicht optimal.

Thema dieser Arbeit ist eine aktive Regelung sowohl des Kühlmittelstroms durch eine elektrische statt mechanische Kühlmittelpumpe als auch der Kühlmitteltemperatur durch ein regelbares Ventil anstatt eines Thermostats. Eine modellbasierte Regelung erfordert eine Modellierung des Gesamtsystems mit allen Komponenten. Das Modell wird anhand von Prüfstandsmessungen validiert und für den Entwurf verschiedener Regler verwendet.

Durch die Verwendung des vorgeschlagenen Thermomanagements kann eine Verbrauchssenkung von ca. 3% bei thermisch stationären Betriebsbedingungen bei Teillast erreicht werden. Zusätzlich verkürzt das Thermomanagement die Kaltstartdauer. Die daraus resultierende Verbrauchssenkung wird bei konstanter Last und Drehzahl im Bereich von 2.8% bis 4.5% gemessen. Kaltstartmessungen von MVEG-A Zyklen ergaben einen Verbrauchsvorteil von ca. 3%. Im Vergleich zu Massnahmen wie Gewichtsreduktion oder innermotorischer Optimierung stellt das vorgeschlagene System eine sowohl kostengünstige als auch flexible Methode der Verbrauchssenkung dar.

Seite Leer /  
Blank leaf

# NOTATIONS

## 1. Symbols

$A$	area	$[\text{m}^2]$
$d$	cylinder wall thickness	$[\text{m}]$
$c_p$	heat capacity	$[\text{Jkg}^{-1}\text{K}^{-1}]$
$D$	cylinder diameter	$[\text{m}]$
$G_c$	controller transfer function	$[-]$
$m$	mass	$[\text{kg}]$
$\dot{m}^*$	mass flow	$[\text{kgs}^{-1}]$
$n$	rotational speed	$[\text{min}^{-1}]$
$H$	cylinder stroke	$[\text{m}]$
$H_F$	fuel heating value	$[\text{Jkg}^{-1}]$
$P$	power	$[\text{W}]$
$\dot{Q}^*$	heat flow	$[\text{W}]$
$T$	temperature	$[\text{°C}]$
$T$	torque	$[\text{Nm}]$
$u$	input	$[-]$
$v$	velocity	$[\text{ms}^{-1}]$
$V_d$	displaced cylinder volume	$[\text{m}^3]$
$V$	volume	$[\text{m}^3]$
$x$	position	$[\text{m}]$
$y$	output	$[-]$
$z$	number of crank revolutions per power stroke	$[-]$
$z_c$	number of cylinder	$[-]$

$\alpha$	coolant heat transfer coefficient	$[\text{Wm}^{-2}\text{K}^{-1}]$
$\eta$	efficiency	[-]
$\Pi_v$	boost pressure ratio	[-]
$\lambda$	thermal conductivity	$[\text{Wm}^{-1}\text{K}^{-1}]$
$\lambda_{A/F}$	air to fuel ratio	[-]
$\tau$	delay	[s]
$\omega$	angular speed	$[\text{rads}^{-1}]$

## 2. Subscripts

<i>amb</i>	ambient
<i>c</i>	coolant
<i>c, eb</i>	from the coolant to the engine block
<i>DES</i>	desired value
<i>eb</i>	engine block
<i>eng, in</i>	coolant entering the engine
<i>eng, out</i>	coolant leaving the engine
<i>ex, eb</i>	from the exhaust gases to the engine block
<i>f</i>	fuel
<i>g</i>	gas
<i>g, w</i>	from the gas in cylinder to the wall
<i>ICE</i>	internal combustion engine
<i>if</i>	internal friction
<i>irr</i>	irradiation
<i>mix</i>	mixing point bypass / radiator
<i>r, in</i>	coolant entering the radiator
<i>r, out</i>	coolant leaving the radiator
<i>w</i>	cylinder wall
<i>w, c</i>	from the wall to the coolant



### 3. Notation

$\Delta$	difference
*	Flux or flow
$\frac{d}{dt}$	Derivative in time

### 4. Abbreviations, Acronyms

ABS	Assisted Braking System
<i>b<sub>mep</sub></i>	break mean effective pressure
<i>f<sub>mep</sub></i>	friction mean effective pressure
ICE	Internal Combustion Engine
<i>fuel mep</i>	fuel mean effective pressure
<i>mep</i>	mean effective pressure
ECE	City part of NEDC
EGR	Exhaust Gas Recirculation
NEDC	New European Driving Cycle
EUDC	Extra Urban Driving Cycle
MVEG	Motor Vehicle Emissions Group
WOT	Wide Open Throttle

# CHAPTER 1

## INTRODUCTION

The importance of individual mobility, especially by means of automotive vehicles, has grown considerably in the past decades to the point where it is now an inevitable part of our daily life. The use of motorized vehicles in urban traffic conditions, where the engine is operated in part load conditions, has increased conspicuously over the last years. In addition, almost 30% of the distances covered by car during a single ride are shorter than 5 km ([4]), which increases the frequency of engine cold starts. Both part load and cold start operating conditions negatively affect engine efficiency by increasing the fuel consumption of the vehicle ([41]).

Simultaneously, due to an increased awareness of damage to the environment and to the pressure imposed by legislation, resources are increasingly being allocated to research focusing on the reduction of fuel consumption and of emissions. These targets are particularly relevant when urban driving conditions are considered. In this context small and light vehicles that are typically used for short distances assume a particularly eminent role.

Various solutions have been proposed for the achievement of these goals, and significant results have been obtained. An overview of the most significant measures taken to reduce fuel consumption is given in the following paragraph. Nevertheless, the potential offered in these fields has not yet been exhausted. The present work focuses on the contribution to the reduction of fuel consumption that can be achieved by improving engine thermomanagement.

## 1.1 Methods for the reduction of fuel consumption

A great number of methods have already been studied in order to reduce vehicle fuel consumption. They can be divided into measures for the improvement of the efficiency of internal combustion (IC) engines, such as thermomanagement, supercharging, or variable valve timing, and in proposals for the improvement of the global powertrain efficiency, such as energy management concepts or hybrid concepts. An overview of some of these methods as well as an indication of the main topics of this work are given in Fig. 1-1.

One of the characteristics of IC engines is that they suffer from different losses (thermal, mechanical, etc.). Engine efficiency can be expressed by the relation between brake mean effective pressure and fuel mean effective pressure:

$$\eta = \frac{bmep}{fuel\ mep}. \quad (1.1)$$

The brake mean effective pressure  $bmep$  is obtained by dividing the work per cycle by the cylinder volume displacement:

$$bmep = \frac{P \cdot z}{V_d \cdot n}, \quad (1.2)$$

while the fuel mean effective pressure  $fuel\ mep$  is the fuel energy released per cylinder volume displacement:

$$fuel\ mep = \frac{z \cdot \dot{m}_f^* \cdot H_f}{V_d \cdot n}.$$

Each energy transformation is characterized by its efficiency. The Willans approach correlates the provided and delivered power for a defined energy transformation ([37]). This representation is often used for combustion

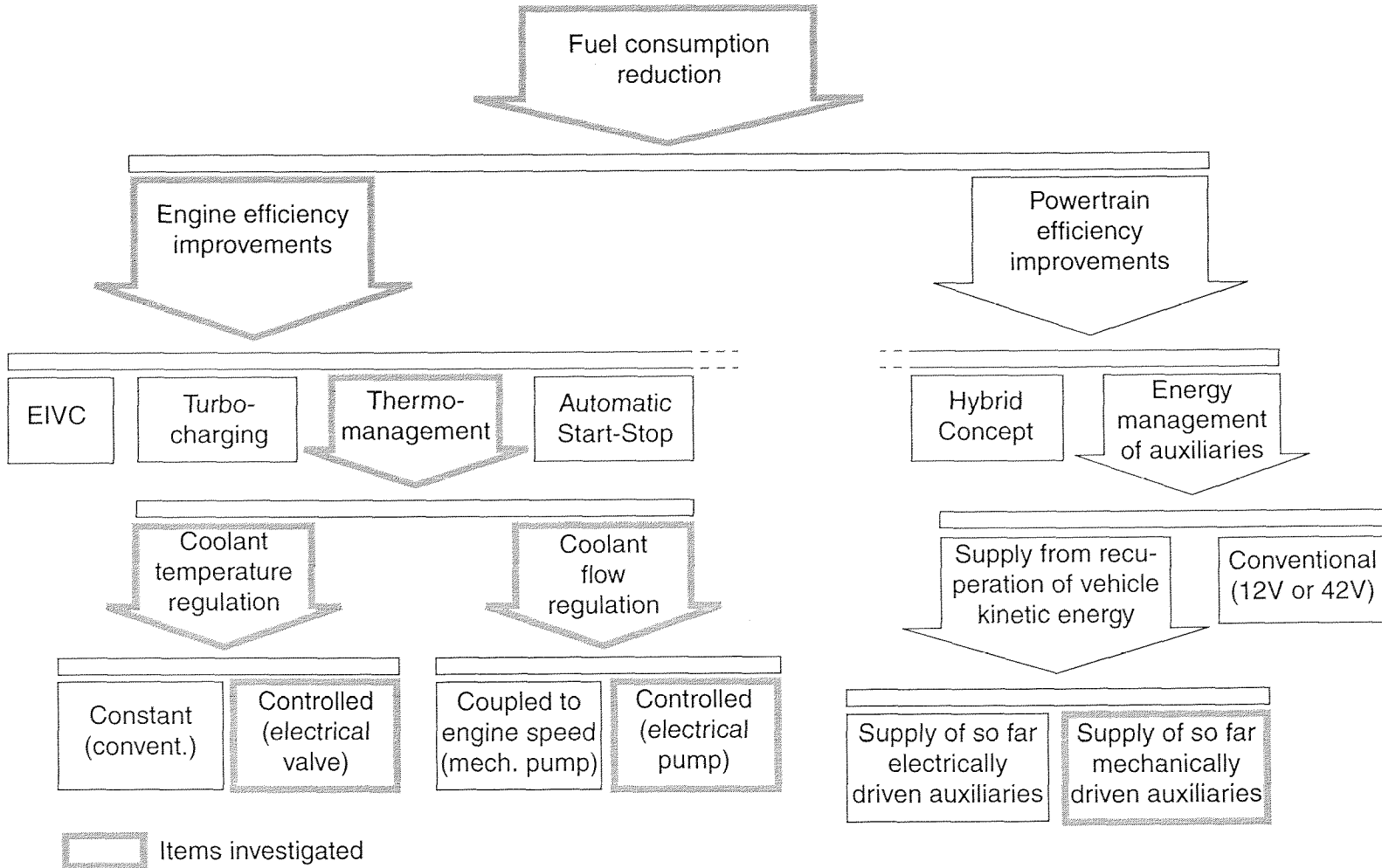
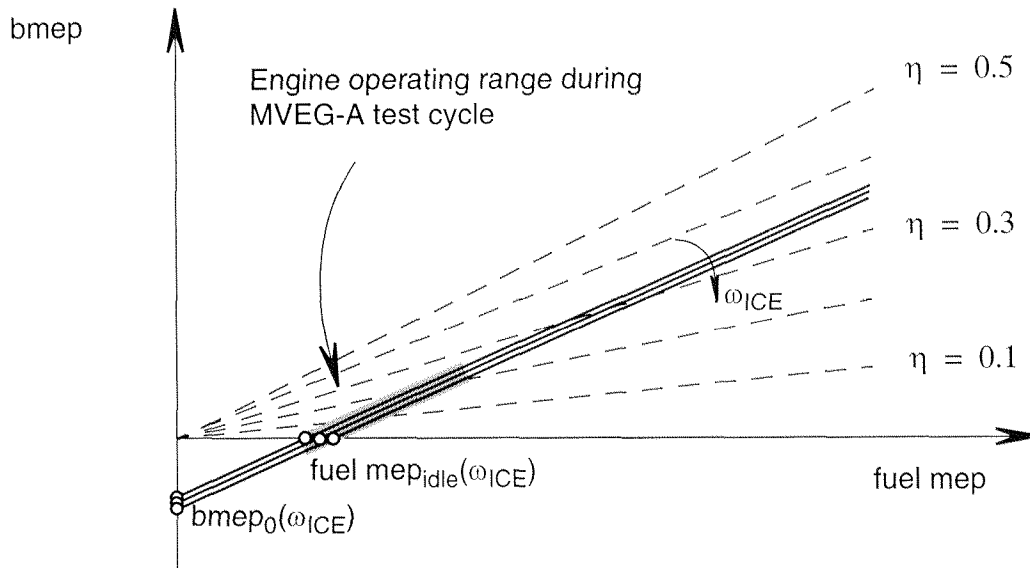


Figure 1-1: Overview of where the items investigated fit within the overall theme of fuel consumption reduction

engines, where for a constant engine speed the brake mean effective pressure shows an affine correlation with the fuel mean effective pressure. The graphical representation of the Willans approach is given in Fig. 1-2.



**Figure 1-2:** Willans representation of engine efficiency

The fuel conversion efficiency for conventional, naturally aspirated engines at wide-open-throttle (WOT) operating conditions varies between 0.31 and 0.34, which also represents their best value ([41], Ch. 2). Radical enhancements of this value in the future are unlikely. As shown in Fig. 1-2, however, the average efficiency of IC engines drops to values between 0.1 and 0.2 during the New European Driving Cycle (MVEG-A, see Appendix A), due to the very low engine loads.

In the Willans representation it is also possible to see that in order to deliver a positive *bmep* the engine internal friction, represented by  $bmep_0$ , is to be compensated first. Two main components of friction are present in IC engines:

1. mechanical friction, needed to overcome the resistance to the relative motion of all the moving parts of the engine (valve train, piston, rings, pins, rods, crankshaft, and seals)

2. auxiliaries work, used for driving the engine auxiliaries (water pump, oil pump, generator, power steering pump, fan, and, as the case may be, the air conditioner).

The cumulative distribution of the two different components of friction for an engine with a displacement of 2 litres is plotted in Fig. 1-3 ([4], [30], [36], [41], Ch. 13).

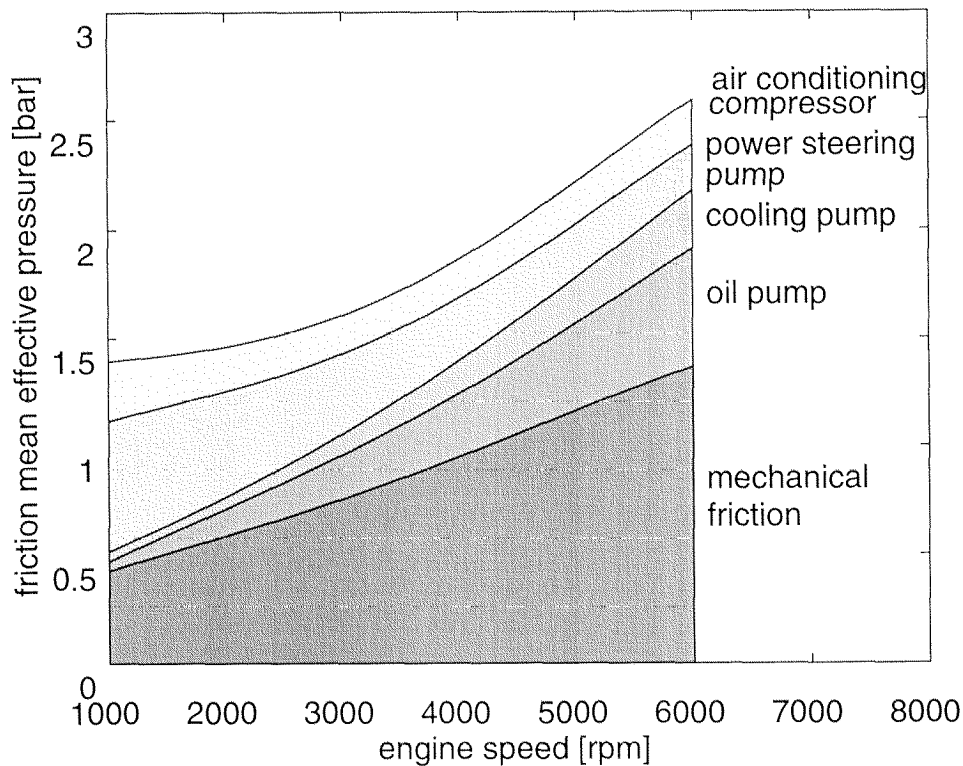


**Figure 1-3:** Friction mean effective pressure for a mid-size engine

The mechanical friction component is a function of engine speed. Due to viscosity variations of the lubricating oil with its temperature, mechanical friction also depends on engine and oil temperature.

One of the main tasks of engine thermomanagement is to maintain the temperature of the coolant as well as of the lubricating oil at a defined level. Unfortunately, especially during engine cold start and part load operating conditions the conventional cooling system cannot guarantee the optimal temper-

ature level. The aim of this work is therefore the development of an improved cooling system capable of raising the engine efficiency in the engine operating conditions mentioned by properly controlling the coolant temperature.

As visible in Fig. 1-3 further sources of engine internal friction are the various engine auxiliaries necessary for proper engine operation. With exception of the air conditioning compressor, which is provided with a clutch, all of the auxiliaries are rigidly coupled with the engine crankshaft since they are belt-driven. In Fig. 1-3 the air conditioner average operating time has been considered for the calculation of the corresponding engine mean effective pressure ([30]). The auxiliaries have to be designed such as to guarantee adequate performance over the whole engine speed range. However, since belt-driven by the engine, they are optimally operated only over a limited range of engine speeds. For instance the direct coupling between engine and cooling pump speeds results in an excessive flow of cooling fluid at part load conditions and at engine cold start. This negatively affects the engine efficiency and, as a consequence, the overall fuel consumption ([3], [4], [26], [47]).

A possible solution to this problem is the “beltless engine” ([36], [78]) where all the conventionally belt-driven auxiliaries are electrified. Since they no longer are coupled to the engine speed, they can run strictly at their optimum operating point. The amount of engine-internal friction is therefore reduced. In the present work the electrification of the cooling pump is considered. The control of the cooling pump is part of the thermomanagement concept proposed.

The electrification of conventionally belt-driven auxiliary devices is justified by other considerations as well. Indeed, in the last years devices for the improvement of driver comfort, such as power assisted steering and air conditioning, as well as those for the increased safety of the occupants, such as airbags and ABS (Assisted Braking System), have ceased to be exclusive characteristics of top-of-the-line vehicles but are being installed in small passenger cars, too. The growth in the complexity as well as in the number of auxiliary devices does not seem to have an immediate end and it is thus responsible for a renewed increase in fuel consumption ([36], [72]). Conventional alternators are hardly capable of producing more than 2.5 KW of power with an average efficiency of ca. 50% ([10], [61]). As a consequence, they can

no longer comply with the increased power demands of the auxiliary devices. As one alternative, a powerful (>6-10 KW) asynchronous machine directly linked to the crankshaft can achieve efficiencies higher than 80% ([78]). In consideration of this, a new energy management for the auxiliaries has to be developed. The higher power available and the higher efficiencies achieved in the production of electrical energy are favourable to the electrification of conventionally belt-driven devices. Other auxiliary devices, like the air conditioner ([70]) or the steering assistance ([13], [23], [60], [70]) can be electrified as well.

In order to limit the level of electrical currents in a more powerful electrical system it is planned to raise the electrical voltage in automotive applications from 12V to 42V ([63], [78]). Volt ages above that level are not recommended because of safety problems.

One of the reasons for the low engine efficiency at part load is the fact that at a fixed throttle position the throttle open area is reduced. The air flow is thus limited and the pumping component of the total friction increases, decreasing the mechanical efficiency of the engine. Unfortunately, due to the consideration of the average operating conditions, internal combustion engines have conventionally been over-dimensioned in automotive applications in order to guarantee sufficient power reserves (e.g. for uphill routes or when overtaking is required), which normally are exploited only for short times.

The specifications of the engine used for the experiments in this thesis work are given in Chapter 2 and in Appendix A. In order to improve the engine performances at part load, an engine supercharged by a pressure wave supercharging device ([2], [39]) is considered.

## 1.2 Importance of heat transfer

During combustion in the cylinder, the burning gases can reach peak temperatures of 2500 K. The maximum temperatures of the metal components of the engine must remain far below this value. Therefore cylinder head and cylinder liner must be cooled. For this reason the heat flux during the combustion period can be substantial, although during the rest of the operating cycle it



drops to almost zero. The heat flux varies considerably, not only depending on the operating phase but also on the location along the chamber wall. In regions with high heat flux thermal stress must be held below levels that would cause fatigue cracking. In addition the gas side surface of the cylinder wall must be maintained below 180 °C in order to guarantee the integrity of the lubricating oil film and to avoid excessive engine wear ([41], Ch. 12, [4]).

A proper heat transfer is not only necessary to maintain the integrity of the engine components, but it also affects engine performance, efficiency, and emissions. For a given mass of fuel within the cylinder, the work per cycle to the piston is influenced by the average gas temperature and pressure. An excessive heat transfer to the combustion chamber wall caused by excessively low wall temperatures will therefore have a negative influence on the engine performance. In addition friction, responsible for a part of the engine losses, is also influenced by the temperature of the cylinder wall and of the engine components more generally (see Chapter 2.2.1). The temperature of the cylinder liner is accountable for the temperature of the oil film lubricating the piston and its rings, and as a consequence for its viscosity. Reducing engine internal friction (see Chapter 1.1) is of considerable importance when improvements of engine efficiency are desired ([3], [4], [47], [50], [76]).

### 1.2.1 Engine energy balance

Although heat flux from the burning gases to the chamber walls  $Q_{g,w}^*$  and from there to the various parts of the engine strongly varies during the engine operating process and along the cylinder wall, earlier investigations have shown that assuming the heat transfer process to be quasi steady is sufficiently accurate for describing the global thermal behaviour of the engine ([41], Ch. 12, [42], [65]).

Fig. 1-4 shows the heat flow partitioning over the engine in case of steady-state operating conditions. The heat developed during the combustion process  $\dot{m}_f \cdot Q_{LHV}^*$  is used for the production of the brake power,  $P_b$ , while a considerable part is dissipated as exhaust gas enthalpy  $H_e^*$ . A portion of the heat developed during the combustion, finally, is transferred to the chamber wall and has to be taken away by the coolant  $Q_c$ . In addition, the coolant is responsible for the removal of the heat produced by means of engine internal friction

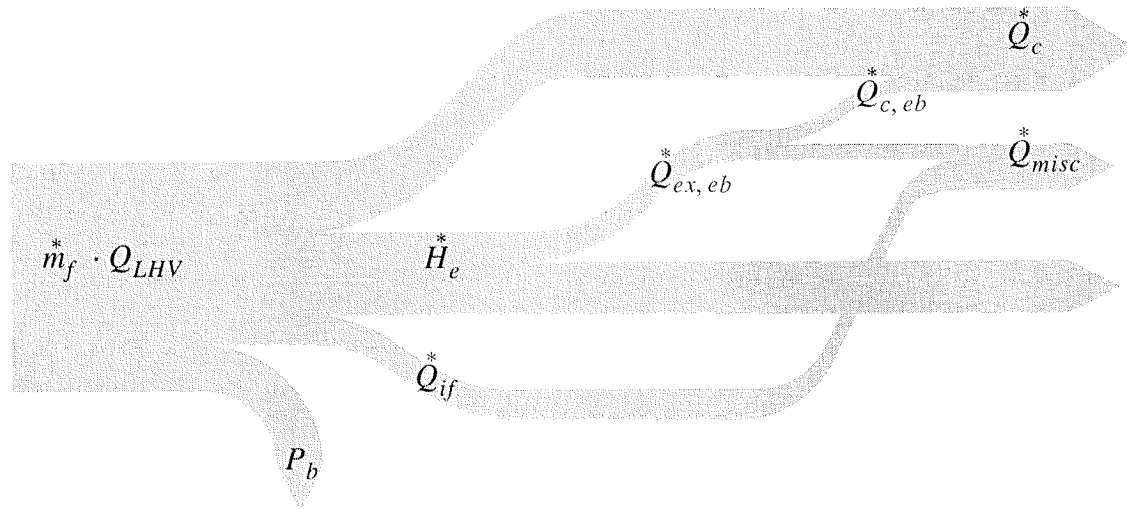


**Figure 1-4:** Energy flow diagram

$\dot{Q}_{if}$  as well as for part of the exhaust gas enthalpy  $\dot{Q}_{ex, eb}$ . The distribution between the different terms mentioned above of the heat produced during the combustion depends furthermore on the particular engine operating point considered. For this purpose, experimental data are shown in Fig. 1-5 describing the brake power and the coolant load as a percentage of the fuel heating value for two different engine loads. The remaining components of the heat produced during combustion such as exhaust enthalpy, exhaust enthalpy due to incomplete combustion, or irradiation are not explicitly plotted in Fig. 1-5. The data are obtained from the engine fuel map shown in Fig. 4-2 and from measurements of the heat removed by the coolant:

$$\dot{Q}_c^* = c_{pc} \cdot \dot{m}_c^* \cdot (T_{eng, out} - T_{eng, in})$$

plotted in Fig. 1-6. As Fig. 1-5 shows, when the engine works in extreme part-load conditions (e.g. 2 bar) only 20% of the heat produced during combustion is used for the production of brake power, while 20 to 25% of the heat is removed by the coolant, depending on the engine speed. The percentage distribution is more favorable when higher loads are considered. A larger part of the heat produced during combustion is transformed into brake power and only 15 to 20% of the total heat needs to be removed by the coolant (see also [41], Ch. 12, [48], [75]).

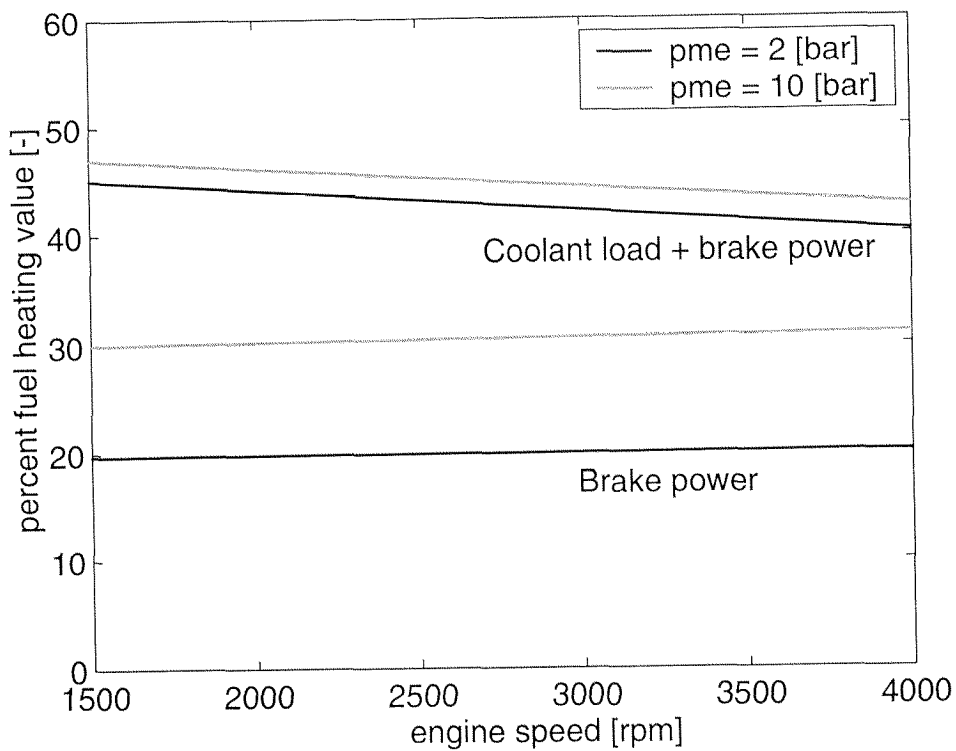


**Figure 1-5:** Brake power and coolant load as a percentage of heat from fuel

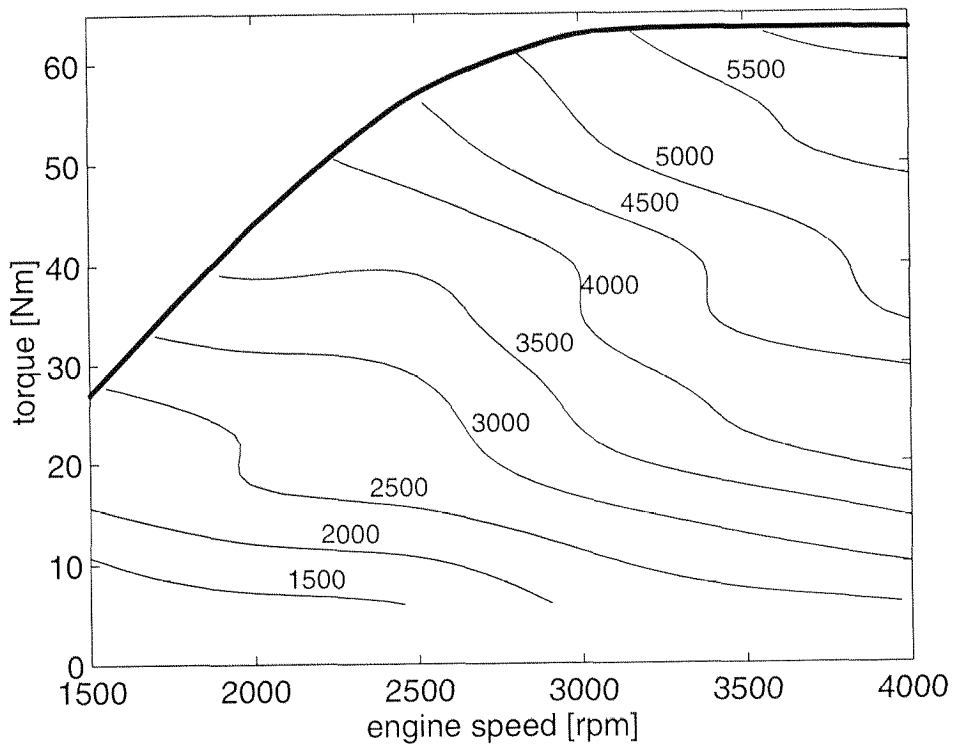


**Figure 1-6:** Coolant heat flow [W]

In Fig. 1-5 it is also evident that the percentage of the coolant load not only depends on the engine load but also on its speed. Indeed, the data plotted are based on a conventional configuration of the cooling system, where the coolant flow is not optimised for each engine speed but designed to remove enough heat at engine full load and speed. The resulting overcooling at low speeds and loads is visible in the fact that the percentage of coolant load is higher for low engine loads and speeds.

These considerations show the relevance of the analysis of the thermomanagement of the engine during part load operating conditions.

### 1.2.2 Other benefits

The cylinder wall and in-cylinder temperatures during and after the combustion process are of great importance for the chemical composition of the emissions. In a cold engine, when fuel vaporization is slow, the fuel flow is increased to provide an easily combustible rich air/fuel mixture in the cylinder ([41], Ch. 11). Thus, until the engine warms up and this enrichment is removed, CO (carbon monoxide) and HC (hydrocarbon) emissions are high. A quicker engine warm-up therefore also positively affects emissions. In addition, the coolant temperature influences HC and NO (nitrogen oxides) emissions also during steady-state engine operating conditions. In this context literature data relative to a decrease of HC with increasing coolant temperatures are available ([45], [46], [58]). In particular, some experiments ([56]) demonstrate a 30% decrease of HC when the coolant temperature is increased from 62 to 108°C. The reason can be found in the fact that the piston top-land crevice decreases in size due to the higher thermal expansion of the aluminium piston relative to the cast-iron bore. The density of the gas in the crevice also decreases due to the higher temperatures. Finally, the solubility of fuel species in the oil layer decreases exponentially with temperature ([64]). Nevertheless, NO emissions increase by approximately 15% over the same coolant temperature range. The reason can be found in the fact that higher gas temperatures due to increased coolant temperatures produce a faster burn and increase the peak pressure.

### 1.3 Methods for improving engine thermomanagement

The accurate design of the coolant jackets in the engine cylinder head is also known as “precise cooling” ([14]). It allows a reduction of the mass of coolant in the system, thus shortening the duration of engine warm-up and reducing the wear of engine components due to lower thermal distortion. Nevertheless, this costly method of improving engine thermomanagement was not considered in this work. Indeed, the approach taken here does not require any modification in the engine coolant jackets.

The present work deals with issues related to the liquid cooling of SI engines, since almost all production engines utilize this method. Air cooling is possible, too. In some cases neither liquid nor air cooling are provided, and the engine is oil cooled. This latter solution, also known as Elsbett engine ([27], [28], [29]) has been developed particularly for DI diesel engines. It provides the so-called duothermic combustion ([1]), which indicates that during combustion two volumes with very different temperatures are present. The discussion of combustion phenomena in DI diesel engine lies outside the main topic of this work and will therefore not be discussed here.

In conventional applications the temperature of the coolant is maintained below the boiling point of water. Higher working temperatures of up to 120 °C are possible as well ([18]) in a procedure known as ‘hot cooling.’ In order to maintain the coolant in its liquid phase, higher than atmospheric pressures would be needed in the cooling circuit ([3], [18], [32], [49]), or cooling fluids other than water have to be used ([19], [31]). As an alternative, nucleate boiling can be allowed. In that case, the liquid and the gas phases of the coolant are simultaneously present in the cooling circuit. By using the change of phase it is possible to achieve a high transfer of heat and to reduce the coolant mass flow ([44], [54], [73]). Nevertheless, it is advisable to increase the temperature of the coolant to the levels mentioned above only when the engine works under part-load operating conditions. At full load, indeed, the torque losses increase with the coolant temperature. Since the density of the aspirated air drops when the in-cylinder temperature rises, the air volume available for combustion and therefore the volumetric efficiency of the cylinder is reduced ([49]). In addition, the engine efficiency drops because of the late ignition

needed in order to prevent knocking ([7]). Nevertheless, due to the modifications needed in the cooling circuit, hot cooling and nucleate boiling are not topics of the present work.

A reduction of coolant flow is mentioned by various authors as an important point for the improvement of engine efficiency. Some authors ([77]) have proposed to throttle the conventional belt-driven cooling pump. It is evident that this method is less efficient than the substitution of the conventional pump with an electrical one ([3], [47], [50]). Nevertheless the importance of a better control of the flow partitioning between the bypass duct and the radiator has been largely ignored. The substitution of the conventional thermostat with an electrically operated bypass valve, as suggested in this work, permits to easily realize a better control of the coolant temperature. In addition, the desired temperature can be easily changed depending on the engine operating point considered. The implementation of variable temperature levels in the expansion-element thermostat, realized by externally heating the wax sensor, has been suggested ([7]). As an alternative, an electronic thermostat has been proposed as well ([49]). However, only few of the aforementioned approaches have been tested on a test bench.

Some authors ([75]) argue that the coolant temperature is not directly related to any engine component temperature. The cylinder wall temperature for instance varies over a wide range although the coolant temperature remains almost constant. This is due to the different time constant and thermal capacity of coolant and engine block. They suggest as a consequence to control the temperature of engine components instead of coolant temperature. This method entails the usage of different sensors placed inside the engine block. This solution can result to be costly, without even considering that high coolant temperatures can be reached.

## **1.4 Objectives of the thesis**

This thesis focuses on the development of a low energy demand engine thermomanagement aiming to the reduction of fuel consumption especially during engine cold start and part-load operating conditions. The analysis and the

experimental tests are conducted on a small supercharged SI engine, whose characteristics and parameters are listed in Appendix A. Nevertheless the results can be extended to engines of middle- and upper-class vehicles.

The following objectives are pursued in this thesis:

- Model of the IC engine from the thermal point of view. Both the conventional (with belt-driven cooling pump and wax-expansion element thermostat) and the improved configuration (electrical cooling pump and electrically controlled valve for the radiator bypass) of the cooling system are to be considered.
- Development of a model-based controller of coolant flow and coolant temperature aiming to fuel consumption reduction
- Verification on a dynamic test bench the fuel consumption reduction achievable with the proposed configuration of engine thermomanagement.

Although thermomanagement also has an important influence on emissions, especially during engine cold start, the composition of the exhaust gases has not been measured on the test bench. The variation of the coolant temperature compared with conventional solutions influences engine emissions as explained in Chapter 1.2.

## **1.5 Main results and new contributions**

The improvements offered by controlling both the coolant flow and the coolant temperature were measured on the test bench. In particular experiments of engine cold start were conducted under constant engine speed and load as well as during the European Test Cycle MVEG-A. The measured fuel consumption reduction due to the better thermal condition of the engine varies between 2.8% and 4.5% depending on the engine operating condition considered. The fuel consumption reduction obtained is significant especially when the realization costs of such a solution are compared with those of other solutions proposed for fuel consumption reduction, like vehicle mass reduction or internal engine improvements.

The thermal behaviour of the system was improved as well. Indeed, the reduction of the coolant mass flow and the simultaneous model-based control of the coolant temperatures permits to reduce the system time constant, avoiding unwanted phenomena such as temperature overshoot during engine cold start.

The fuel consumption reduction achieved here is due only to the improved thermal conditions of the engine. This research does not take into consideration the fact that the coolant flow and as a consequence the pump energy demand of the proposed configuration amount to just a fraction of the original configuration. Indeed in both cases an electrical cooling pump externally driven is implemented on the test bench. It delivers the same coolant mass flow as the mechanical pump does when the conventional configuration is considered. On the contrary, when the improved configuration of the cooling system is considered the electrical pump delivers the mass flow imposed by the controller designed.

For practical realizations, in order to supply the electrical cooling pump, mechanical energy has to be transformed in electrical energy by the alternator. The efficiency of this process typically amounts to about 60%, but it is likely to increase to more than 80% in the future ([78]). With ca. 90% the efficiency of a belt transmission is clearly higher. Nevertheless this difference is obviously more than compensated by the fact that the need for the cooling pump energy in the new configuration can be reduced to just a fraction of that required in the original case. The substitution of the mechanical pump with an electrical one reflects a general tendency for all the auxiliary devices in automotive applications.

The global energy balance of electrified auxiliary devices and of the cooling pump as well is increasingly favourable when the possibility of recuperating vehicle kinetic energy to supply auxiliary devices is considered ([15], [78]).



Seite Leer /  
Blank leaf

## CHAPTER 2

# MODELING FOR ENGINE THERMOMANAGEMENT

In this chapter the modelling of the thermal behaviour of the engine is explained. Both the conventional and the improved configurations of the cooling system are considered in the modelling. The components that characterize each of the configurations considered are modelled and analysed in detail. They consist of the belt-driven mechanical cooling pump and the thermostat for the conventional configuration as well as the electrical cooling pump and the electrically driven bypass valve for the improved configuration of the cooling system.

In order to quantify the benefits of an improvement in engine thermomanagement a model of the thermal behaviour of the conventional configuration of the cooling system is proposed first. For all the simulations and the measurements performed the engine considered is a boosted small IC engine. The engine parameters are given in Appendix A.

In a second step an improved configuration of the engine thermomanagement is proposed. The elements typical of the new cooling system configuration, namely the electrical pump and the controlled bypass valve, are modelled as well. The resulting model of the improved cooling system is validated and afterwards used for the development of a model-based controller (Chapter 3). Experimentally verified improvements of the fuel consumption and of the temperature performances of the new cooling system are presented in Chapter 5.

## 2.1 Main components of the cooling circuit and their models

The main components of a conventional automotive cooling circuit are a mechanically driven cooling pump and a thermostat, while the proposed configuration of the cooling circuit is characterized by an electrically driven pump and by an electrically actuated bypass valve. The modelling of these components is described in the following.

### 2.1.1 Cooling pump

Constructive characteristics of the cooling pump are not considered in this work. However, the investigation of the energy directly used by the cooling pumps for the two different strategies proposed is rather important.

For a better comparison of the two different configurations of the cooling circuit, the experiments related to the conventional configuration have been conducted with an electrical cooling pump instead of a mechanical one. The measurements of the coolant mass flow for the mechanical and the electrical pumps are shown in Figs. 2-1 and 2-2, respectively. Fig. 2-1 shows the correlation between engine speed and mass flow for the mechanical pump, while Fig. 2-2 shows the correlation between the pump mass flow and the power absorbed by the electrical pump. An engine driven at 1500 rpm for instance, has a coolant mass flow of 0.14 l/s with the conventional pump. In order to deliver the same mass flow with the electrical pump, it has to be powered with 17 W. Therefore, in measurements relative to the basic configuration, the electrical pump is powered such as to guarantee the same coolant flow as with the conventional pump.

### 2.1.2 Conventional thermostat

In conventional applications an expansion-element thermostat is used: the most conventional type of thermostat is a solid-liquid wax actuator. The brass housing (cup) of the thermostat is filled with expansive wax material of various components to provide accurate and repeatable temperature responses.

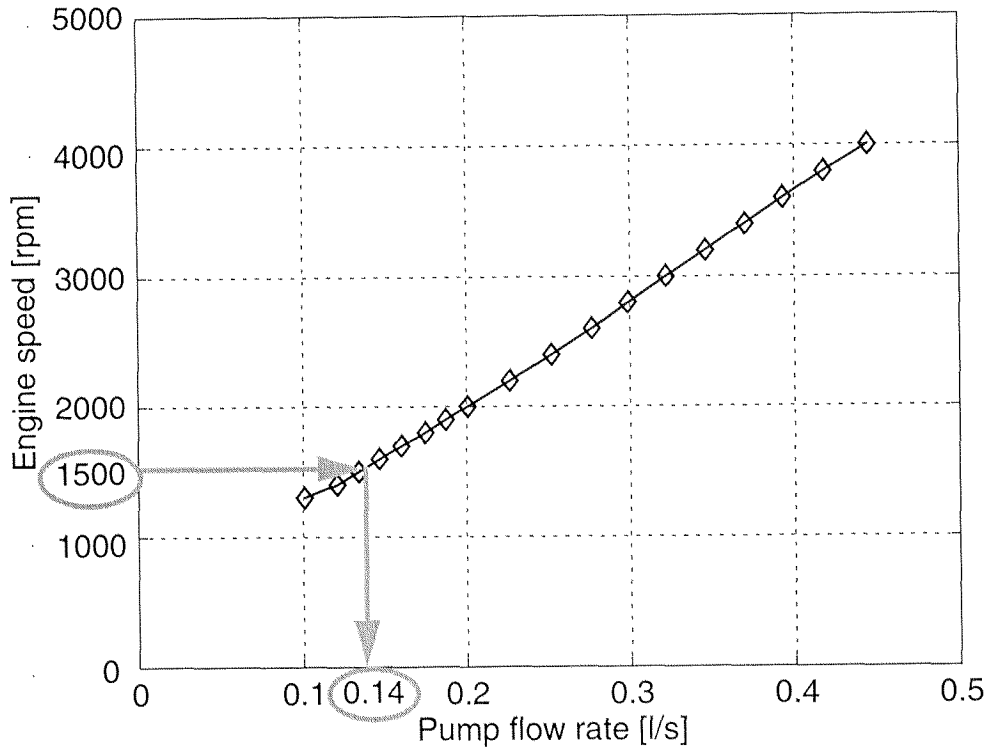


**Figure 2-1:** Flow rate for the mechanical cooling pump

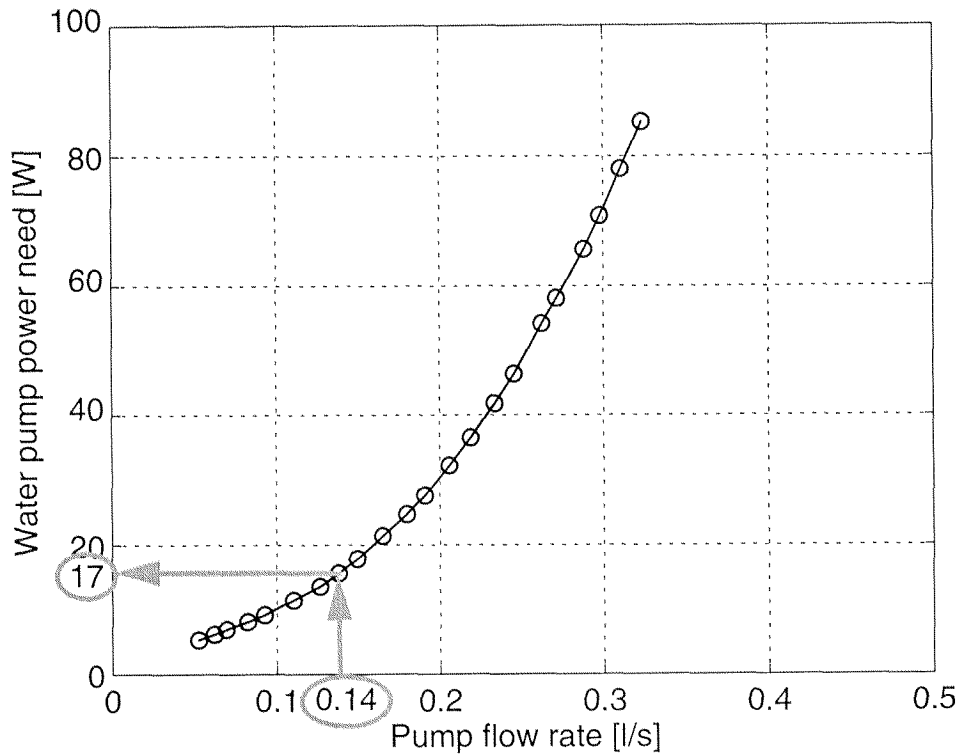


**Figure 2-2:** Flow rate for the electrical cooling pump

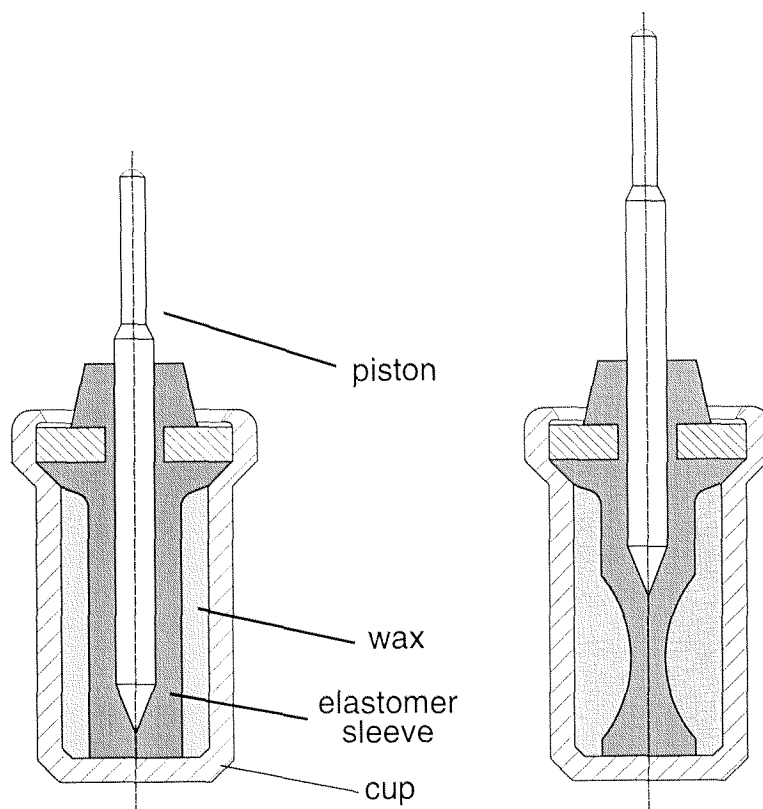
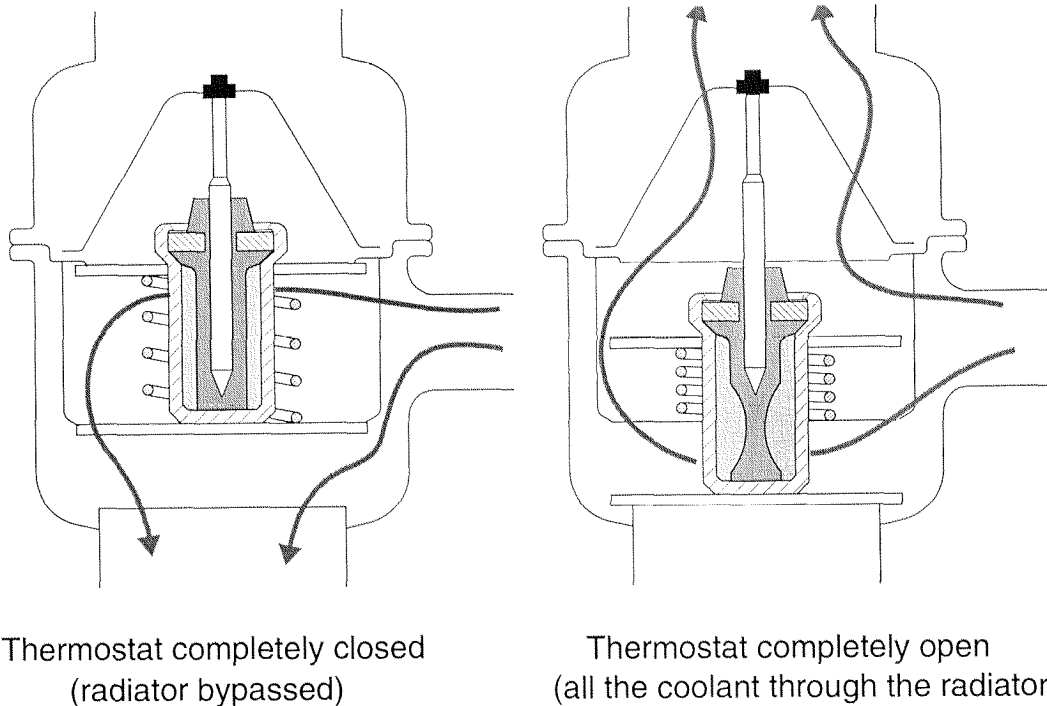


**Figure 2-3:** Thermostat expansion element

The wax is then sealed within the cup by an elastomer sleeve. The sleeve envelops a polished stainless steel piston with tapered ends. A seal and a brass cover complete the unit.

The thermostat begins to open when the liquid into which it is immersed, in this case the coolant leaving the engine  $T_{eng, out}$ , reaches the thermostat start-to-open temperature, which is also called the activation temperature. As shown in Fig. 2-3, part of the wax melts and begins to expand, compressing the elastomer sleeve that envelops the polished stainless steel piston with tapered ends. The piston position determines the valve open area. In Fig. 2-4 the two extreme valve positions are shown. For all the remaining valve open positions, the flow is partitioned over the valve and some liquid is directed through the radiator. When the temperature continues to rise, the valve further opens directing more and more coolant to the radiator until it opens up completely. When the temperature sinks, the reverse action takes place.



Thermostat completely closed  
(radiator bypassed)

Thermostat completely open  
(all the coolant through the radiator)

**Figure 2-4:** Coolant flow for different thermostat positions

To appropriately model the thermostat the processes happening in succession when the thermostat is actuated are:

1. Heat transfer by convection from the coolant to the outer face of the brass cup in contact with the coolant
2. Heat transfer by convection through the cup to its inner surface
3. Heat transfer by convection to and through the wax
4. Melting and volume increase of the wax
5. Movements of the piston and actuation of the valve

The dynamic behaviour of the thermostat can be approximated with a first-order system with a time delay ([4], [52]). The time delay models the steps 1 and 2 listed above. It amounts to ca. 5 seconds, while the system time constant of ca. 30 seconds characterizes the subsequent steps 3 to 5.

The stationary behaviour of a conventional thermostat can be characterized by an opening characteristic where a proportional relationship between the lift and the coolant temperature is given, as shown in the small frame in Fig. 2-14 ([4], [49], [52]).

As shown in Fig. 2-14 the thermostat begins to open at relatively low coolant temperatures. It would be possible to raise the engine operating temperature by simply shifting the thermostat opening characteristics to higher temperatures. However, since this would narrow the reserve to critical coolant temperature conditions (boiling), the problem of the response of the thermostat to variations of the coolant temperature would be aggravated compared to conventional systems. In addition, negative effects (knocking) would appear at engine full-load operating conditions ([25]). This obviated the necessity of realizing a controlled bypass valve.

### **2.1.3 Electrically operated bypass valve**

For the investigation conducted, the thermostat is substituted by an electrically operated 3-way bypass valve. The valve opening characteristics, i. e. the relationship between the valve opening position and the mass flow through the bypass has been measured. They are shown in Fig. 2-5; at 100% the valve is completely opened and the heat exchanger is completely bypassed. Clearly, the relationship between the valve opening position and the mass flow partitioning over the valve is characterized by a strong nonlinearity.

The dynamic behaviour of the valve has been measured as well. The results of the frequency analysis between the desired valve position and the effective valve opening is shown in Fig. 2-6. The constant gain shown in Fig. 2-6 is due to the different scaling of the input and output signals. The effective gain amounts to 1 dB. The valve dynamic behaviour can be well approximated by a lowpass element.

The valve used has an internal position controller, with a time constant of 15 seconds.

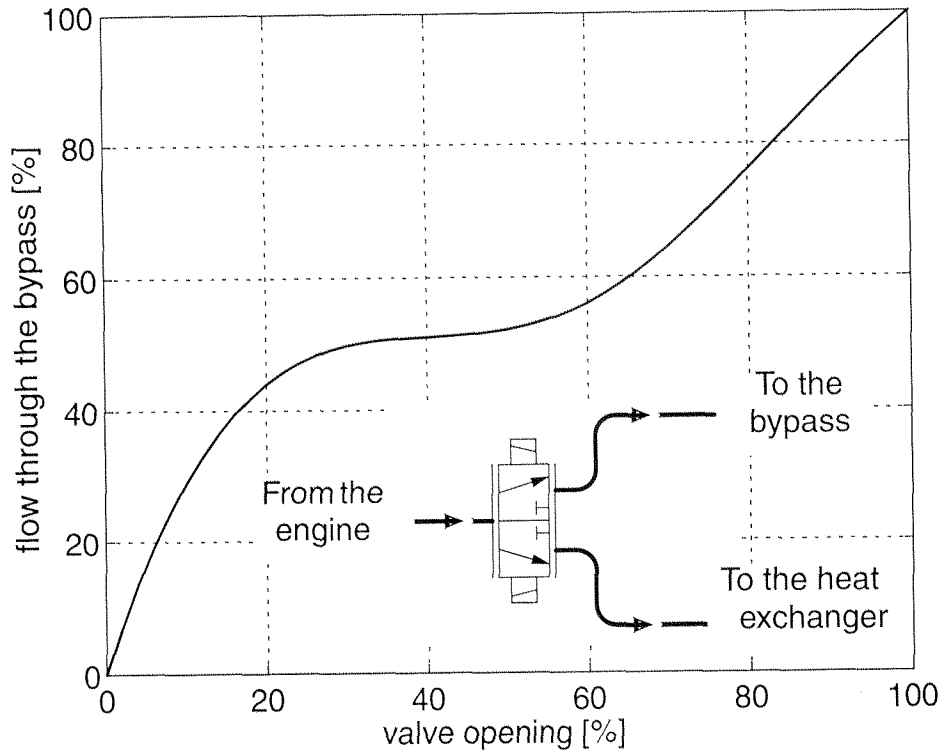


Figure 2-5: Valve opening characteristic

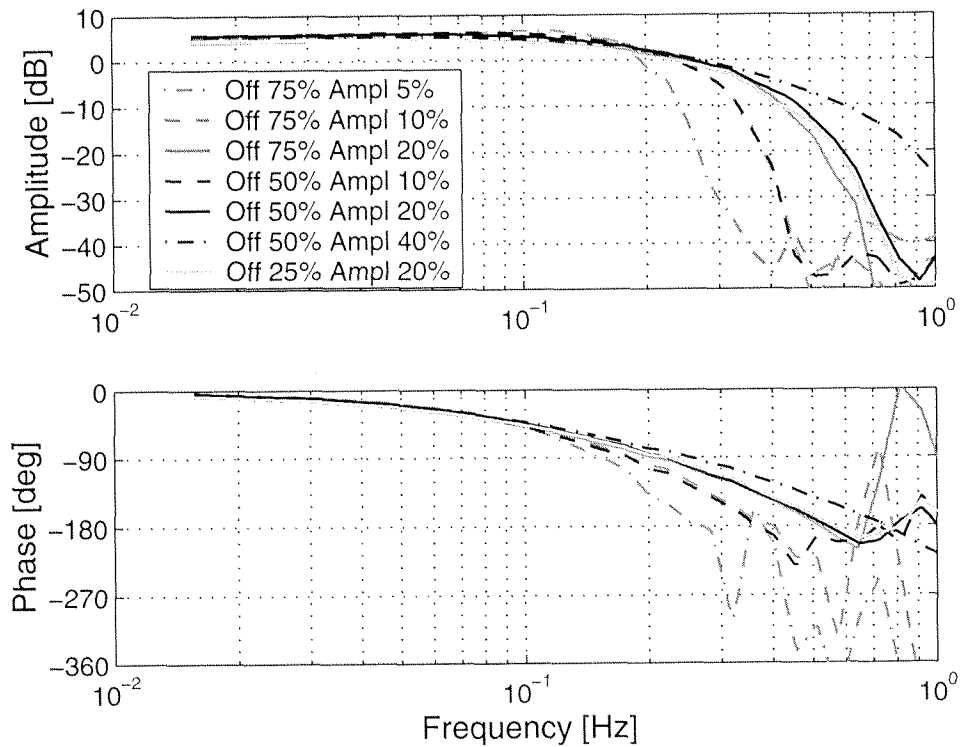


Figure 2-6: Frequency response of the valve



## 2.2 System modeling

A fourth-order mean value model of the system is developed ([16]). Local differences in the coolant temperature or in the coolant flow speed are neglected and only the overall system behaviour is considered. A lumped parameter model is developed. The delays caused by the coolant flowing in the tubes are considered in the simulation. The goal of the model is the prediction of the system thermal behaviour at various operating conditions (i.e. engine cold start, steady-state operating points, or test cycles) as well as the realization of a model-based controller. The results are verified with experiments on a dynamic test bench.

A schematic representation of the cooling circuit in automotive applications is given in Fig. 2-7. Part of the energy delivered during the combustion of fuel is lost due to heat transfer through the cylinder walls. To avoid overheating of the materials a coolant is forced to flow through the engine and the fluid is cooled before it re-enters the engine. To avoid an excessive cooling effect (for example at engine cold start or at part-load conditions), a heat exchanger bypass is installed. The flow partitioning between the bypass and the heat exchanger is realized in the bypass valve, also known as thermostat.

Inputs to the system are the coolant flow rate through the engine and the position of the bypass valve. In conventional automotive applications the static position  $u_1$  of the thermostat is a function of the temperature of the coolant leaving the engine  $T_{eng, out}$ :

$$u_1 = \frac{m_{by}^*}{m_c^*} = f_1(T_{eng, out}). \quad (2.1)$$

The dynamics of conventional expansion-element thermostats was explained in Section 2.1.2 above.

The coolant mass flow is directly coupled with the engine speed since the cooling pump is directly driven by the engine. Therefore:

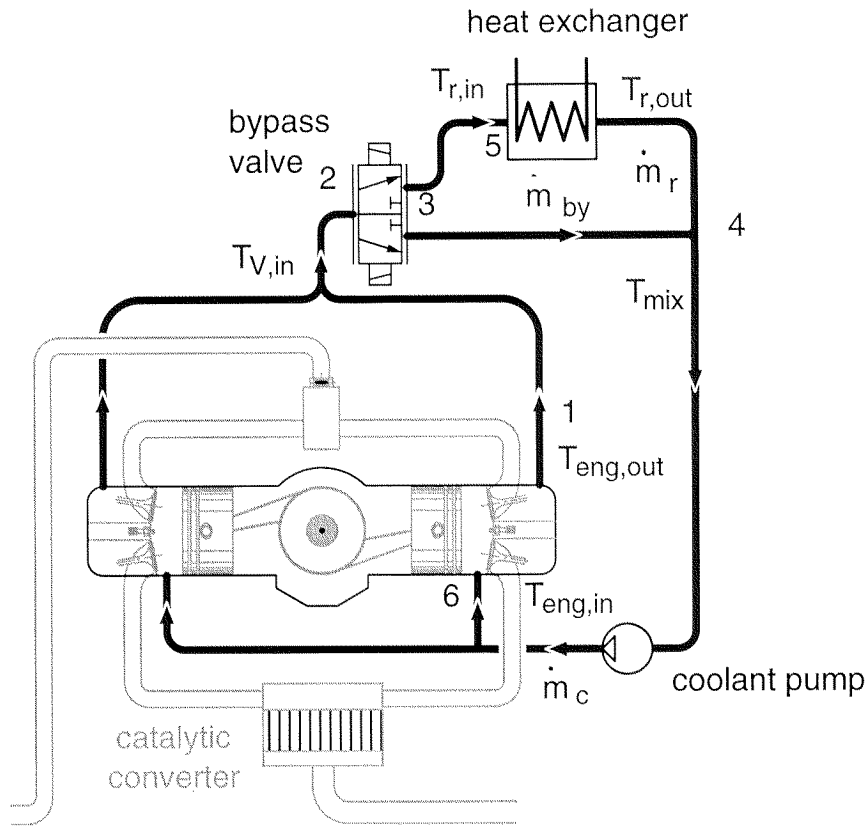


**Figure 2-7:** Schematic representation of the cooling circuit

$$u_2 = \dot{m}_c^* = f(n_{ICE}). \quad (2.2)$$

Outputs of the system are the temperatures of the various subsystems. The cooling system consists of the engine internal and the engine external cooling circuits, as represented in Fig. 2-8. The disturbances acting on the system are shown in Fig. 2-8 as well. A more precise definition of the disturbances is given in the following sections.

While considering the engine internal cooling system the temperature at the output of the engine can be calculated if the coolant mass flow and the temperature of the coolant entering the engine are known. Similarly, since the temperature of the coolant entering the external cooling system, the flow distribution in the bypass valve, and the global coolant mass flow are known,

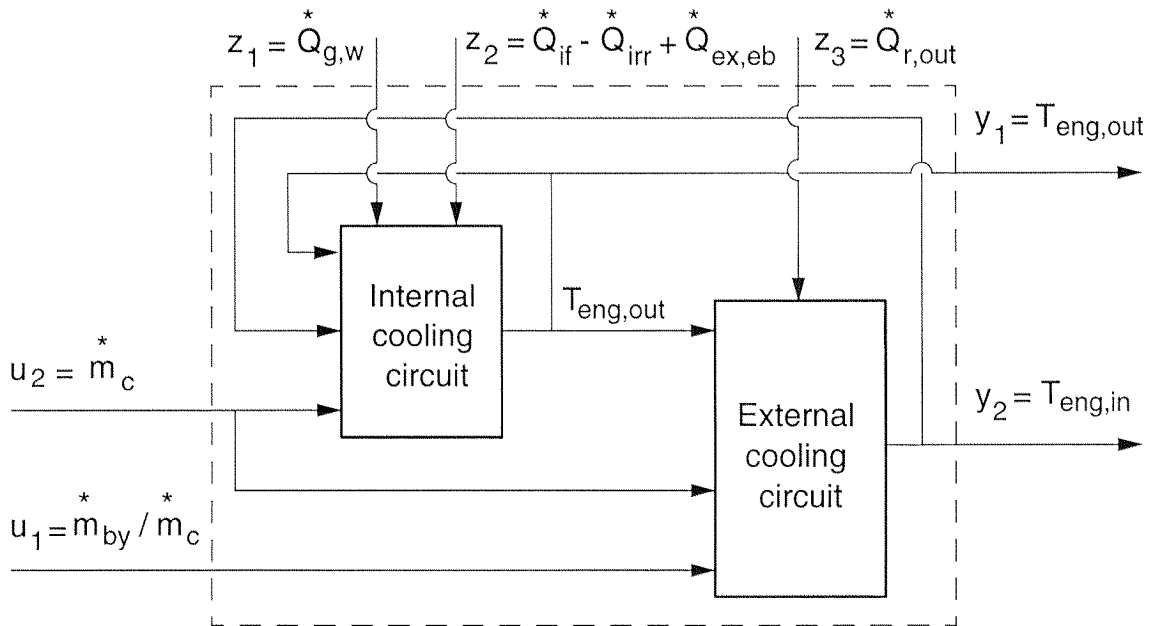


**Figure 2-8:** Cooling circuit model

the coolant temperature exiting the external cooling circuit can be determined. This temperature is also the temperature of the coolant entering the engine. Considering Fig. 2-8, the two subsystems of the cooling circuit can be modelled as described below.

### 2.2.1 Engine internal cooling circuit

Since a lumped parameter model is considered the engine is divided into three different zones as shown in Fig. 2-9. The first zone represents the cylinder, the second one the coolant fluid, while the third zone models the thermal behaviour of the engine block.

The first zone is characterized by the cylinder wall temperature. Eq. (2.3) calculates this temperature as a function of the heat balance:

$$\frac{dT_w}{dt} = \frac{\dot{Q}_{g,w}^* - \dot{Q}_{w,c}^*}{c_{pw} \cdot m_w} \quad (2.3)$$

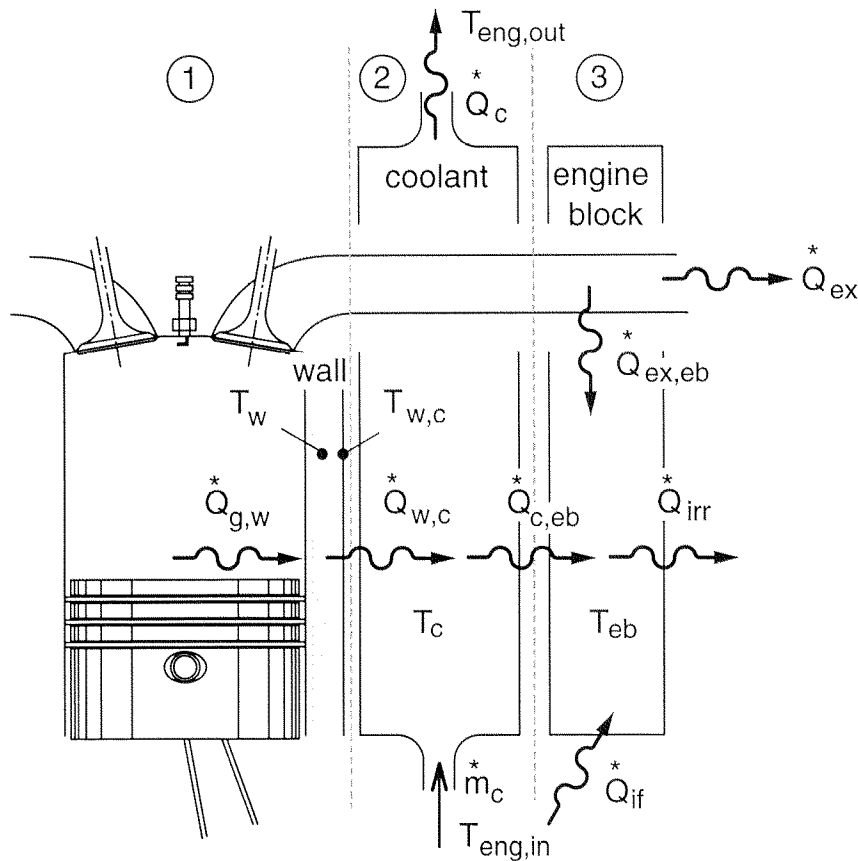


**Figure 2-9:** Temperatures and heat flows at the cylinder

As shown in eq. (2.4), the cycle-averaged heat flow  $\dot{Q}_{g,c}^*$  transferred from the burning gases to the cylinder wall for a particular operating point is predicted using thermodynamics-based cycle calculations ([41], [42]). For these calculations the geometry of the engine has to be known. The results obtained from the cycle calculation in case of *warm* wall temperatures over the whole engine operating region are shown in Fig. 2-10.

$$\dot{Q}_{g,w}^* = f(bmep, n_{ICE}, T_w). \quad (2.4)$$

The heat transfer data from the burning gases to the cylinder wall can be obtained from the cycle calculation only under steady-state operating conditions. Since during an engine cold start the wall temperature increases steadily, the steady-state working conditions for various wall temperatures are calculated, and the current heat flow from the gases to the wall during the warm-up process is interpolated. In Fig. 2-11 the cycle-averaged heat flow

from the gas to the cylinder wall is plotted as a function of the wall temperature and for constant engine operating conditions. For the simulation the cycle-averaged heat flow  $\dot{Q}_{g,w}^*$  is obtained from a three-dimensional map, as represented by eq. (2.4).

In the following calculations the mean coolant temperature:

$$T_{eng,m} = \frac{T_{engin} + T_{eng,out}}{2} \quad (2.5)$$

is considered.

The heat flow from the wall to the coolant is calculated considering the heat transfer due to conduction through the cylinder wall area  $A_w$  in contact with the coolant.

$$\dot{Q}_{w,c}^* = z_c \cdot \alpha_c \cdot A_w \cdot (T_{w,c} - T_{eng,m}) \quad (2.6)$$

The coolant heat transfer coefficient  $\alpha_c$  is calculated as an area-averaged value. Some authors ([40]) propose the definition of a local heat exchanger heat transfer coefficient. Nevertheless in this case the zero-dimensional description of the heat propagation from the cylinder wall to the surrounding coolant is precise enough to describe the thermal behaviour of the system ([42]).

The coolant flow around the cylinder can be described with the help of the Nusselt, Prandtl, and Reynolds numbers ([42], [67], [74]):

$$Nu = \frac{\alpha_c \cdot H}{\lambda} \quad Re = \frac{v \cdot H}{\nu} \quad Pr = \frac{v \cdot c_p \cdot \rho}{\lambda} \quad (2.7)$$

In this way the heat transfer coefficient  $\alpha_c$  can be calculated with reference to the coolant properties (viscosity  $\nu$ , thermal conductivity  $\lambda$ , heat capacity  $c_p$ , density  $\rho$ ), its flow characteristics (velocity  $v$ ) and some engine-geomet-

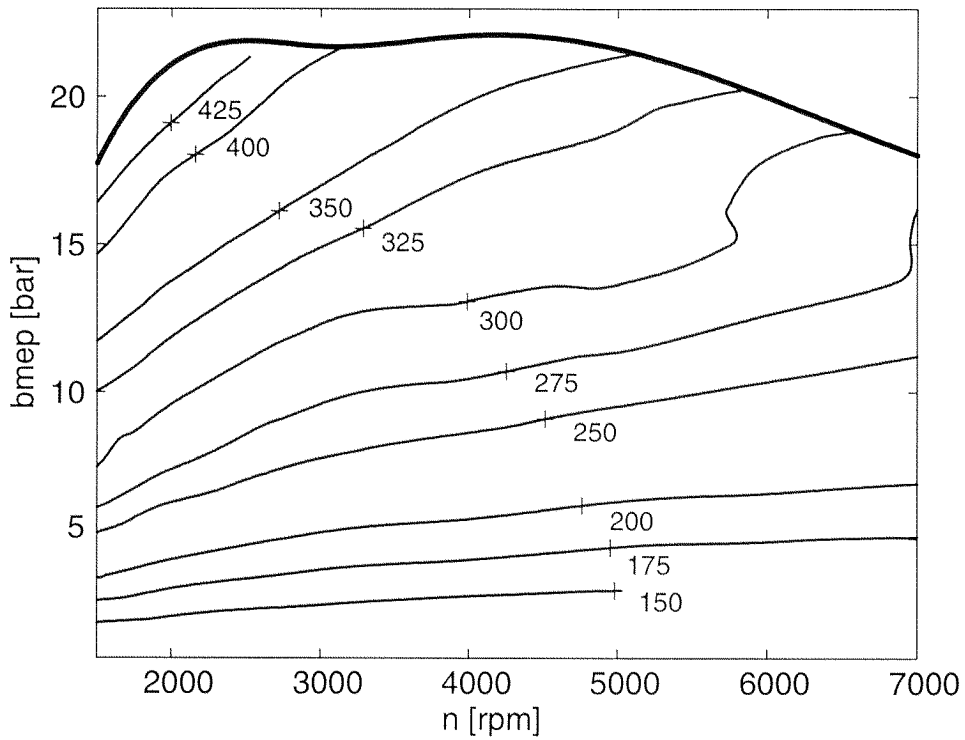


**Figure 2-10:** Cycle-averaged heat flow [J/cycle] from the gas to the wall

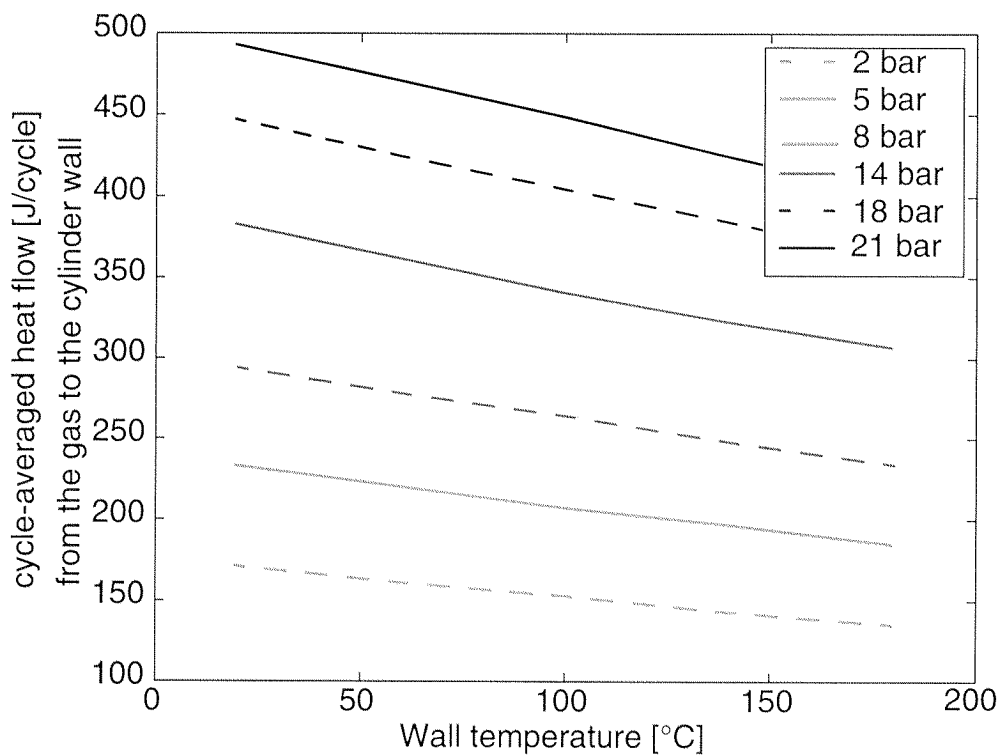


**Figure 2-11:** Heat flow to the wall as a function of wall temperature

rical factors. For the coolant flow both a laminar and a turbulent behaviour are considered:

$$Nu = \left( 0.3 \cdot \sqrt{Nu_{lam}^2 + Nu_{turb}^2} \right) \cdot (1 + (z_c - 1) \cdot f_a) \cdot z_c^{-1}, \quad (2.8)$$

$$Nu_{lam} = 0.664 \cdot \sqrt{Re} \cdot \sqrt[3]{Pr}, \quad (2.9)$$

$$Nu_{turb} = \frac{0.037 \cdot Re^{0.8} \cdot Pr}{1 + 2.443 \cdot Re \cdot (Pr^{2/3} - 1)}, \quad (2.10)$$

where with  $f_a$  a form coefficient is expressed ([42]).

As Fig. 2-9 shows, the wall temperature considered for the calculation of the heat transferred from the cylinder wall to the coolant is the cylinder-external temperature (coolant side). Nevertheless, the wall temperature used for calculations is the average wall temperature  $T_w^*$  (see Fig. 2-9). The conduction heat transferred from the wall to the coolant  $\dot{Q}_{w,c}$  can be also calculated as follows:

$$\dot{Q}_{w,c}^* = \frac{z_c \cdot \lambda_w \cdot A_w}{d/2} \cdot (T_w - T_{w,c}). \quad (2.11)$$

From eq. (2.6) and eq. (2.11) the heat transferred from the wall to the coolant can be calculated on the basis of the difference between the mean wall temperature and the mean coolant temperature:

$$\dot{Q}_{w,c}^* = z_c \cdot \frac{2 \cdot \alpha \cdot \lambda_w \cdot A_w}{2 \cdot \lambda_w + \alpha \cdot d} \cdot (T_w - T_{eng,m}) \quad (2.12)$$

The second zone is characterized by the coolant. The temperature in this zone is assumed to be equal to the temperature of the coolant leaving the engine. The differential equation describing the variation in the coolant temperature leaving the engine is thus:

$$\frac{dT_{eng, out}}{dt} = \frac{\dot{Q}_{w, c}^* - \dot{Q}_{c, eb}^* - \dot{Q}_c^*}{c_{pc} \cdot \dot{m}_c} \quad (2.13)$$

The heat transfer between the coolant and the engine block is described by the following equation:

$$\dot{Q}_{c, eb}^* = z_c \cdot \alpha_c \cdot A_{eb} \cdot (T_{eng, m} - T_{eb}), \quad (2.14)$$

where  $A_{eb}$  indicates the engine block area in contact with the coolant. The enthalpy flow due to the temperature difference over the engine is:

$$\dot{Q}_c^* = c_{pc} \cdot \dot{m}_c \cdot (T_{eng, out} - T_{eng, in}). \quad (2.15)$$

The last differential equation (needed to determine the behaviour of the engine internal cooling system) permits the calculation of the engine block temperature:

$$\frac{dT_{eb}}{dt} = \frac{\dot{Q}_{c, eb}^* + \dot{Q}_{if}^* - \dot{Q}_{irr}^* + \dot{Q}_{ex, eb}^*}{c_{peb} \cdot m_{eb} + c_{poil} \cdot m_{oil}}, \quad (2.16)$$

with engine block temperature  $T_{eb}$  meaning the temperature of the engine block as well as of the oil. Nevertheless in eq. (2.16) the different heat capacities of engine block and oil are considered. The amount of heat transferred from the exhaust gases to the engine block  $\dot{Q}_{ex, eb}^*$  depends on the engine operating point and on the engine block temperature. In the simulations its value is determined by means of cycle calculations.



The value  $\dot{Q}_{if}^*$  represents the heat transferred to the engine block due to internal friction. When warm steady-state operating conditions are considered, for instance when:

$$T_{eng, m0} = \frac{T_{eng, out} + T_{eng, in}}{2} = 90 \text{ }^\circ\text{C} \quad (2.17)$$

$$T_{eb0} = 100 \text{ }^\circ\text{C}$$

the mean pressure due to internal friction can be empirically expressed as ([42], [24]):

$$mp_{if0} = 0.052 + \left( \left( 0.464 + \frac{0.072 \cdot \omega_{ICE}}{2 \cdot \pi} \cdot 2 \cdot H \right) \cdot \Pi_v + 0.0215 \cdot bmep \right) \cdot \sqrt{\frac{0.075}{D}}, \quad (2.18)$$

where  $\Pi_v$  indicates the boost-pressure ratio. The friction work, here defined as the difference between the net indicated power  $\int p dV$  and the brake power delivered to the drive shaft ([41], Ch. 13, [53], [69]), is used for:

1. overcoming the resistance to the relative motion of all the moving parts of the engine (mechanical friction work),
2. driving the engine auxiliaries, including the fan, the water pump, the oil pump, the generator, the power steering pump, and the air conditioner (auxiliaries work).

The work needed for drawing the fresh mixture through the intake system and into the cylinder and to expel the burned gases from the cylinder and out of the exhaust system (pumping work) is not considered here as part of the engine internal friction.

In the configuration examined on the test bench, the oil and the water pumps are the only accessories present of those listed above. However, the water pump is externally driven. For this reason, the friction work due to the acces-

sories can be neglected and the mechanical friction work, which amounts to about half of the global friction as plotted in Figure 1-3 on page 5, is the only component of the friction considered in the following.

When the coolant and the oil temperatures differ from the steady-state value considered, the mean pressure from friction is calculated as ([42]):

$$\begin{aligned} mp_{if} = & mp_{if0} \cdot (1 - 0.006 \cdot (T_{eng,m} - T_{eng,m0}) - \\ & 2.25 \cdot 10^{-6} \cdot (T_{eng,m} - T_{eng,m0})^3 - \\ & 0.006 \cdot T_{eb} - T_{eb0} - 2.25 \cdot 10^{-6} \cdot T_{eb} - T_{eb0}^3 + 1). \end{aligned} \quad (2.19)$$

The heat transferred to the engine block due to internal friction is finally:

$$\dot{Q}_{if}^* = mp_{if} \cdot \frac{V \cdot 10^5}{4 \cdot \pi} \cdot \omega_{ICE}, \quad (2.20)$$

$$\dot{Q}_{if}^* = f\left(\Pi_v, T_{eb}, \frac{T_{eng,out} + T_{eng,in}}{2}, n_{ICE}, bmep\right). \quad (2.21)$$

A similar approach for the calculation of engine internal friction during engine warm-up can be found in [58].

The engine heat losses due to irradiation and convection are considered in the term

$$\dot{Q}_{irr}^* = \sigma \cdot \varepsilon \cdot (T_{eb}^4 - T_{amb}^4) + \lambda \cdot A_{eb,irr} \cdot (T_{eb} - T_{amb}). \quad (2.22)$$

The simulated variations in  $\dot{Q}_{if}^*$  and  $\dot{Q}_{irr}^*$  are considered as disturbances. A flowchart representation of the engine internal cooling system is given in Fig. 2-12.

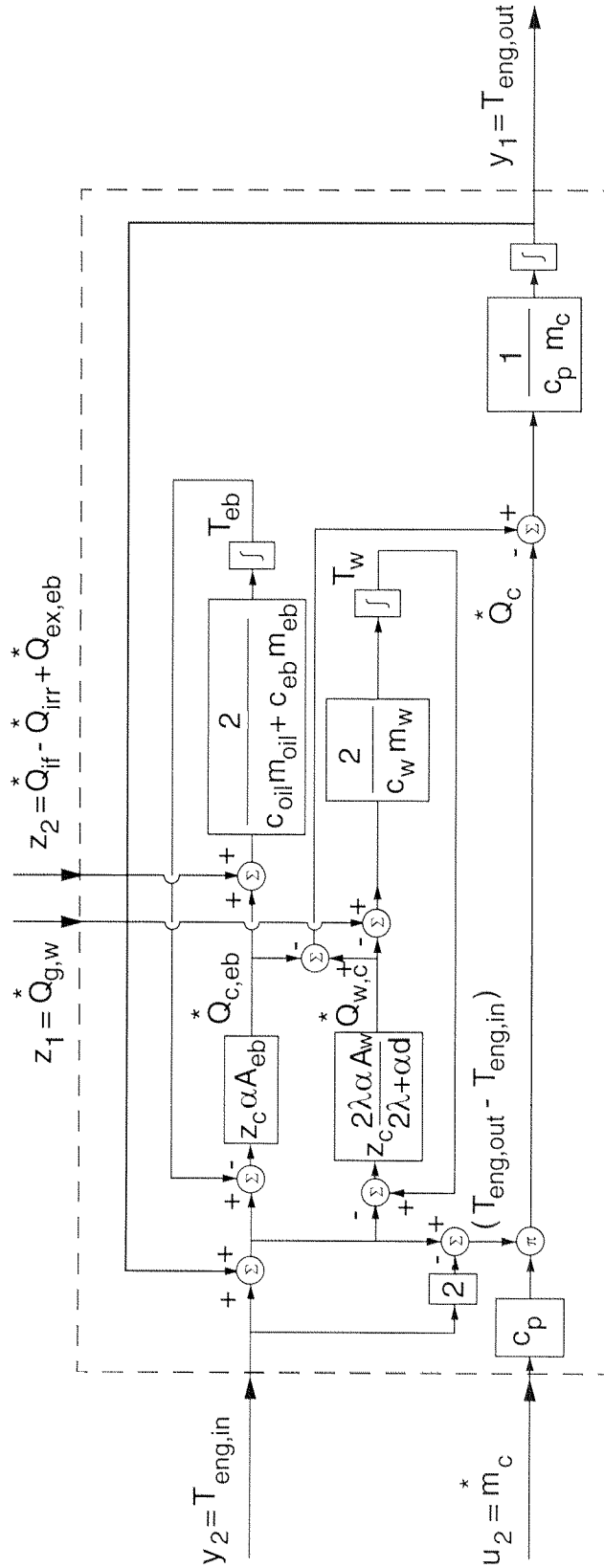


Figure 2-12: Flowchart of the internal cooling system as modeled

### 2.2.2 Engine external cooling circuit

The main components of this part of the cooling circuit are the bypass valve and the heat exchanger.

For each bypass valve construction, a dependence of the flow partitioning between the bypass and the heat exchanger on the valve position is given. Since the total coolant mass flow  $\dot{m}_c^*$  is known, the flow through the bypass

$$\dot{m}_{by}^* = f(\dot{m}_c^*, x_{valve}) \quad (2.23)$$

and through the heat exchanger

$$\dot{m}_r^* = \dot{m}_c^* - \dot{m}_{by}^* \quad (2.24)$$

can be determined.

The various parts of the cooling system are connected by tubes where the coolant flows with different velocities depending on the mass of the pump conveyance. These connections are characterized by varying delays, whose influences on the behaviour of the system cannot be neglected.

The size of the delays in the various parts of the system can be determined assuming plug flow conditions on the basis of the known volume of interest and the fluid mass flow through the section under consideration:

$$\tau = \frac{V}{\dot{m}^*}. \quad (2.25)$$

The coolant flows in hard hosepipes that connect the different components of the cooling circuit. The heat loss in the tubes is neglected since it only amounts to ca. 1% of the heat globally removed by the coolant.

A simplified model for the heat exchanger is proposed. More complex models are discussed in [4], [8], [18], and [59]. The differential equation used to describe the temperature variation in the heat exchanger is

$$\frac{dT_r}{dt} = \frac{\dot{Q}_{r,in}^* - \dot{Q}_{r,out}^*}{c_{pc} \cdot \dot{m}_r}, \quad (2.26)$$

where the additional heat flow to the heat exchanger is

$$\dot{Q}_{r,in}^* = (T_{r,in} - T_{r,out}) \cdot c_{pc} \cdot \dot{m}_r. \quad (2.27)$$

The temperature of the coolant entering the heat exchanger  $T_{r,in}$  can be calculated as a function of the temperature of the coolant leaving the engine and taking into account the mass flow through the various tubes:

$$T_{r,in}(t) = T_{eng,out}(t - \tau_1(\dot{m}_c^*) - \tau_2(\dot{m}_r^*)).$$

The heat transferred from the heat exchanger to the environment is calculated considering the heat transfer due to conduction through the tube walls and due to convection on the coolant and on the air side. Therefore, assuming a mean temperature difference between the coolant and the air, we obtain:

$$\dot{Q}_{r,out}^* = \alpha_r \cdot A_r \cdot \left( \frac{T_{r,in} + T_{r,out}}{2} - T_{amb} \right). \quad (2.28)$$

A more detailed definition of the heat transfer coefficient  $\alpha_r$  can be found in ([8]).

The heat exchanger is modelled as a lumped system. Thus:

$$T_{r,out} = T_r. \quad (2.29)$$

In conventional automotive applications the heat removal from the engine is realized by means of coolant-to-air heat exchangers. However, for the tests performed on the test bench for this thesis research, a coolant-to-water heat exchanger is used. The quantity of water that flows to the heat exchanger simulates the air ramming the heat exchanger and is controlled by a valve. The circuit cooling the heat exchanger is referred to as secondary cooling circuit while the secondary valve is the valve controlling its water flow. This valve can be operated either with a constant opening (which implies a constant water flow to the heat exchanger) or it can be controlled as a function of the temperature of the coolant leaving the engine. Because of the large diameters of the secondary cooling circuit tubes connected to the heat exchanger and of the low cooling water temperature (15 °C) even small openings of the thermostat (or of the bypass valve) cause a significant decrease in the coolant temperature entering the engine.

The coolants from the bypass and from the heat exchanger mix before entering the engine. Since it is assumed that no heat dissipation takes place in the tube connecting the mixing point and the engine, we obtain the following values:

$$T_{mix}(t) = T_{eng, out}(t - \tau_1 - \tau_4) \cdot \frac{m_{by}^*}{m_c^*} + T_{r, out}(t - \tau_3) \cdot \frac{m_r^*}{m_c^*} \quad (2.30)$$

$$T_{eng, in}(t + \tau_5) = T_{mix}(t) \quad (2.31)$$

where

$$\begin{aligned}
 \tau_1 &= f(m_c^*) = \frac{V_{1-2}}{m_c^*} \\
 \tau_3 &= f(m_r^*) = \frac{V_{3-5}}{m_r^*} \\
 \tau_4 &= f(m_{by}^*) = \frac{V_{3-4}}{m_{by}^*} \\
 \tau_5 &= f(m_c^*) = \frac{V_{4-6}}{m_c^*}
 \end{aligned} \tag{2.32}$$

The meaning of each of the volumes  $V_{i-j}$  is explained in Fig. 2-2. The numerical values of the volumes relative to the different segments of the tubes can be found in Appendix A.

Fig. 2-13 shows a flowchart representation of the model of the engine external cooling circuit and of the delays that characterize it.

### 2.2.3 Parameters used for modeling

The general validity of a model is guaranteed when the parameters used for the modelling of a precise configuration can be used for different system configurations. In the case considered here, the system has been validated for a defined engine operating point. Successive validations for other engine operating points confirmed the validity of the model, since no adjustment of the parameters was needed.

In order to successfully model the cooling system of a defined engine some data are needed on the geometry of the engine and on the thermal properties of the different materials involved (coolant, oil, aluminium, etc.). In the following, an overview is given of the parameters used.

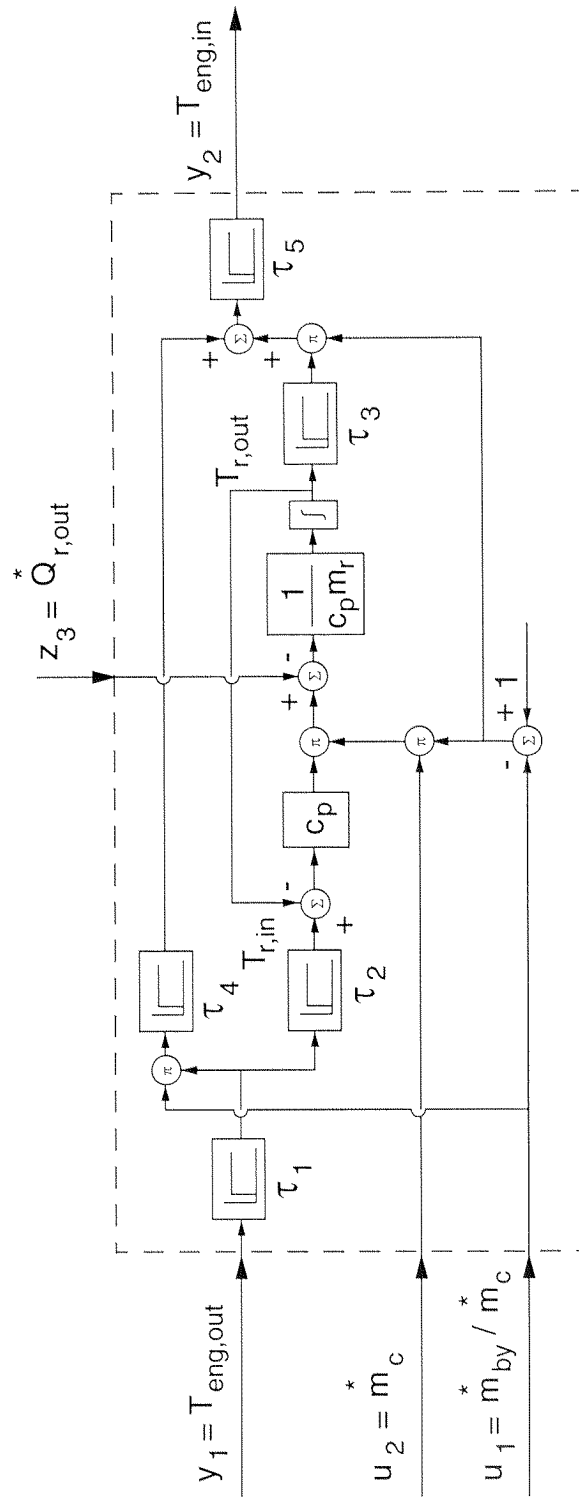


Figure 2-13: Flowchart of the engine external cooling circuit as modeled



The parameters relative to the geometry of the engine that are known or that can be easily measured are summarized in Table 2-1. A few of the parameters,

**Table 2-1:** Known or easily measurable engine parameters

Stroke	$H$	0.054	[m]
Cylinder internal diameter	$D_{in}$	0.065	[m]
Number of cylinders	$z_c$	2	[-]
Cylinder wall thickness	$d$	0.009	[m]
Thickness of coolant channels surrounding the cylinder	$d_{cool}$	0.01	[m]
Cylinder wall surface in contact with the coolant	$A_w$	0.0125	[m <sup>2</sup> ]
Engine block mass	$m_{eb}$	35	[kg]
Oil mass	$m_{oil}$	4.2	[kg]

e. g., the surface of the engine block in contact with the coolant, cannot be measured but could only be calculated with elaborate methods. As an alternative the values of these parameters were estimated. For this purpose measurements and simulations of engine cold-start procedures for a defined operating point were compared. Considering the cold-start procedure has the advantage that the greatest variations in engine thermal conditions are represented and that therefore the influence of the various parameters is emphasized. In order to estimate the values of the parameters listed in Table 2-2 the optimization procedure described below was realized with the aim of minimizing the following cost function:

$$G = \min \left( (T_{eng, out_{MEAS}}^{(i)} - T_{eng, out_{SIM}}^{(i)})^2 \right), \forall i [0..10 \text{ min}]. \quad (2.33)$$

**Table 2-2:** Parameters estimated comparing measurements and simulations.

Engine block surface in contact with the coolant	$A_{eb}$	0.0159	[m <sup>2</sup> ]
Engine block surface in contact with the exhaust gases	$A_{ex, eb}$	0.006	[m <sup>2</sup> ]
Coolant mass in the engine block	$m_c$	0.7	[kg]
Heat transfer coefficient for irradiation	$\alpha_{eb, irr}$	40	[Wm <sup>-2</sup> K <sup>-1</sup> ]
Heat transfer coefficient for the exhaust gases	$\alpha_{ex, eb}$	250	[Wm <sup>-2</sup> K <sup>-1</sup> ]

The estimated values of the parameters obtained from the minimization of the function in eq. (2.33) are listed in Table 2-2. Clearly, these parameters do have a physical significance, which further confirms their plausibility. With the values of the estimated parameters listed in Table 2-2 the maximal relative error for the operating point considered between the measured and the simulated temperatures of the coolant leaving the engine amounts to 3%. Moreover, the same maximum error results when other engine operating points are considered as well as for the temperature of the coolant entering the engine.

The parameters that refer to the thermal properties of the different components (aluminium for the engine block, coolant and oil) such as specific heat, thermal conductivity, and specific density, can be found in [22].

Fig. 2-14 shows plots of the results obtained from measurements as well as from simulation for the temperature of the coolant leaving the engine.

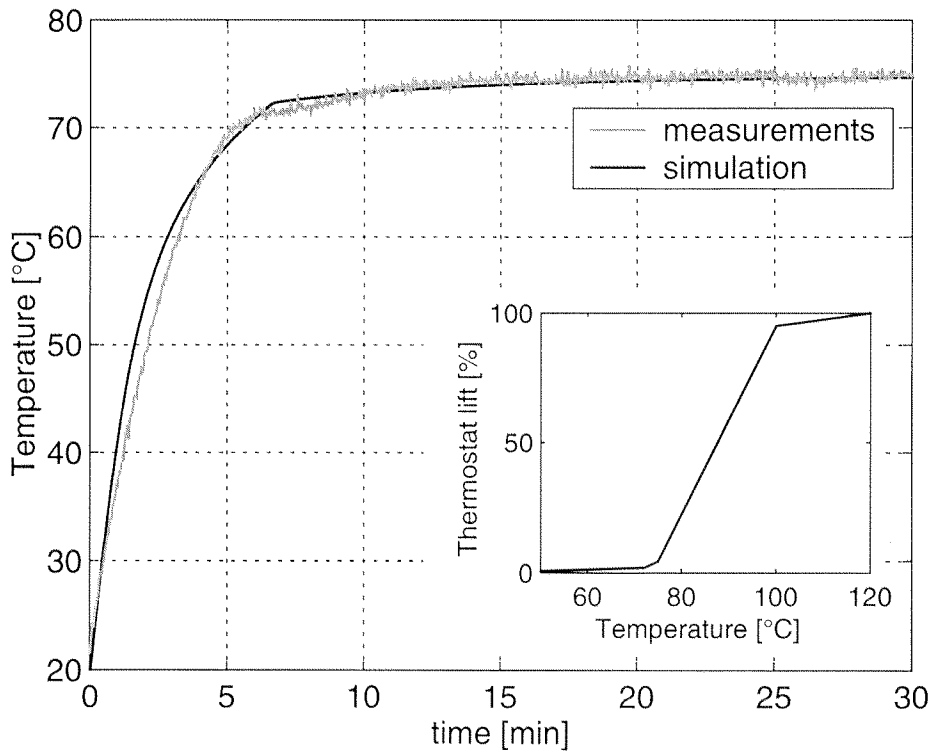


**Figure 2-14:** Temperature of coolant exiting the engine at cold start

## 2.3 Model validation

The model was first validated for the conventional configuration of the cooling circuit. For this purpose, experiments have been conducted on the engine specified in Chapter 2. The following setup was chosen for the measurements and the simulation:

- Constant engine operating point ( $n_{ICE} = 2500$  [rpm] and  $p_{me} = 2$  [bar]).
- Electrical cooling pump operated such as to obtain a constant mass flow. The coolant mass flow is the same as measured in the case of the conventional water pump configuration (water pump mechanically coupled with the engine shaft) for the chosen engine operating point. The coolant flow rate for this particular operating point is, as shown in Fig. 2-2:  $m_c = 0.266$  [l/s].

- Conventional thermostat. The opening characteristics of the conventional thermostat are a function of the coolant temperature. For the experimentally used thermostat the lift characteristic is given in the small frame in Fig. 2-14. This lift characteristic has been implemented in the simulation as well.
- Since on the test bench the heat exchanger is water-cooled,  $T_r$  remains almost constant at  $T_r = 25$  [°C].

The results obtained from the simulation and from the measurement under these operating conditions in the case of an engine cold start are plotted in Fig. 2-14.

The dynamic behaviour of the system has been validated with the help of step responses as well. The position of the bypass valve was used as input. For simulations and measurements both the resulting values of the temperature of the coolant leaving the engine are shown in Fig. 2-15 and in Fig. 2-16. The behaviour of the system in case of a reduction or an increase of the coolant mass flow through the heat exchanger is shown in Fig. 2-15 and Fig. 2-16 respectively.

## 2.4 Conclusion

In this chapter a model of the cooling system has been developed based on physical characteristics of the system and on information from the literature. The model developed has been successfully validated on the test bench and can therefore be used for the design of a model-based controller for the bypass valve opening position and the cooling pump mass flow.

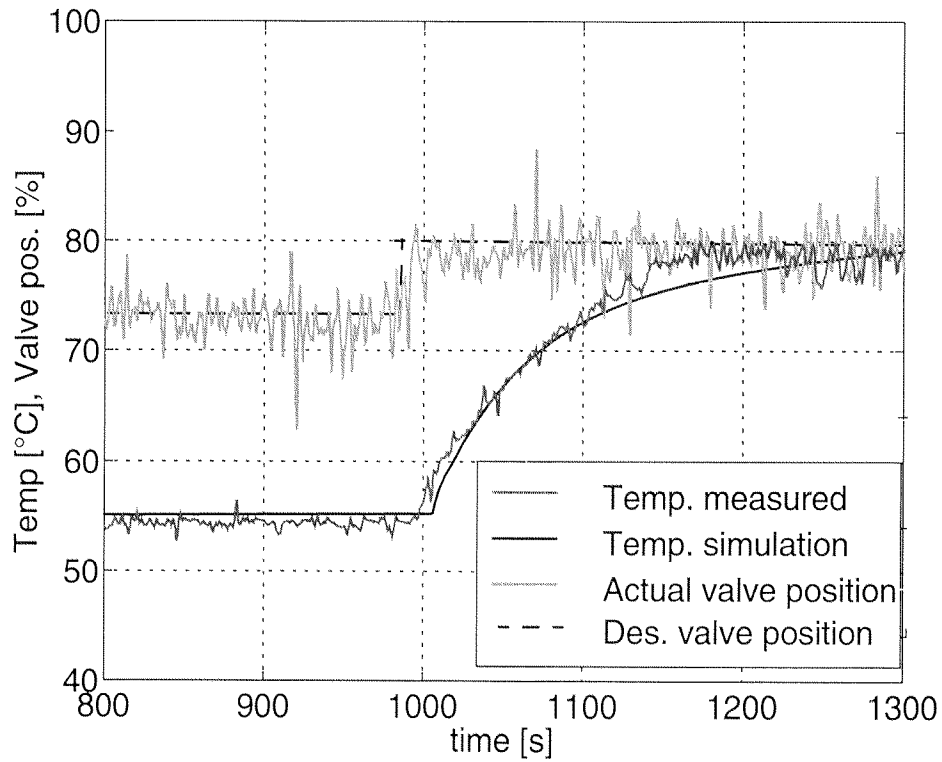


**Figure 2-15:** Temperature step responses when the valve position is excited

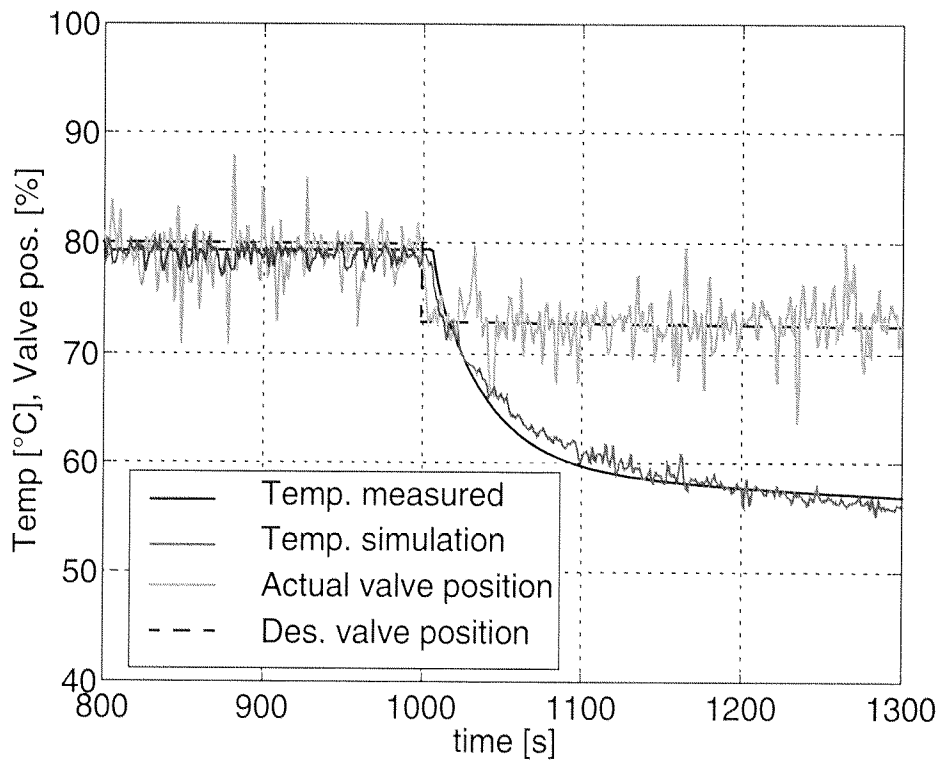


**Figure 2-16:** Temperature step responses when the valve position is excited

## CHAPTER 3

### CONTROLLER DESIGN

The thermal behaviour of an engine is strongly determined by the partitioning of the flow between the heat exchanger and the bypass as well as by the flow of the coolant mass pumped through the system. These two values have already been defined in Chapter 2 as inputs  $u_1$  and  $u_2$  of the model describing the thermal behaviour of the engine. In the conventional realization of the cooling system

$$\dot{u}_1 = \frac{1}{T} \cdot u_1 - \frac{1}{T} \cdot f_1(T_{eng, out}), \quad (3.1)$$

where  $u_1 = \dot{m}_{by}^* / \dot{m}_c^*$  and

$$u_2 = \dot{m}_c^* = f_2(n_{ICE}) \quad (3.2)$$

since the opening characteristic of the expansion-element thermostat only depends on the temperature of the coolant leaving the engine and the cooling pump is belt driven by the IC engine.

Choosing an electrical cooling pump and an electrically controlled bypass valve allows the inputs to be controlled individually and thus opens new possibilities in controlling the engine thermal behaviour. In this chapter the desired control specifications are defined, then a model-based feedforward controller as well as a feedback controller are designed and tested in simulations and on

the test bench. The results obtained on an engine test bench when the improved configuration of the cooling circuit is applied are presented in Chapter 5.

### 3.1 Control specifications

The main objectives of an improved engine thermal behaviour are a better energy management and, as a consequence, a reduction of the fuel consumption. The new configuration of the engine cooling circuit proposed should therefore satisfy the following demands:

1. Minimize the energy demand of the cooling pump.
2. Reduce the duration of an engine cold start by rapidly bringing the engine to the desired thermal conditions.
3. Optimize the thermal behaviour of the engine by maintaining a high engine temperature even during part-load operating conditions.

The control objectives of the proposed cooling system and the respective possibilities for controlled actuators are summarized in Table 3-1. Besides the controlled actuators considered others are possible, e.g. the cooling fan or an additional air shutter on the radiator to modify the heat transfer coefficient in the radiator ([47]). Those devices are not considered in the present analysis.

### 3.2 Definition of the minimal coolant mass flow

As described in the modelling of the internal cooling circuit in Chapter 2, the amount of heat to be removed from the engine by the coolant results from the balance of the various heat flows that characterize the internal combustion process. Furthermore (cf. eq. (2.15)), assuming that the heat  $Q_c^*$  to be removed from the engine by the coolant remains constant, there is an inverse proportionality between the coolant mass flow through the engine  $\dot{m}_c^*$  and the temperature difference  $\Delta T_{eng}$  between the coolant entering and leaving the engine (here defined as the coolant temperature difference over the engine)

$$\Delta T_{eng} = T_{eng, out} - T_{eng, in} \quad (3.3)$$

**Table 3-1:** Control objectives for the improved engine thermomanagement

Control objectives	Contribution to development goal	Actuator control
Minimum power requirement for the cooling system	Fuel consumption reduction	Adjustment of pump speed
Minimize the cold start phases	Fuel consumption and emission reduction Maximum comfort and driving safety	Valve position for maximal radiator bypass
Modification of steady-state engine thermal conditions at part-load operating conditions	Fuel consumption reduction Maximum comfort and driving safety	Adjustment of pump speed Control of valve position for radiator bypass
Maximum cooling power in critical thermal conditions	Protection of the engine components	Maximal pump speed Valve position for minimal or no radiator bypass

The engine considered in this thesis has been measured on the test bench in its whole operating range with a conventional configuration of the cooling system and under steady-state operating conditions. The resulting coolant temperature difference over the engine is plotted in Fig. 3-1. The relationship between the coolant mass flow and the engine speed is given in the plot in Figure 2-2 on page 19 and is summarized in Table 3-2 for some representative engine speeds. Since the coolant flow remains constant for a given engine speed, the coolant temperature over the engine increases proportionally with the load. The resulting flow of the heat removed from the engine by the coolant is plotted in Figure 1-6 on page 10.



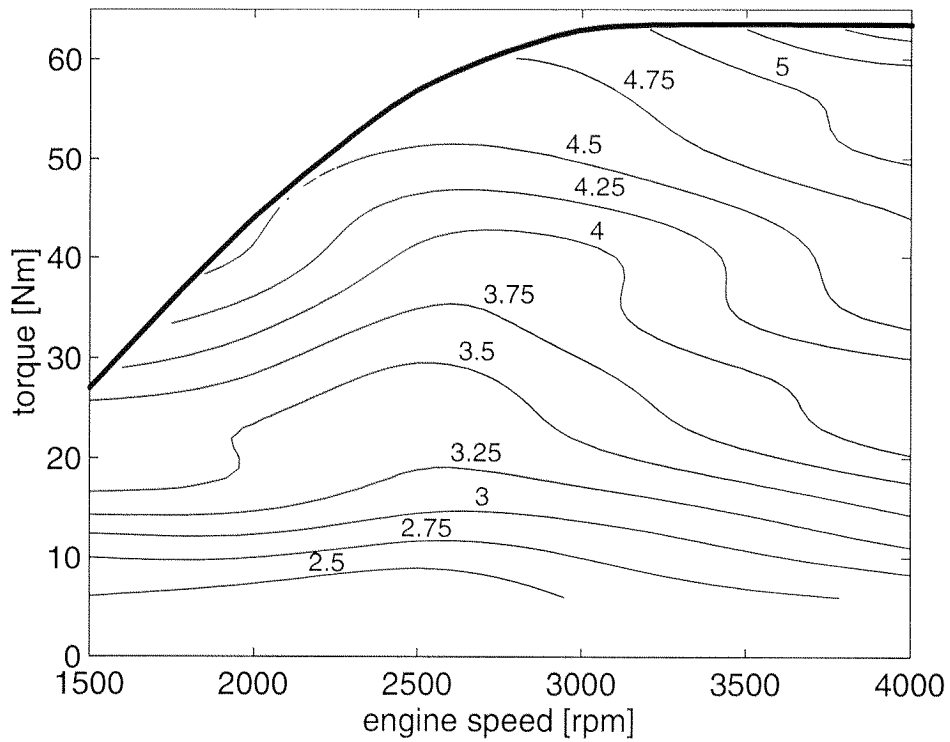


**Figure 3-1:**  $\Delta T_{eng}$  for the conventional cooling system ( $^{\circ}\text{C}$ )

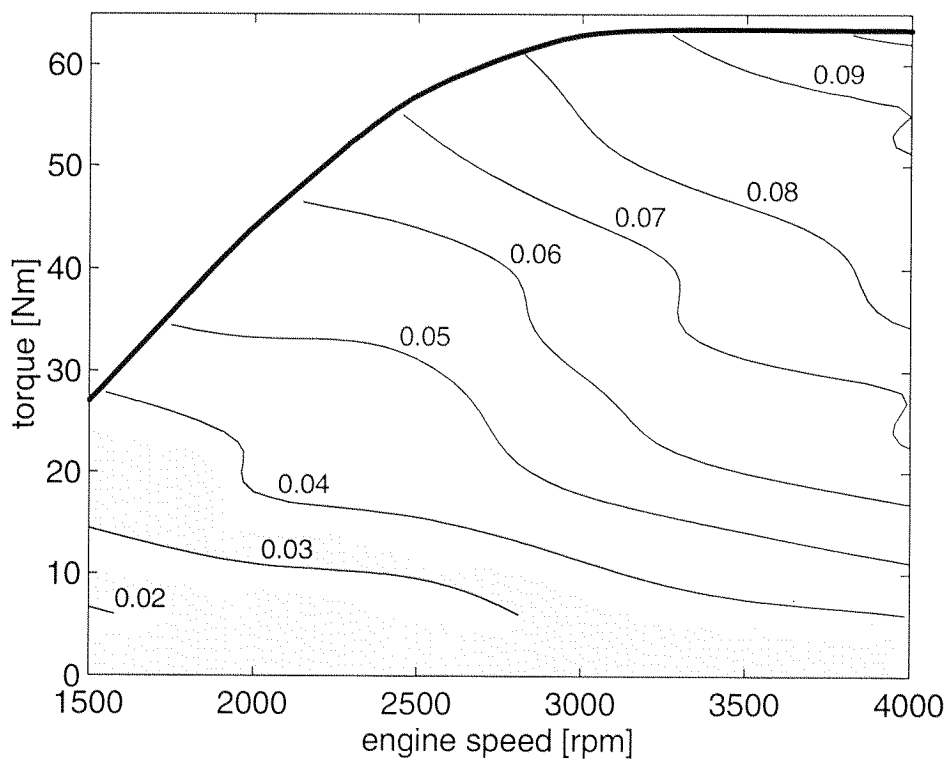


**Figure 3-2:** Minimal coolant flow for  $T_{eng,out} - T_{eng,in} = 15^{\circ}\text{C}$ , [l/s]

**Table 3-2:** Coolant mass flow in the conventional cooling system

Engine speed [rpm]	Coolant mass flow [l/s]
1500	0.19
2000	0.24
2500	0.29
3000	0.33

In order to reduce the power requirement for the cooling pump, the coolant mass flow should be reduced to a minimum. A possible approach is to define a constant coolant temperature difference over the engine, such that no local fatigue and no thermal stress occurs. According to [54] this value can be set to 15 °C. Since the heat to be removed from the engine in order to maintain steady-state operating conditions only depends on the operating point of the engine, the minimum mass flow can be calculated as a function of the defined coolant temperature difference over the engine and the measured coolant heat flow as plotted in Figure 1-6 on page 10. The resulting minimum coolant mass flow is shown in Fig. 3-2. Due to hardware limitations imposed on the measurements of the power absorbed by the electrically driven cooling pump, the minimum flow rate measurable amounts to 0.04 l/s. Therefore this value has been assumed for all the engine operating points included in the filled area in Fig. 3-2.

### 3.3 Model linearization

The input  $u_1$ , which represents the valve position and thus the flow partitioning between the heat exchanger and its bypass, is defined such that under steady-state conditions the desired coolant temperature at engine output is obtained. The linearisation has been performed at various steady-state engine operating conditions, e.g., for  $T_{eng, out} = 90, 70, 50$  °C .

The results of the linearisation are shown in Fig. 3-3, where the system responses to a cold start for the nonlinear system and for the system linearised for 70 °C are plotted. The position of the bypass valve remains constant.

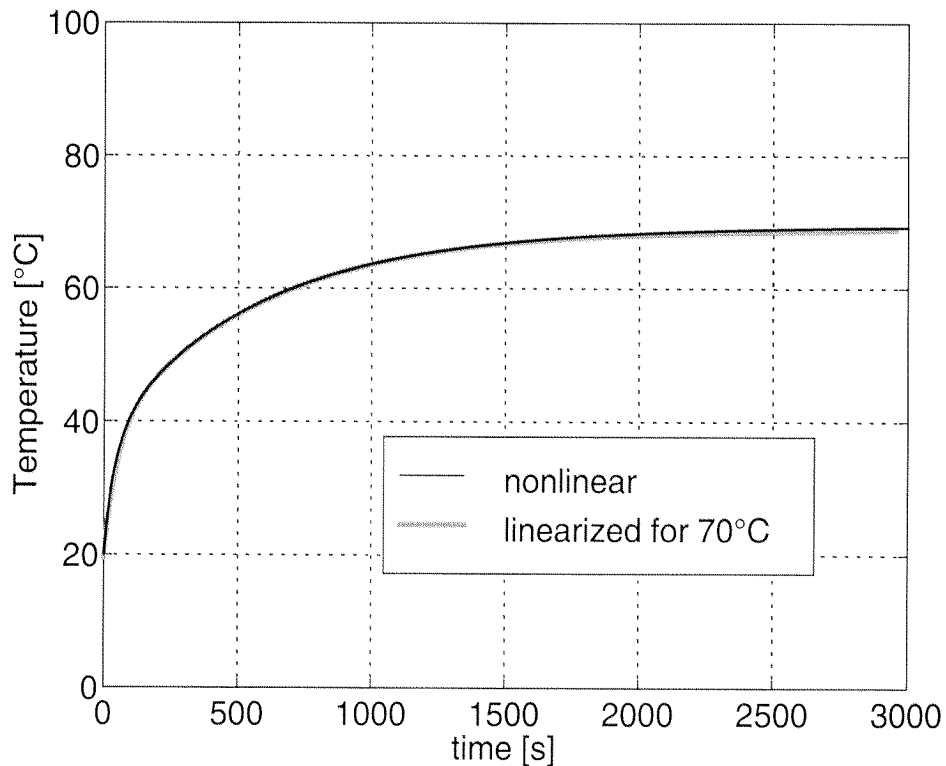


**Figure 3-3:** Coolant temperatures of nonlinear and linearized models

The behaviour of the system linearised for the steady-state temperature (70 °C) quite well approximates the behaviour of the nonlinear system. The influence of the delays is not relevant since the inputs remain constant.

### 3.4 Feedforward controller

Based on the model of the engine thermal behaviour presented in Chapter 2, a feedforward controller for the actuation of the bypass valve has been developed ([34]). Due to time delays and heavy nonlinearities a feedback-only structure cannot meet the desired performance criteria, i. e. minimal overshoot of the temperature at cold start and stable, non-oscillating behaviour in steady state at low loads. A feedforward controller is therefore additionally needed.

During cold start the controller should ensure that the desired temperature level, here  $T_{eng, out, DES} = 90 \text{ }^\circ\text{C}$ , is reached as soon as possible and is then maintained constant.

The structure of the feedforward controller is described in the following sections.

### 3.4.1 Reduction to a SIMO system

The system object of study can be modelled with a Multiple Input, Multiple Output (MIMO) structure. Nevertheless, under the particular operating conditions that characterize the warm-up phase, it is possible to reduce the system to a SIMO (Single Input, Multiple Output) structure. Indeed, in order to reach the desired engine operating temperature as quickly as possible, only the minimal coolant flow for the particular engine operating point considered is needed, as defined in the previous section. In this particular case this means that:

$$u_2 = \dot{m}_{c, min}^* = \text{constant}, \quad (3.4)$$

and the system assumes a SIMO structure.

In addition, the temperature  $T_{r, out}$  of the coolant leaving the radiator is assumed to be constant and equal to the ambient temperature. Indeed, in this case a situation is simulated in which the vehicle powered by the engine considered drives at low constant speed and at very low loads. For these particular operating points of the engine the radiator is over-dimensioned, since it is designed to guarantee a sufficient heat removal at high loads ([4], [8]). Since the temperature  $T_{r, out}$  is assumed to be constant, it is possible to reduce the order of model relative to the engine thermal behaviour from four to three.

These operating conditions are reproduced on the test bench. The new configuration of the model is given in Fig. 3-4.

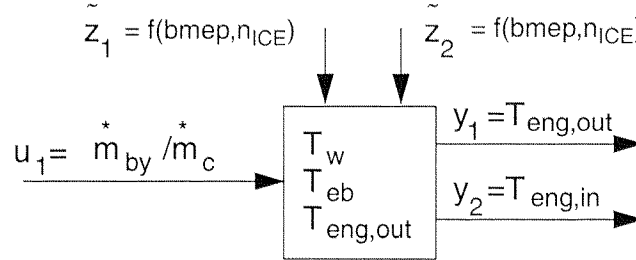


**Figure 3-4:** Simplified model of the cooling circuit

It has to be pointed out that the disturbances  $\tilde{z}_1$  and  $\tilde{z}_2$  exclusively depend on the engine operating point. As plotted in Figure 2-8 on page 26, three different disturbances act on the system. The first one concerns the in-cylinder process. The heat flow from the combustion gas to the cylinder wall  $Q_{g,w}^*$  depends on the engine operating point and therefore acts as a disturbance on the system:

$$z_1 = Q_{g,w}^*(\text{bmep}, n_{ICE}) = \tilde{z}_1(\text{bmep}, n_{ICE}). \quad (3.5)$$

When the engine block thermal behaviour is considered, the heat developed by internal friction  $Q_{if}^*$ , the heat dissipated by irradiation  $Q_{irr}^*$ , as well as the heat  $Q_{ex,eb}^*$  transferred from the exhaust gases to the engine block are a function of the engine operating point as well as of the engine block temperature and of the coolant mean temperature:

$$T_{eng,m} = \frac{T_{eng,in} + T_{eng,out}}{2}.$$

Therefore:

$$\begin{aligned} z_2 = (Q_{if}^* - Q_{irr}^* + Q_{ex,eb}^*) &= \tilde{z}_2(T_{ICE}, n_{ICE}) + f_1(T_{eb}) \\ &+ f_2(T_{eng,m}) \cong \tilde{z}_2(T_{ICE}, n_{ICE}) + f_1(T_{eb}) + f_2(T_{eng,in}), \end{aligned} \quad (3.6)$$

where the coolant mean temperature is approximated by the temperature of the coolant entering the engine.

The third disturbance acting on the system is the heat  $\dot{Q}_{r, out}^*$  removed from the coolant in the heat exchanger:

$$z_3 = \dot{Q}_{r, out}^*(T_{r, in}, T_{r, out}). \quad (3.7)$$

In the particular case considered here this term is no longer relevant since the temperature of the coolant leaving the heat exchanger  $T_{r, out}$  is assumed to be constant.

Based on the equations (2.3) to (2.16) presented in Section 2.2.1, the internal cooling circuit can be described by the following equations:

$$\begin{aligned} \frac{dT_{eng, out}}{dt} &= \frac{\dot{Q}_{w, c}^* - \dot{Q}_{c, eb}^* - \dot{Q}_c^*}{c_{pc} \cdot m_c} = \\ & \frac{1}{c_{pc} \cdot m_c} \cdot [a_1 \cdot (T_w - T_{eng, m}) - a_2 \cdot (T_{eng, m} - T_{eb}) \\ & - a_3 \cdot (T_{eng, out} - T_{eng, in})] \end{aligned} \quad (3.8)$$

$$\begin{aligned} \frac{dT_w}{dt} &= \frac{\dot{Q}_{g, w}^* - \dot{Q}_{w, c}^*}{c_{pw} \cdot m_w} = \\ & \frac{1}{c_{pw} \cdot m_w} \cdot \left[ \tilde{z}_1(T_{ICE}, n_{ICE}) - a_1 \cdot (T_w - T_{eng, m}) \right] \end{aligned} \quad (3.9)$$

$$\begin{aligned} \frac{dT_{eb}}{dt} = & \frac{\dot{Q}_{c,eb}^* + \dot{Q}_{if}^* - \dot{Q}_{irr}^* + \dot{Q}_{ex,eb}^*}{c_{peb} \cdot m_{eb} + c_{poil} \cdot m_{oil}} = \\ & \frac{1}{c_{peb} \cdot m_{eb} + c_{poil} \cdot m_{oil}} \cdot \left[ a_2 \cdot (T_{eng,m} - T_{eb}) \right. \\ & \left. + \tilde{z}_2(bpme, n_{ICE}) + f_1(T_{eb}) + f_2(T_{eng,in}) \right]. \end{aligned} \quad (3.10)$$

A definition of the coefficients used in eqs. (3.8), (3.9) and (3.10) is given in Appendix B.

The modelling of the external cooling circuit is simplified by the assumption that the temperature of the coolant leaving the radiator remains constant. The temperature of the coolant entering the engine can therefore be derived from equations (2.30) and (2.31) as:

$$T_{eng,in}(t + \tau_5) = T_{eng,out}(t - \tau_1 - \tau_4) \cdot \frac{m_{by}^*}{m_c^*} + T_{r,out} \cdot \frac{m_r^*}{m_c^*}, \quad (3.11)$$

$$\begin{aligned} T_{eng,in}(t) = & T_{eng,out}(t - \tau_1 - \tau_4 - \tau_5) \cdot u_1(t - \tau_5) \\ & + T_{r,out} \cdot (1 - u_1(t - \tau_5)) \end{aligned} \quad (3.12)$$

A flowchart of the cooling system described above is shown in Fig. 3-5.

### 3.4.2 Approximation of the delays

The delays that characterize the external cooling circuit of the engine are not constant, as they depend on the current mass flow through the corresponding section of tube. During engine warm-up the pump mass flow is assumed to be constant. Under these conditions the delays  $\tau_1$  and  $\tau_5$  relative to the section where all the coolant flows, like for example the lengths of pipe used for the

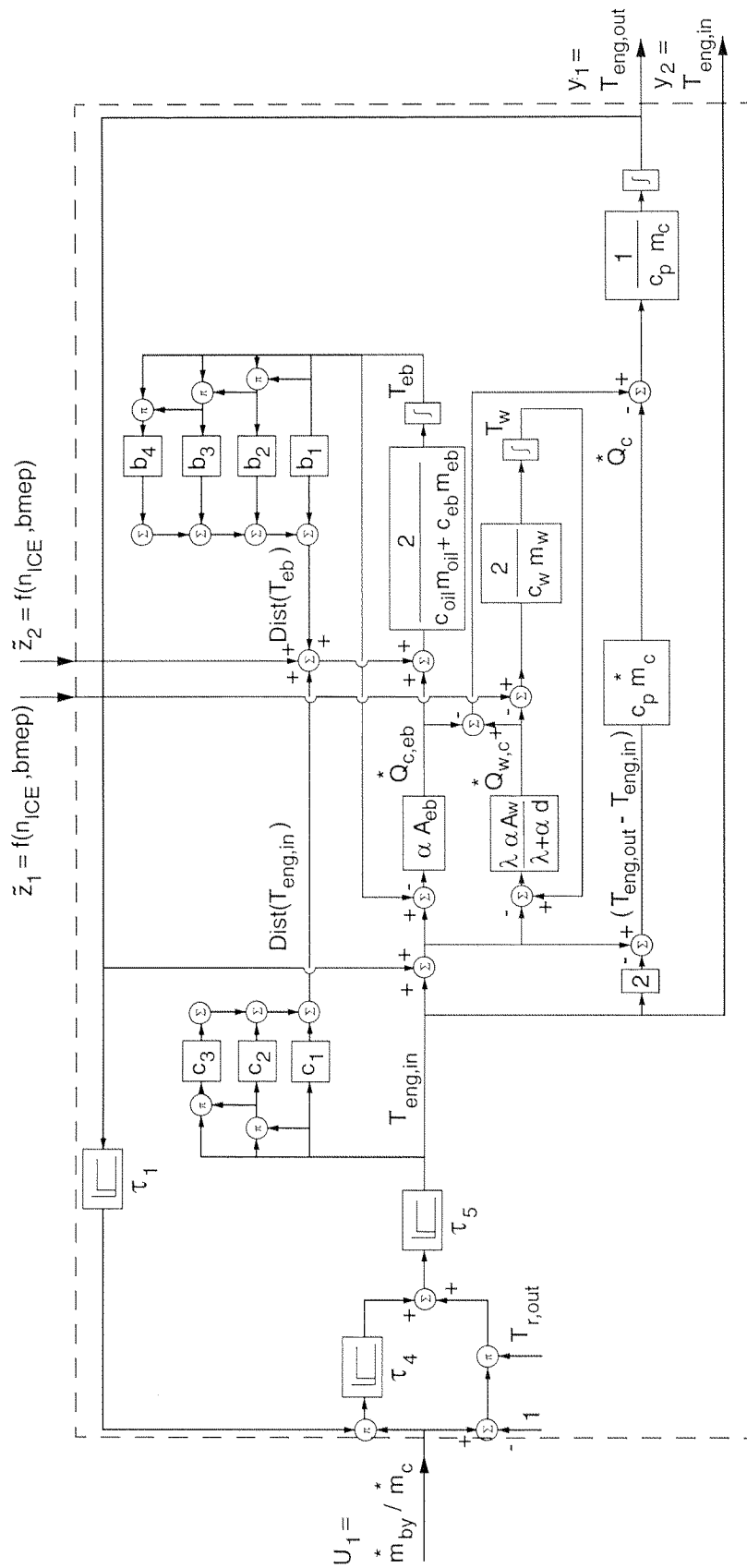


Figure 3-5: Flowchart of the model used for the design of the feedforward controller



coolant entering and leaving the engine, are constant since they only depend on the global coolant mass flow and not on the actual flow partitioning over the bypass duct.

The delay  $\tau_3$  defined to occur in the section of tube from the radiator output to the point where the coolant from the bypass duct and the coolant from the radiator mix is unimportant since the temperature of the coolant leaving the heat exchanger is assumed to be constant.

The only assumption to be met concerns the delay in the temperature of the coolant flowing through the bypass tube. The delay  $\tau_4 = f(\dot{m}_{by}^*)$  is in fact proportional to the value of the input  $u_1$  representing the mass flow partitioning over the bypass duct. It is assumed that this delay also remains constant and is:

$$\tau_4 = f(\dot{m}_{by}^*) \cong f(\dot{m}_c^*) = \text{constant}. \quad (3.13)$$

This assumption holds for the engine operating points studied at almost fully open bypass valve.

### 3.4.3 Controller design

Based on eq. (3.8), the temperature of the coolant entering the engine  $T_{eng, in}$  can be expressed as a function of the three state variables of the model and of the derivative of the coolant temperature  $T_{eng, out}$ :

$$T_{eng, in} = f\left(T_{eng, out}, \frac{dT_{eng, out}}{dt}, T_w, T_{eb}\right) \quad (3.14)$$

When the temperature of the coolant leaving the engine first reaches the desired temperature, the following behaviour is chosen:

$$T_{eng, out} = T_{eng, out, DES}, \quad (3.15)$$

$$\frac{dT_{eng, out}}{dt} = 0. \quad (3.16)$$

In order to obtain this behaviour the demanded value for the temperature  $T_{eng, in, DES}$  of the coolant entering the engine can be calculated as:

$$T_{eng, in, DES} = f(T_{eng, out, DES}, \hat{T}_w, \hat{T}_{eb}) \quad (3.17)$$

where the temperature of the cylinder wall  $\hat{T}_w$  and the temperature of the engine block  $\hat{T}_{eb}$  are not measurable and thus must be estimated (see Section 3.4.4). Therefore the desired temperature of the coolant entering the engine  $T_{eng, in, DES}$  also depends on the temperature of the cylinder wall and of the engine block. Indeed, the coolant temperature difference over the engine is lower during engine warm-up than at steady-state operating conditions. In this particular case, part of the heat is used for raising the temperature of the engine block and of the cylinder wall. Under the assumptions that:

$$\begin{aligned} u_2 &= m_{c, min}^* = \text{constant} \\ T_{r, out} &= \text{constant} \\ \tau_1, \tau_4, \tau_5 &= \text{constant} \end{aligned} \quad (3.18)$$

it is possible to calculate the flow partitioning between the bypass and the heat exchanger  $u_1$  needed to maintain the temperature  $T_{eng, out}$  of the coolant leaving the engine at the desired value as follows:

$$u_1(t) \cong u_1(t - \tau_5) = \frac{m_{by}^*}{m_c^*} = \frac{T_{eng, in, DES}(T_{eng, out, DES}, \hat{T}_w, \hat{T}_{eb}) + T_{r, out}}{T_{eng, out}(t - \tau_1 - \tau_4 - \tau_5) + T_{r, out}} \quad (3.19)$$

As eq. (3.19) shows, the flow partitioning over the bypass at the instant  $t$  is approximated to the value of the same variable at the instant  $(t - \tau_5)$ . Indeed, in order to calculate the value of  $u_1(t)$ , a predictor for the corresponding temperature of the coolant entering the engine  $T_{eng,in}(t + \tau_5)$  would be needed. However, the approximation made here allows to obtain a satisfying system response, as shown in Sections 3.4.5 and 3.4.6.

Since the delay  $\tau_5$  reaches its maximal value when the coolant flow rate  $\dot{m}_c^*$  is at its minimum the conditions presented above represent the worst case for the approximation of  $u_1(t - \tau_5)$  to  $u_1(t)$ .

### 3.4.4 Model-based estimator

The basic structure of the model-based estimator is shown in Fig. 3-6 and is derived from the model of the thermal behaviour of the engine. As Fig. 3-6 shows, rather than a full state observer a reduced-order model-based estimator is realized. Indeed, only two of the three state variables are estimated.

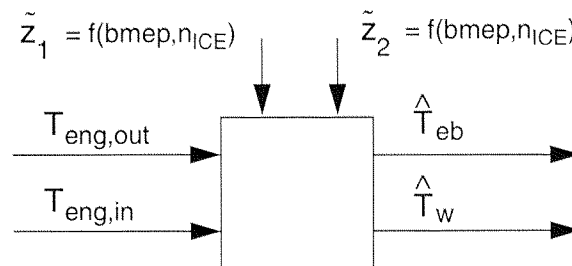


**Figure 3-6:** Model-based estimator structure

The equations needed to calculate the estimator values are based on the model of the system. In particular:

$$\frac{d\hat{T}_w}{dt} = \frac{\dot{Q}_{g,w}^* - \dot{Q}_{w,c}^*}{c_{pw} \cdot m_w} = \frac{1}{c_{pw} \cdot m_w} \cdot \left[ \tilde{z}_1(T_{ICE}, n_{ICE}) - a_1 \cdot (\hat{T}_w - T_{eng,m}) \right], \quad (3.20)$$

$$\begin{aligned}
\frac{d\hat{T}_{eb}}{dt} &= \frac{\dot{Q}_{c,eb}^* + \dot{Q}_{if}^* - \dot{Q}_{irr}^* + \dot{Q}_{ex,eb}^*}{c_{peb} \cdot m_{eb} + c_{poil} \cdot m_{oil}} = \\
&\frac{1}{c_{peb} \cdot m_{eb} + c_{poil} \cdot m_{oil}} \cdot \left[ a_2 \cdot (T_{eng,m} - \hat{T}_{eb}) \right. \\
&\left. + \tilde{z}_2(bpme, n_{ICE}) + f_1(\hat{T}_{eb}) + f_2(T_{eng,in}) \right].
\end{aligned} \tag{3.21}$$

The definition of the coefficients used in eqs. (3.20) and (3.21) is given in Appendix B. A detailed flowchart of the model-based estimator is shown in Fig. 3-7.

The model-based estimator for the engine block and cylinder wall temperatures  $T_{eb}$  and  $T_w$ , respectively, uses measured values of the temperature of the coolant entering and leaving the engine ( $T_{eng,in}$  and  $T_{eng,out}$ ). For this reason, a feedback loop is present within the feedforward path. Nevertheless, the feedforward structure is preserved since the measured values are only used in the model-based estimator and not for the calculation and feedback of the observation error.

The structure of the system with the model-based estimator and the feedforward controller is displayed in Fig. 3-8.

### 3.4.5 Simulation results

The performance of the system with feedforward control was first simulated. For both the simulations and the subsequent measurements three different engine operating points were chosen;

- Operating point OP1:  $n_{ICE} = 2500$  [rpm];  $bmep = 2$  [bar]
- Operating point OP2:  $n_{ICE} = 2500$  [rpm];  $bmep = 4$  [bar]
- Operating point OP3:  $n_{ICE} = 2500$  [rpm];  $bmep = 6$  [bar]

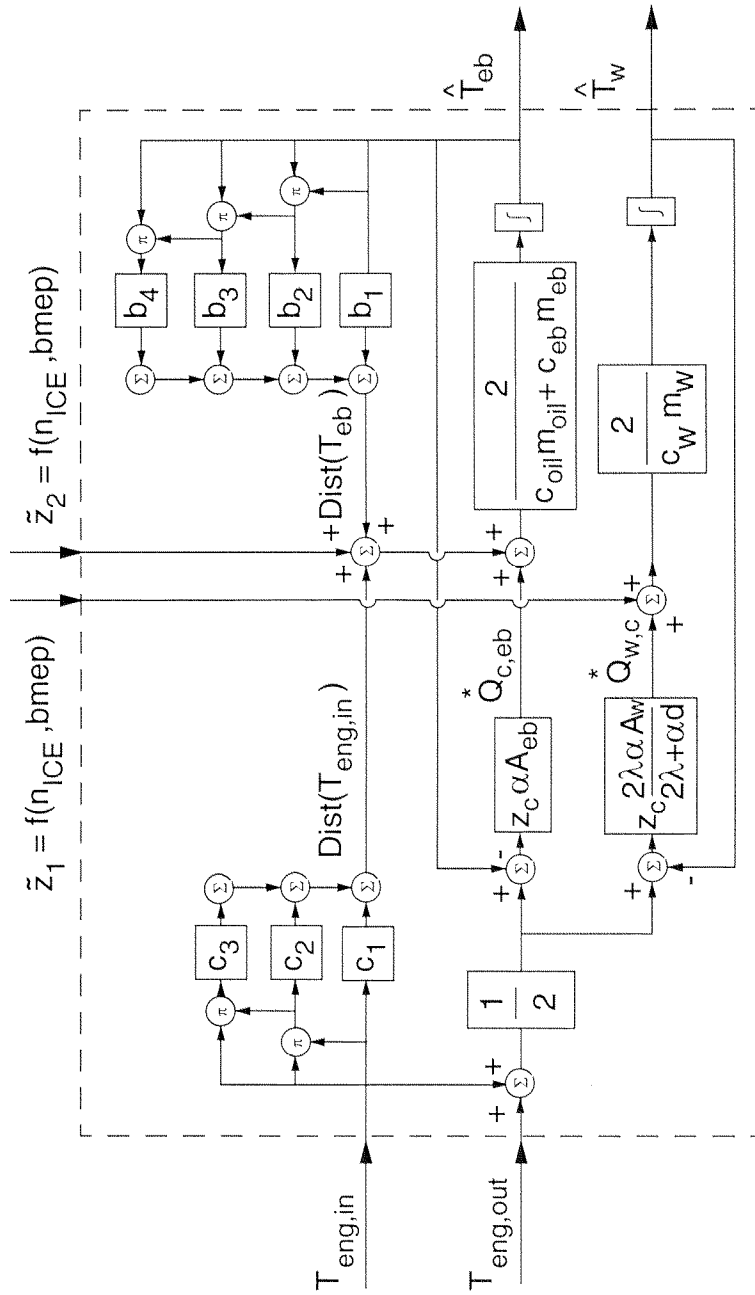
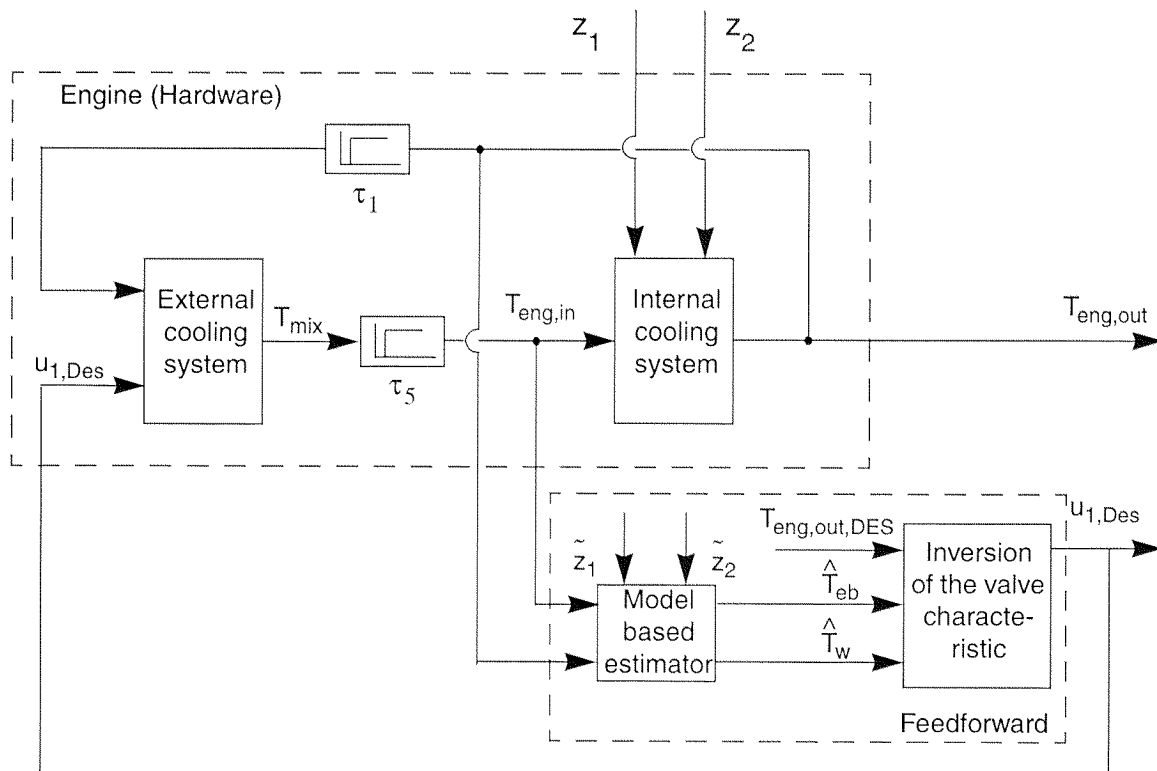


Figure 3-7: Flowchart of the model-based estimator

The possibility of an improvement in fuel consumption by means of engine thermomanagement is particularly promising when engine part-load operating conditions are considered. In addition, the chosen operating points are representative of the MVEG-A test cycle often used for fuel consumption prediction in this thesis work.



**Figure 3-8:** System with model based estimator and feedforward controller

The results obtained from simulation for the first engine operating point are plotted in Fig. 3-9. The heat exchanger is completely bypassed until the temperature of the coolant that leaves the engine reaches the desired temperature. In this phase the coolant temperature difference over the engine is only caused by the delay that characterizes the engine external cooling circuit. Once the temperature of the coolant leaving the engine  $T_{eng,out}$  reaches the desired value, it is evident that the feedforward controller successfully maintains this temperature at the desired level by gradually opening the bypass valve. In this way more and more coolant is sent to the heat exchanger, which causes a decrease in the temperature of the coolant entering the engine  $T_{eng,in}$ . For the reasons explained in Section 3.2, the chosen flow through the pump is

larger than the minimum possible for the engine operating point considered. Therefore, the steady-state operating conditions are reached long before the coolant temperature difference over the engine reaches the limit of  $15^{\circ}\text{C}$ .

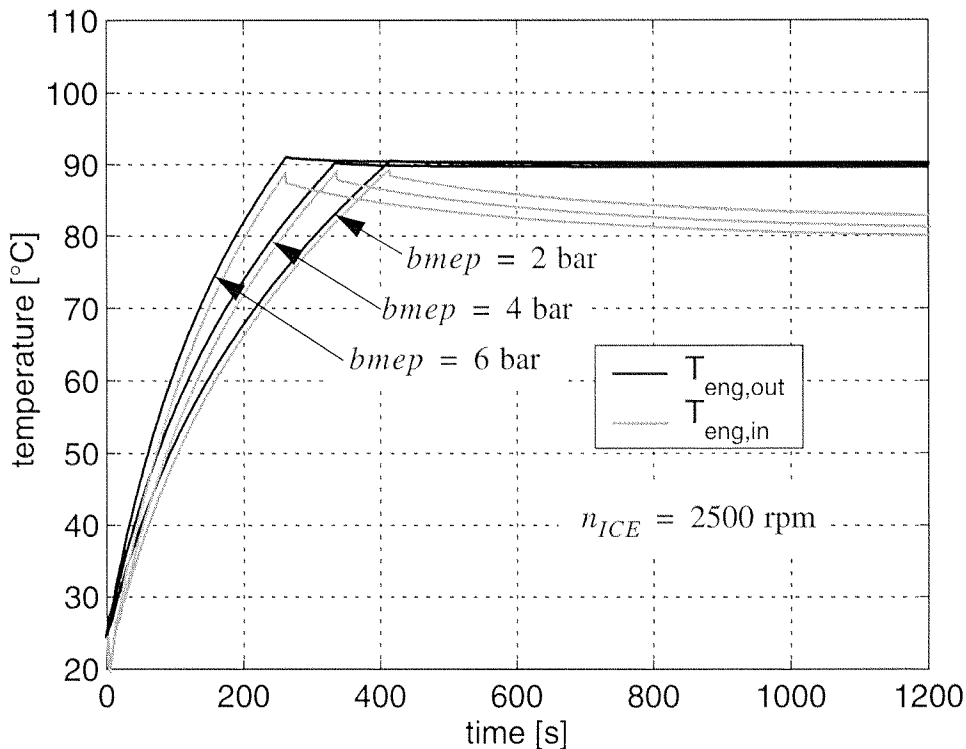


**Figure 3-9:** Simulated coolant temperature with feedforward controller

Fig. 3-9 also shows the results obtained from the simulations using the feedforward controller for the two other engine operating points. The values of the disturbances and of the coefficients used in the model as well as in the model-based estimator depend on the engine operating point considered. For this reason, for each engine operating point considered they have been accordingly modified. In addition, the parameters that characterize the estimator are calculated in function of the engine geometry as well as of its operating point, as explained in Appendix B.

As for the engine operating point considered above, in the first phase after starting the engine, the bypass valve stays closed and all the fluid completely flows through the bypass. Indeed, since the heat developed during combustion is proportional to the engine load (see Figure 2-10 on page 29), the coolant

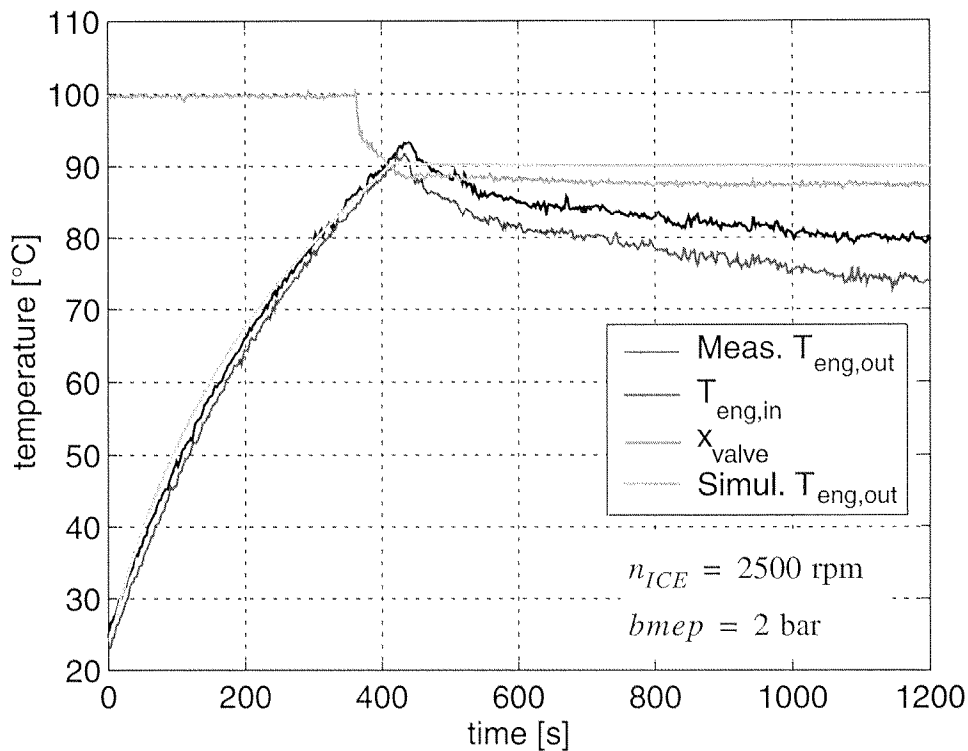


**Figure 3-10:** Measured coolant temperatures with feedforward controller

leaving the engine reaches the desired temperature  $T_{eng,out,DES} = 90$  °C earlier and the temperature difference of the coolant  $\Delta T_{eng}$  (see eq. (3.3)) over the engine increases with increasing engine loads.

### 3.4.6 Measurements

The performances of the feedforward controller have not only been simulated but experimentally tested on the test bench as well. The thermal behaviour of the engine for the first of the three operating points listed in Section 3.4.5 in terms of the temperature difference of the coolant over the engine are plotted in Fig. 3-10. The measured valve position is shown as well.

It has to be pointed out that in the case of the simulated system response the value of the mass flow distribution over the bypass as calculated by the feedforward controller immediately acts on the system, whereas on the test bench the valve as hardware has to be considered. The way in which the signal calculated by the feedforward controller is implemented is shown in Fig. 3-11. The



desired valve position  $x_{Des}$  is the effective valve input. It is calculated as a function of the desired mass flow partitioning over the bypass  $u_{1,Des}$  and of the inverted valve characteristic (plotted in Figure 2-5 on page 23). The effective valve position  $x_{act}$  is controlled by a proportional controller. The corresponding effective flow partitioning  $u_{1,act}$  over the bypass duct acts on the system in function of the effective valve position.

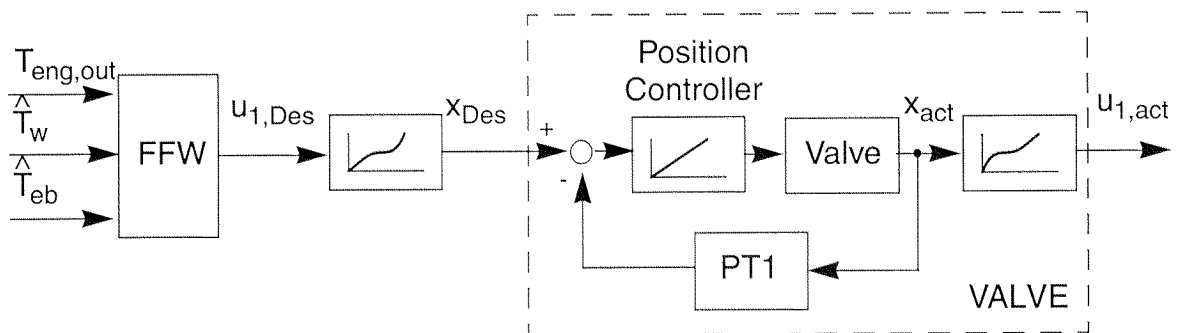


**Figure 3-11:** Realization of the output signal of the feedforward controller

Because of measurements errors in the valve opening characteristic a discrepancy between the desired and the effective mass flow partitioning over the bypass valve is unavoidable. In addition on the test bench the inputs of the feedforward control are measured as well as observed values. The last can differ from the effective values. Although the measured system response does not perfectly correspond to the response obtained by simulation, the feedforward controller performance can be considered as good. Indeed, the controlled temperature of the coolant leaving the engine has an overshoot of 6% of the desired value, while a stationary error of 11% of the desired value can be found for stationary thermal conditions. The same considerations are valid for the measurements carried out for the two other engine operating points. Those results are shown in Figs. 3-12 and 3-13. The temperatures of the coolant at engine output under steady-state operating conditions are slightly different for the engine operating points considered due to even small differences of the simulated correlation between coolant temperature and valve opening position from the real one.

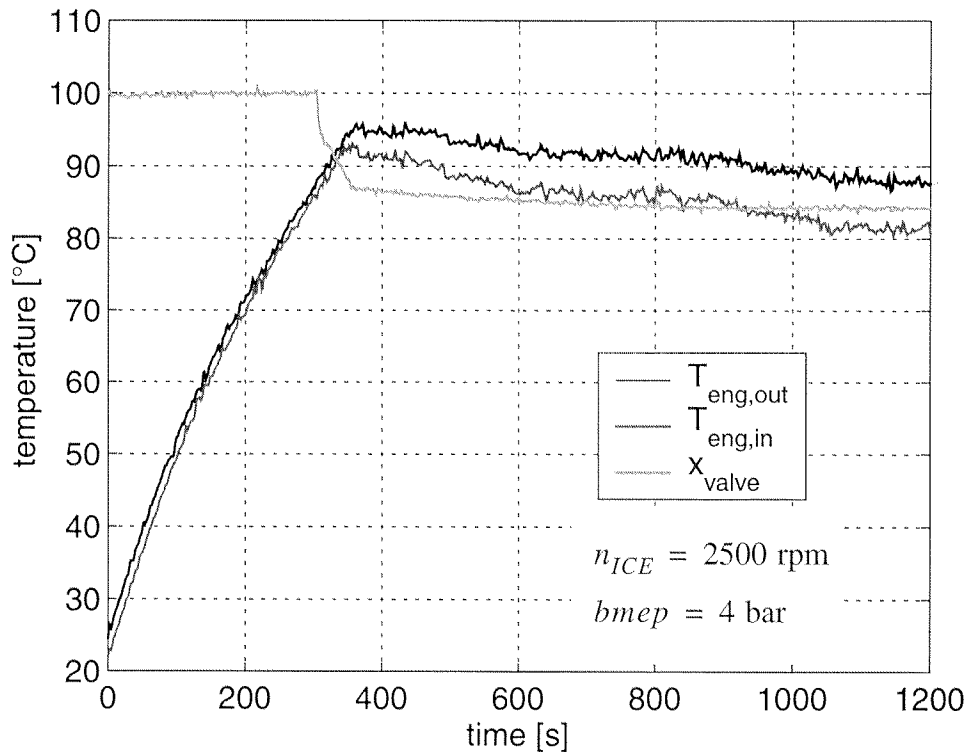


Figure 3-12: Measured coolant temperatures with feedforward controller

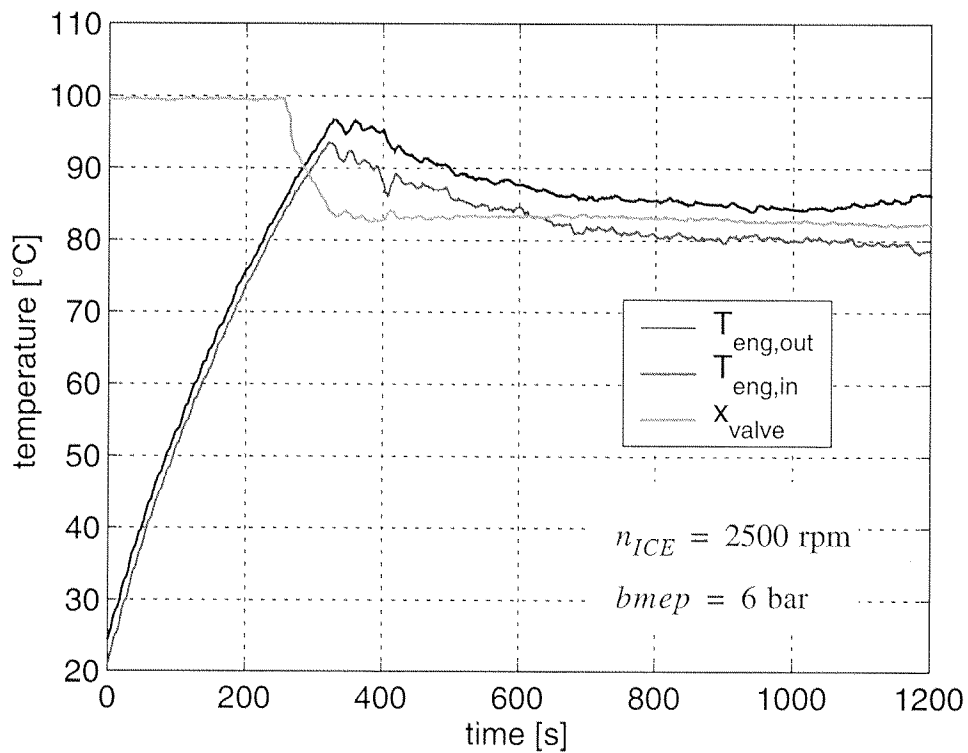


Figure 3-13: Measured coolant temperatures with feedforward controller

When the feedforward controller alone is applied the system response does not satisfy the specifications listed in Section 3.1. A feedback controller is thus needed as well. Its design is explained in the following sections.

### 3.5 Feedback controller

Whereas the feedforward controller presented above was designed in order to improve the engine temperature response during cold starts, the feedback controller is designed for the more general working conditions of the engine. The coolant temperature leaving the engine should reach the desired level as soon as possible and maintain it:

$$T_{eng, out, DES} = 90 \text{ }^\circ\text{C}, \quad (3.22)$$

while the temperature of the coolant entering the engine should not fall below the limit:

$$T_{eng, in, DES} = 75 \text{ }^\circ\text{C}. \quad (3.23)$$

Indeed, the temperature of the coolant entering the engine is not controlled to the value defined above, since temperature levels higher than  $75^\circ\text{C}$  are tolerable. The controller only guarantees that the temperature of the coolant entering the engine does not fall below the value of  $T_{eng, in, DES}$  defined above, in order to avoid an excessive coolant temperature gradient over the engine and the local material stress caused nearby.

#### 3.5.1 System reduction

The feedback controller should have universal validity at several engine operating points and working conditions. The particular operating conditions considered for the design of the feedforward controller (i.e. constant mass flow of the pump and constant coolant temperature after the heat exchanger) are thus no longer valid. As a consequence, the feedback controller has to be developed for the global system. The global MIMO system structure is therefore considered. Nevertheless, it is possible to reduce the system described in

Section 2.2 to various SISO subsystems. Different controllers are therefore designed for each of the subsystems. Switching conditions between the different subsystems are also defined.

### 3.5.2 Control strategy

The temperatures of the coolant  $T_{eng, out}$  leaving and  $T_{eng, in}$  entering the engine are measured on the test bench and can be used for control purposes. An alternative would be for example to control the temperature of the coolant leaving the engine and the coolant temperature difference over the engine. Since the first solution offers more flexibility it was chosen for this research. The temperature difference over the engine is not forced to maintain the limit value, only its amplitude may not exceed the defined value.

During engine warm-up the temperature of coolant and engine block as well as of the cylinder wall strongly varies between atmospheric conditions and up to operating conditions. For this reason during engine warm-up different engine thermal conditions can occur. The following control strategy for engine cold start is therefore proposed:

1. At start, the heat exchanger is completely bypassed. As a consequence the coolant leaving the engine reenters it without any change in its temperature. The temperature difference over the engine is only determined by the fact that the coolant leaving the engine reenters the engine with a delay that depends on the amount of the coolant mass flow:

$$T_{eng, in}(t) = T_{eng, out}(t - \tau_1(\dot{m}_c^*) - \tau_4(\dot{m}_{by}^*) - \tau_5(\dot{m}_c^*))$$

This procedure is typical of conventional configurations as well, where the thermostat conveys all the coolant flow to the radiator bypass for coolant temperatures below the activation temperature. Nevertheless for the configuration of the cooling system here proposed, the coolant flow through the engine (that means the mass flow through the pump) is minimized. This way the power need of the cooling pump is minimized as well. The minimum coolant flow for

the engine considered has been defined in Section 3.2. This configuration is applied until the coolant temperature leaving the engine reaches the desired temperature (in this case  $T_{eng, out, DES} = 90 \text{ }^\circ\text{C}$ )

2. Still maintaining the pump flow at a minimum, the temperature of the coolant leaving the engine is controlled to  $T_{eng, out, DES}$  by gradually closing the bypass valve (realized by the controller  $G_{c1}(s)$ ). This way, part of the warm fluid flows through the heat exchanger and the temperature of the coolant entering the engine is reduced.
3. In order to avoid large temperature differences inside the engine, the coolant temperature at engine input should not fall below a minimum (e.g.  $T_{eng, in, DES} = 75 \text{ }^\circ\text{C}$ ). When the temperature at engine output corresponds to  $T_{eng, out, DES}$  and if a temperature lower than  $T_{eng, in, DES}$  at engine input has been reached, the coolant mass flow through the engine obviously is insufficient to guarantee a proper cooling. In this case the temperature of the coolant entering the engine is controlled with the coolant flow through the water pump (controller  $G_{c2}(s)$ ).
4. Under high loads and at high ambient temperatures the valve will fully open, thus letting all the coolant flow through the heat exchanger. The temperature of the coolant leaving the engine will rise above the desired value. As a consequence, the coolant temperature at engine input would also rise above its desired value. In this case the temperature of the coolant leaving the engine has to be controlled with the coolant flow through the pump (controller  $G_{c3}(s)$ ).
5. As the coolant temperature is getting lower again, steps 1 to 3 are followed in reverse order.

In order to prevent constant switching among the different controllers, appropriate bands for the switching are used instead of fixed values.

**Table 3-3:** Schematic representation of the control law used.

	$y_2 = T_{eng, in}$	$y_1 = T_{eng, out}$	$u_1 = x_{valve}$	$u_2 = \dot{m}_c^*$
case 1	$< T_{eng, out, DES}$	$< T_{eng, out, DES}$	100 %	<i>minimal</i>
case 2	$> T_{eng, in, DES}$	$> T_{eng, out, DES}$	$\Delta T_{eng, out} \cdot G_{c1}(s)$	<i>minimal</i>
case 3	$< T_{eng, in, DES}$	$> T_{eng, out, DES}$	$\Delta T_{eng, out} \cdot G_{c1}(s)$	$\Delta T_{eng, in} \cdot G_{c2}(s)$
case 4	$> T_{eng, in, DES}$	$> T_{eng, out, DES}$	0 %	$\Delta T_{eng, out} \cdot G_{c3}(s)$

A schematic representation of the control law is given in Table 3-3. The term  $\Delta T_{eng}$  represents the difference between the desired temperature value  $T_{eng, DES}$  and the actual temperature  $T_{eng}$ , whereas  $G_{ci}(s)$  indicates the transfer functions of the controllers.

### 3.5.3 Controller design

In order to satisfy the specifications defined above, three different controllers have to be designed ([33]):

1. the controller  $G_{c1}$  that affects the output  $y_1 = T_{eng, out}$  by variations of the input  $u_1 = \dot{m}_{by}^*/\dot{m}_c^*$ ,
2. the controller  $G_{c2}$  that affects the output  $y_2 = T_{eng, in}$  by variations of the input  $u_2 = \dot{m}_c^*$ ,
3. the controller  $G_{c3}$  that affects the output  $y_1 = T_{eng, out}$  by variations of the input  $u_2 = \dot{m}_c^*$ .

All three are PI controllers. The parameters have been chosen such as to make the system robust (i.e, with sufficient large phase and magnitude reserves).

The temperature of the fluid leaving the engine (also defined as output  $y_1$ ) is controlled by the position of the bypass valve (input  $u_1$ ). The Nyquist diagram showing the influence of  $u_1$  on  $y_1$  (the complex frequency response of the open-loop system) is presented in Fig. 3-14. The influence of the delays can be seen clearly.

A critical gain of

$$K_{P1cr, L(model)} = 0.09$$

can be obtained in the simulation using the Ziegler-Nichols method. A value for this parameter can also be gained by a nonlinear simulation:

$$K_{P1cr, NL(model)} = 0.03.$$

The discrepancy between these two values of the critical proportional gain can be explained as follows: While the global delay remains constant in the linearised model, this is not the case in the nonlinear model, since variations in the bypass valve position influence the mass flow through the tubes and therefore the delays. Moreover, the strong non linearity that characterizes the opening characteristic of the bypass valve does not appear in the linearised model.

Experiments conducted on the test bench lead to a value of the critical proportional gain of

$$K_{P1cr, TestBench} = 0.03,$$

and of a corresponding critical period of:

$$T_{1cr, NL(model)} = 94 \text{ [s]}.$$

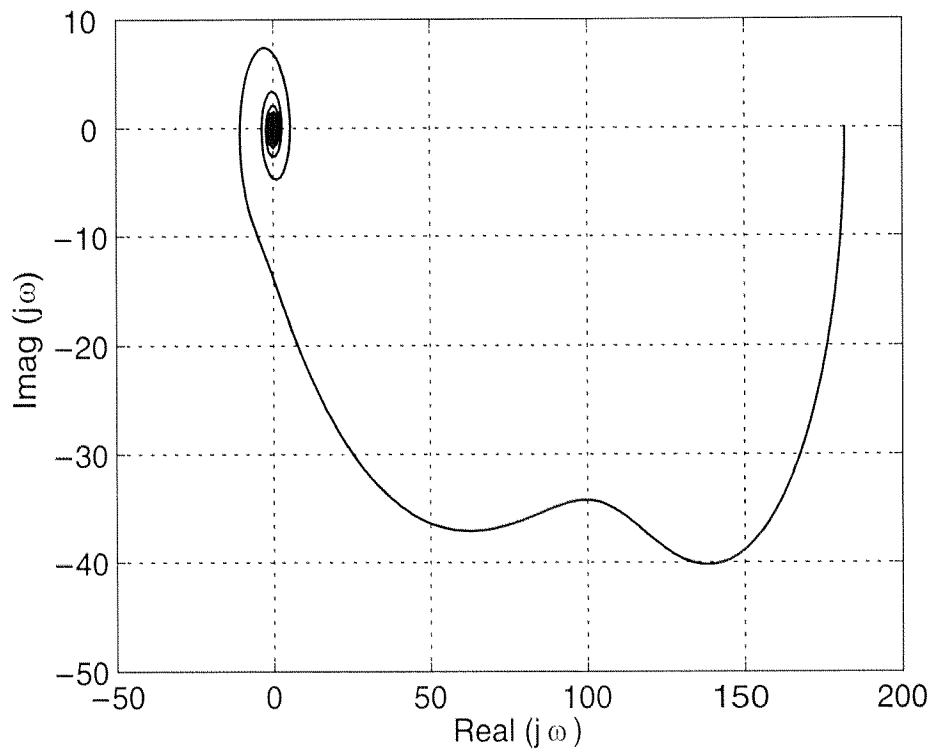


**Figure 3-14:** Transfer function from input  $u_1$  to output  $y_1$

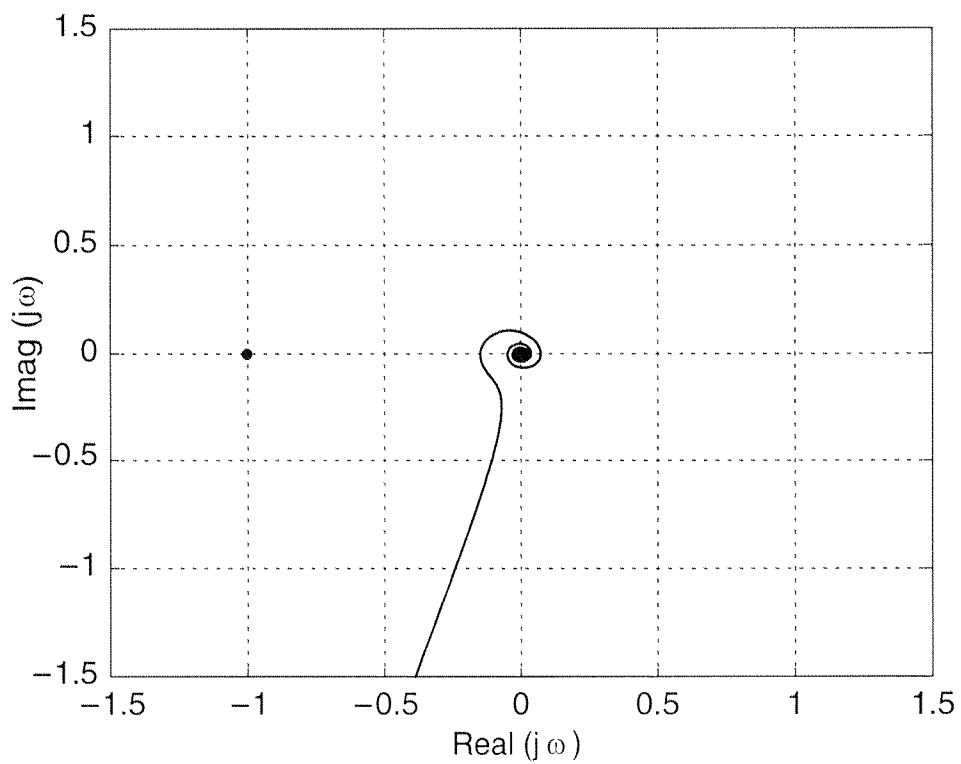


**Figure 3-15:** Open-loop transfer function  $u_1$  to  $y_1$  with the PI controller



These values have also been identified with the nonlinear simulation and have been used for the design of the PI controller  $G_{c1}$ , which reads as follows:

$$G_{c1}(s) = 0.0135 + \frac{1.05 \cdot 10^{-3}}{s}. \quad (3.24)$$

A Nyquist plot of the open-loop system with this PI controller is shown in Fig. 3-15.

Finally, Fig. 3-16 shows the temperature of the coolant leaving the engine during a cold start, both for the measurement results on the test bench and the simulations of the nonlinear system. The engine in this case is operated at  $n_{ICE} = 2500$  [rpm] and  $bmep = 2$  [bar]. The coolant mass flow is sufficient to guarantee that the temperature of the coolant entering the engine does not sink below the level defined earlier. Therefore, only the controller  $G_{c1}$  is activated. The overshoot of the temperature  $T_{eng, out}$  is clearly visible both in the simulated and in the measured system response. While the measured value of the system output exhibits clear limit cycles, they are not present in the simulation since an ideal valve is modeled.

When the temperature of the coolant leaving the engine is controlled to the desired value and the temperature difference of the coolant over the engine does not exceed the imposed limit  $T_{eng, out, DES} - T_{eng, in, DES}$ , only the controller  $G_{c1}$  is activated, as already seen. When this condition is no longer satisfied, the temperature of the coolant entering the engine (output  $y_2$ ) can be controlled by changing the pump mass flow (input  $u_2$ ) in the case where part of the cooling flow still bypasses the heat exchanger (case 3 in Table 3-3).

The parameters for the controller  $G_{c2}$  can be calculated based on the Nyquist plot of the open-loop system represented in Fig. 3-17. In this case the risk of neglecting important nonlinearities is not as large as for the controller  $G_{c1}$ . Simulations conducted on the linearised system yield a critical gain of:

$$K_{P2cr} = 0.09,$$

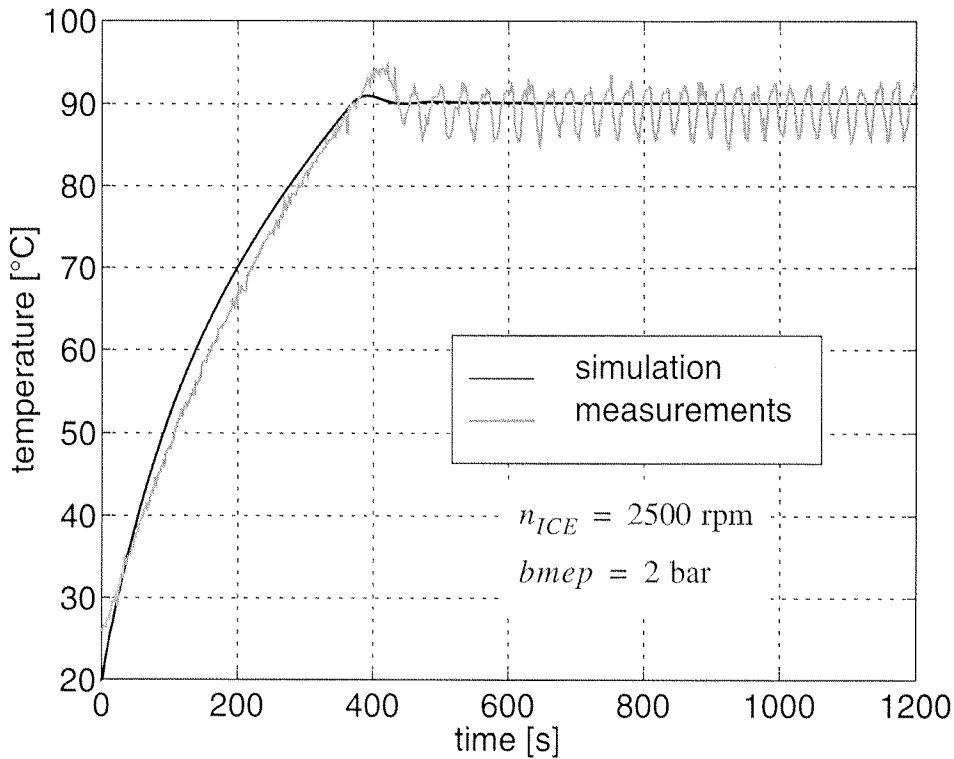


**Figure 3-16:** Measured and simulated coolant temperatures,  $G_{c1}$  activated and a critical period of:

$$T_{2cr} = 36 \text{ [s]}.$$

The parameters for the controller can thus be defined as follows:

$$G_{c2}(s) = 0.04 + \frac{8 \cdot 10^{-3}}{s}. \quad (3.25)$$

Note that the controller increases the input  $u_2 = \dot{m}_c^*$  if the value of the output  $y_2 = T_{eng,in}$  is too low.

The same procedure is applied for the choice of the parameters of the third controller  $G_{c3}$  influencing the temperature of the coolant leaving the engine (output  $y_1$ ) with variations of the pump mass flow (input  $u_2$ ) when the cool-

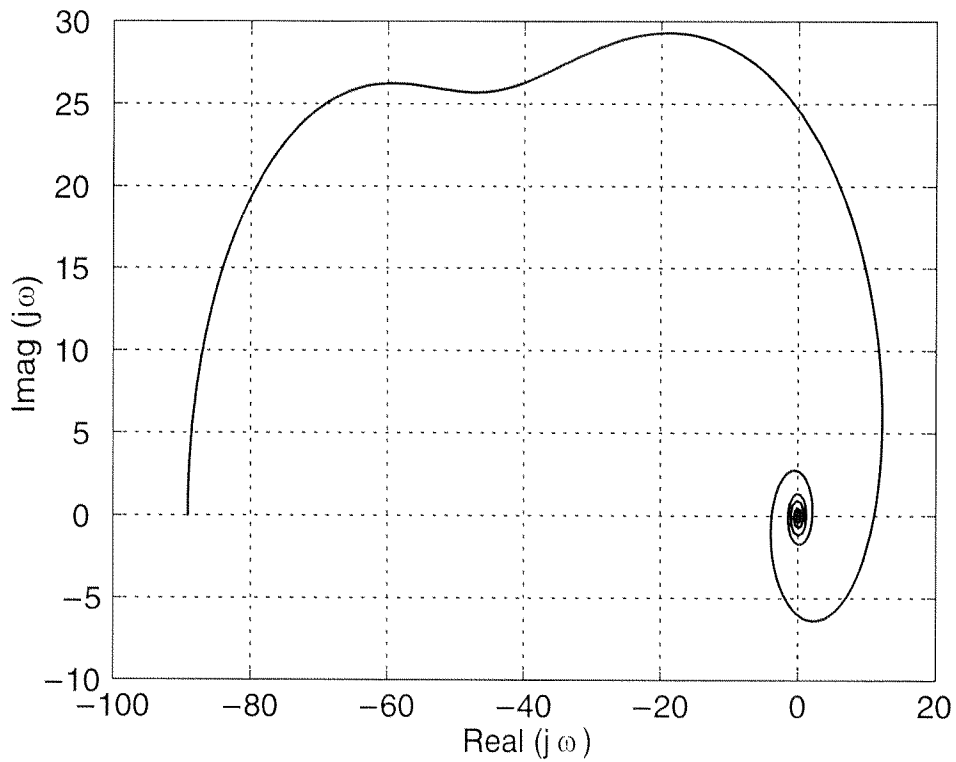


**Figure 3-17:** Transfer function from input  $u_2$  to output  $y_2$

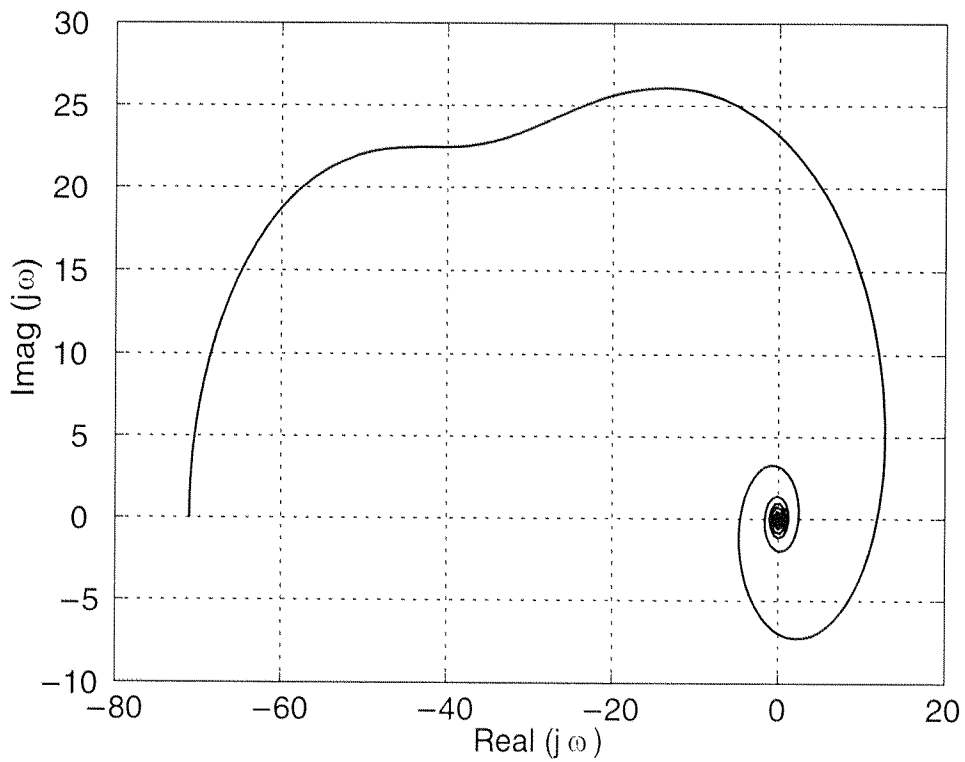


**Figure 3-18:** Transfer function from input  $u_2$  to output  $y_1$

ant completely flows through the heat exchanger (case 4 in Table 3-3). The critical gain calculated from the Nyquist plot represented in Fig. 3-18 is:

$$K_{P3cr} = 0.08.$$

The parameters for the controller  $G_{c3}$  are defined as follows:

$$G_{c3}(s) = 0.036 + \frac{7.2 \cdot 10^{-3}}{s}. \quad (3.26)$$

The feedback controller alone presents the drawback that the valve works with clear limit cycles. The effect can be clearly seen on the temperature of the coolant leaving the engine as plotted in Fig. 3-16.

During the engine cold start plotted in Fig. 3-16 only the two controllers  $G_{c1}$  and  $G_{c2}$  are active. Indeed, for low engine speeds and loads due to hardware limitations of the test bench (Section 3.2), the coolant flow through the pump is higher than the coolant flow needed to maintain a coolant temperature difference over the engine of 15 °C (cf. Fig. 3-2). As a consequence, for the engine operating conditions considered in Fig. 3-16, case 3 of Table 3-3 never occurs and the controller  $G_{c3}$  is never active.

### 3.6 Feedforward and feedback controllers

The system behaviour can be improved by combining the feedback and the feedforward controllers. In this case the feedforward controller only acts on the system output  $y_1 = T_{eng, out}$  by calculating the desired value of the input  $u_1 = \dot{m}_{by}^* / \dot{m}_c^*$ , improving the engine thermal behaviour in particular in case of cold-start operating conditions. On the other hand, the additional feedback controller keeps the value of the output  $y_1 = T_{eng, out}$  to the desired value and additionally ensures that the value of the output  $y_2 = T_{eng, in}$  does not drop below the desired limit. The feedback controller acts on the two system inputs  $u_1$  and  $u_2$ . A flowchart representation of the system with both controllers designed is given in Fig. 3-19.

Because of the concurrent action of the feedforward controller, the effect of the controller  $G_{c1}$  on the input  $u_1 = \dot{m}_{by}^*/\dot{m}_c^*$  can be reduced. For this reason, the proportional and the integral gains of the controller  $G_{c1}$  defined in Chapter 3.5.3 are now cut in half, which improves robustness.

The performance of the coolant temperatures entering and leaving the engine during engine cold start has been measured when only the feedback controller is activated and when both the feedback and the feedforward controllers are applied. In both cases the engine was operated at constant  $n_{ICE} = 2500$  rpm and  $bmeP = 2$  bar. The results are shown in Figs. 3-20 and 3-21. The advantages of using the combination of feedback and feedforward controllers over using the feedback controller alone can be recognized in the facts that the temperature of the coolant leaving the engine does not overshoot when the desired operating temperature is reached and that both the controlled coolant temperatures do not show any limit cycles.

Fig. 3-21 shows the valve opening position during the defined engine cold start for both controller configurations considered. One major improvement of the combination of feedback and feedforward controllers is the fact that the valve position does not oscillate. Indeed, because of the combination of feedback and feedforward controllers the control loop gains a better stability since the gain of the feedback controller can be cut in half. In addition, the performances of the complete system are improved due to the presence of the feedforward controller. Furthermore the feedforward controller acts on the bypass valve causing its immediate opening when the desired coolant temperature at engine output is reached. This globally improves the dynamics of the system, as evident in Fig. 3-21.

Some difficulties have been encountered in controlling the valve position: the use of a better valve and in particular of a better position controller would surely simplify the definition of the feedback controller and reduce the amplitude of the measured limit cycles.

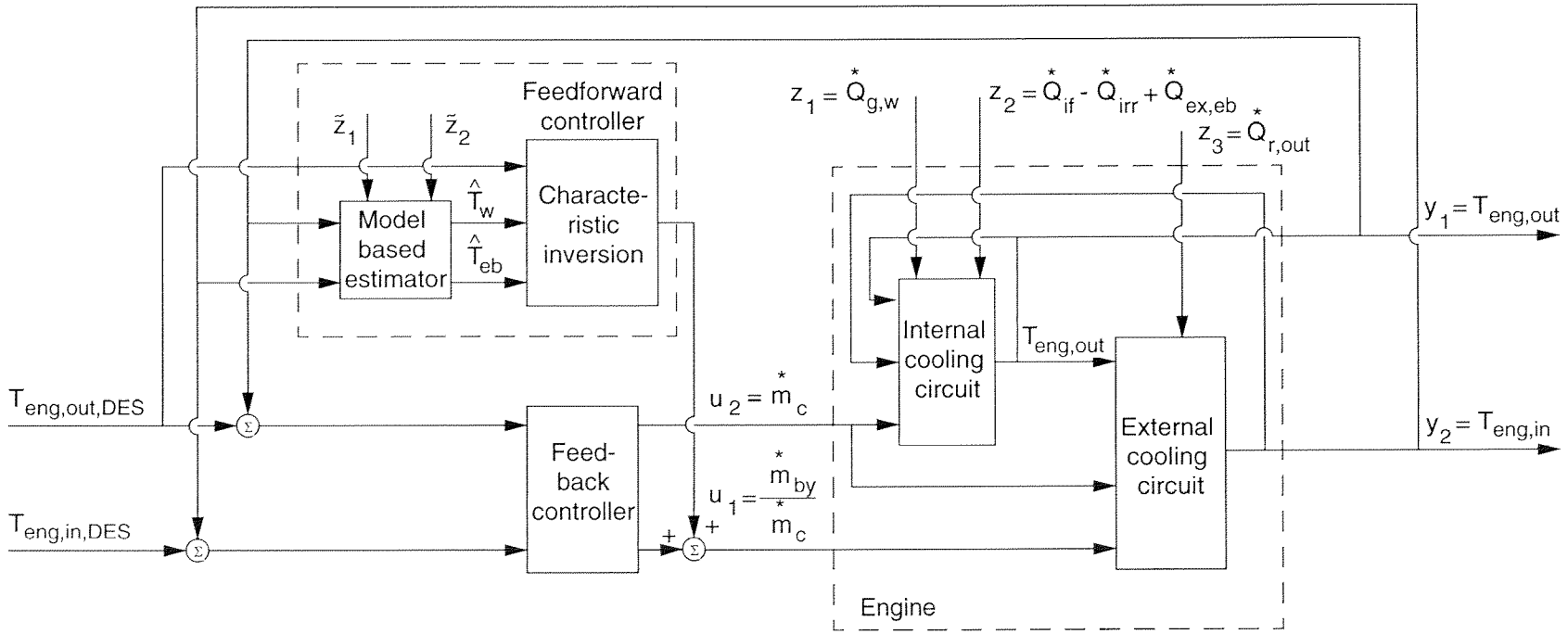
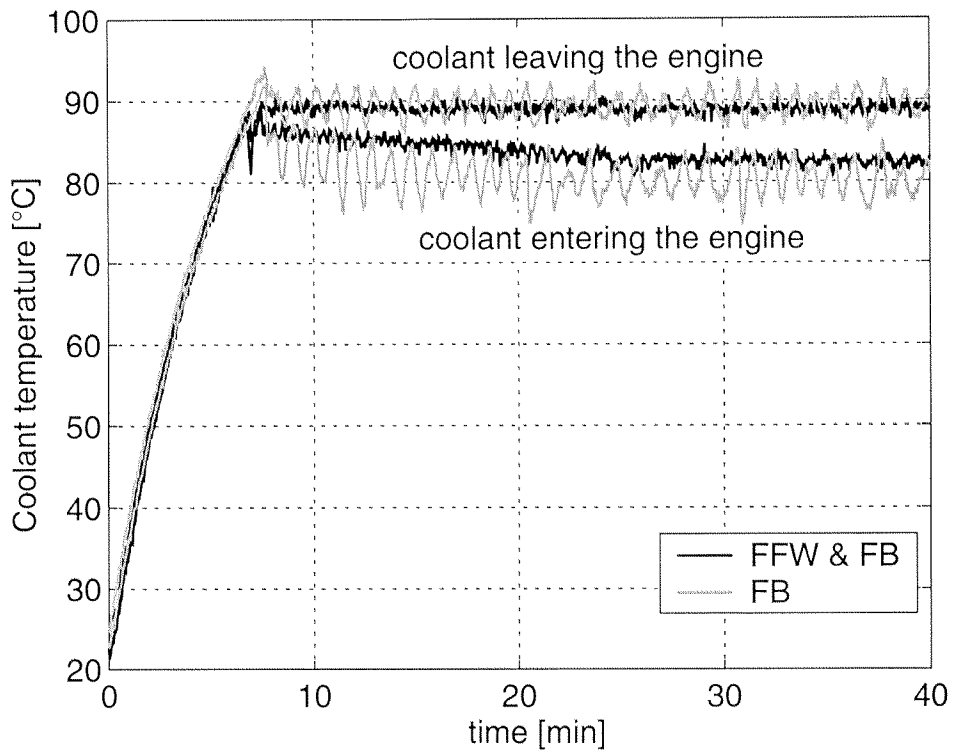
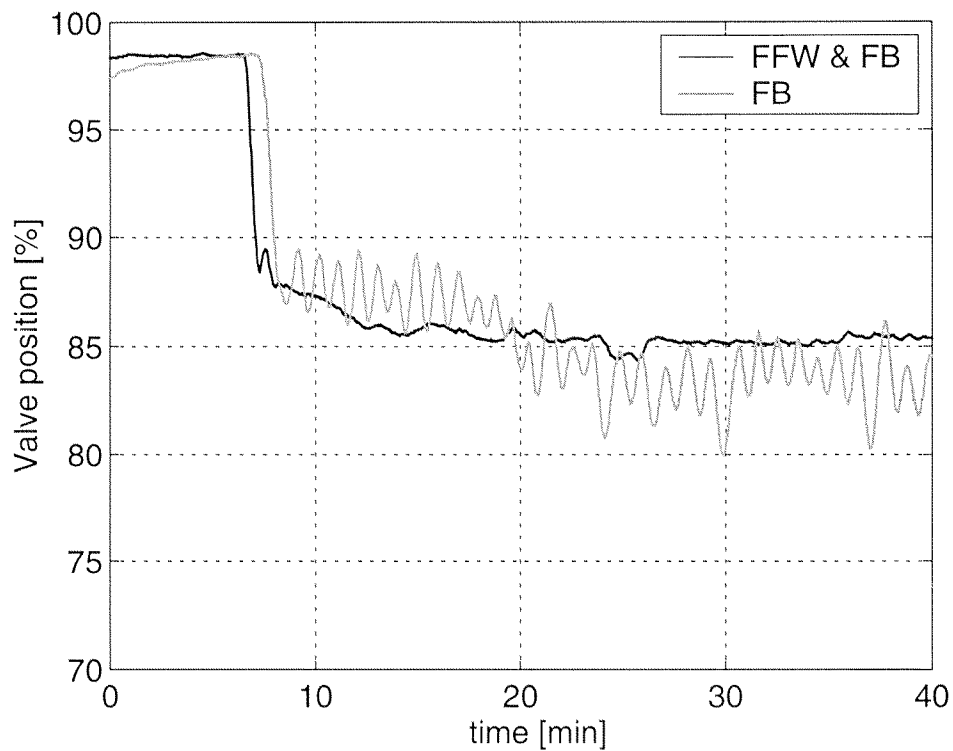


Figure 3-19: Combined controller system



**Figure 3-20:** Measured coolant temperatures (cold start, different controllers)



**Figure 3-21:** Measured valve positions at cold start for different controllers

## 3.7 Conclusions

The control of the bypass valve is a key element for the optimization of the global thermal behaviour of the engine. The most critical operating conditions are encountered during engine warm-up phases when the system is characterized by low coolant flows and therefore by high transport delays. These delays are not constant, but proportional to the coolant mass flow and the flow partitioning over the radiator. Furthermore, the heat balance during engine warm-up is different from that observed during steady-state operating conditions, since part of the heat produced during combustion is used for warming up the engine block and the coolant itself. For these reasons a feedforward controller is designed for the more critical engine warm-up operating conditions.

Once the engine is warmed up, the feedback controller can guarantee good thermal performance. Both system inputs (flow partitioning over the radiator as well as coolant flow) are now controlled.



Seite Leer /  
Blank leaf

## CHAPTER 4

### EXPERIMENTAL SETUP

In this chapter the experimental setup and the most important hardware components are described, followed by measurement results obtained using the conventional as well as the improved configuration of the cooling system on the dynamic test bench. Later on, cold-start experiments performed under constant engine load and speed as well as emulated test cycles are documented. A brief description of the emulation of test cycles on the test bench closes this chapter.

#### 4.1 Test bench configuration

The experiments have been performed on a dynamic test bench by *APICOM*, type *SM 200 L-4*. The water-cooled asynchronous generator runs with a maximum power of 300 KW and a maximum speed of 10'000 rpm, although for the experiments conducted the maximum speed was limited to 5'500 rpm. The experimental set-up is schematically presented in Fig. 4-1.

The engine is instrumented with thermocouples for the measurement of various temperatures (oil, water, intake air, exhaust gases). The sensors for the measurements of temperatures in the range of 0 °C up to 200 °C are of the type *Thermocoax*, type *K*. Various pressures (intake manifold, exhaust collector, ports of pressure wave supercharger, etc.) are measured as well. Further, some additional values are measured, such as the air-to-fuel ratio by means of a lambda sensor, pressure wave supercharger and cooling pump speed, as well as the electrical power needed and the position of the cooling circuit valve for

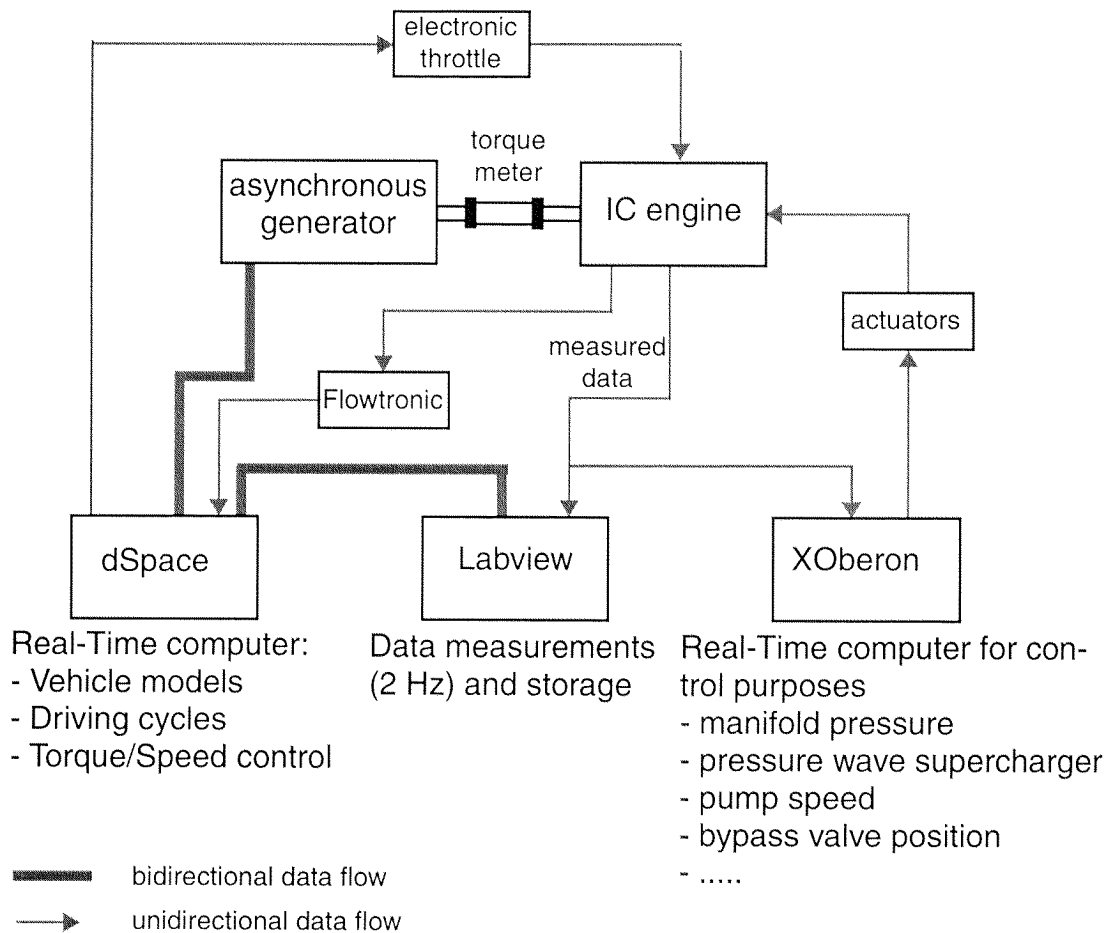


**Figure 4-1:** Test bench configuration

the bypass of the radiator. The fuel consumption is measured with a dedicated flow meter (*Flowtronic, Quicky AG*). According to the manufacturer's specifications the accuracy in the measurements of fuel flow is 0.3%.

The engine is directly coupled with the brake, i.e. there is no gear box in-between. Of the engine auxiliary devices only the oil pump is conventionally driven by the engine. There is no alternator for the production of 12 V electrical energy. All the electrical devices (engine electronics, fuel pump, ignition, injection, fan, and cooling pump) are externally powered. A vibration absorber is mounted between asynchronous generator and combustion engine. The torque meter by *CCT Transducer*, type *TR 20 C* provides an accuracy in the torque measurements smaller than 0.03% of the full range value, according to the manufacturer's specifications.

A dSpace real-time computer is responsible for controlling engine speed and torque as well as for implementing all the Simulink models emulating the test cycle, the vehicle, and the powertrain components. The asynchronous generator can thus be kept at the desired engine speed which is calculated based on the velocity profile and gear demanded by the cycle as well as on the desired engine torque which is calculated based on vehicle and powertrain specifications. The control of the engine speed is realized by controlling the asynchronous generator speed while engine torque is controlled with the engine throttle.

A further real-time system, denominated XOberon, is mainly used for controlling the pressure wave charger and the proposed cooling system. Indeed, manifold pressure, pressure wave supercharger and cooling pump speed as well as bypass valve position are controlled by appropriate algorithms implemented in XOberon. The control of these variables is realized by proper actuators.

Some of the measured signals are supplied to both dSpace and XOberon. Additionally, all the measured data flow to a computer where they are processed and stored by means of a specifically developed LabView program. Since the sampling rate of the LabView system is limited to ca. 2 Hz, the processing and the storage of fast sampling data is realized by dSpace with sampling rates of 1000 Hz. The maximum possible sampling rate depends on the number of channels considered.

## 4.2 Engine

For all the measurements and simulations a small boosted engine with flat twin configuration has been considered ([38], [65], [66]). The parameters characterizing the engine are given in Appendix A. Measurements of the brake-specific fuel consumption relative to the engine considered have been performed on the test bench under stationary operating conditions. The engine map obtained is plotted in Fig. 4-2.

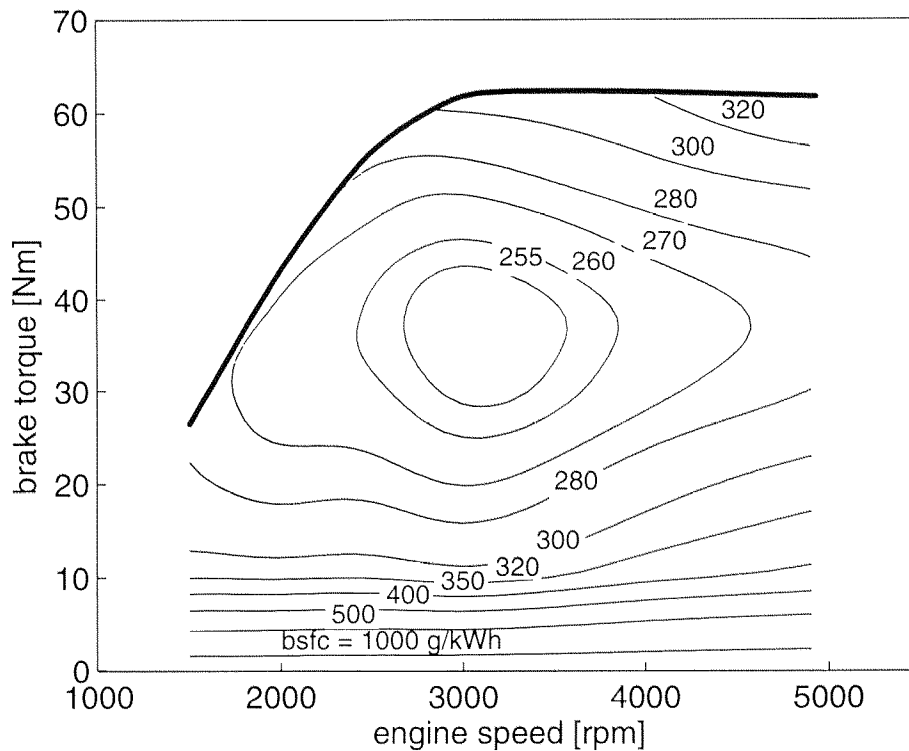


**Figure 4-2:** Measured brake-specific fuel consumption [g/kWh]

### 4.3 Cooling system components

All the components of the cooling system are present in hardware on the engine test bench, both for the conventional and the improved configuration considered. An overview of the conventional cooling system configuration is given in Fig. 4-3.

The cooling pump for both of the configurations tested is an electrical one (*Webasto* cooling pump, type *U4814*). The pump is externally supplied with 12 V DC and can be powered up to 105 W. When working against a pressure of 0.2 bar the maximum pump mass flow amounts to 2500 l/h.

The thermostat visible in Fig. 4-3 has the opening characteristic plotted in Figure 2-14 on page 42.

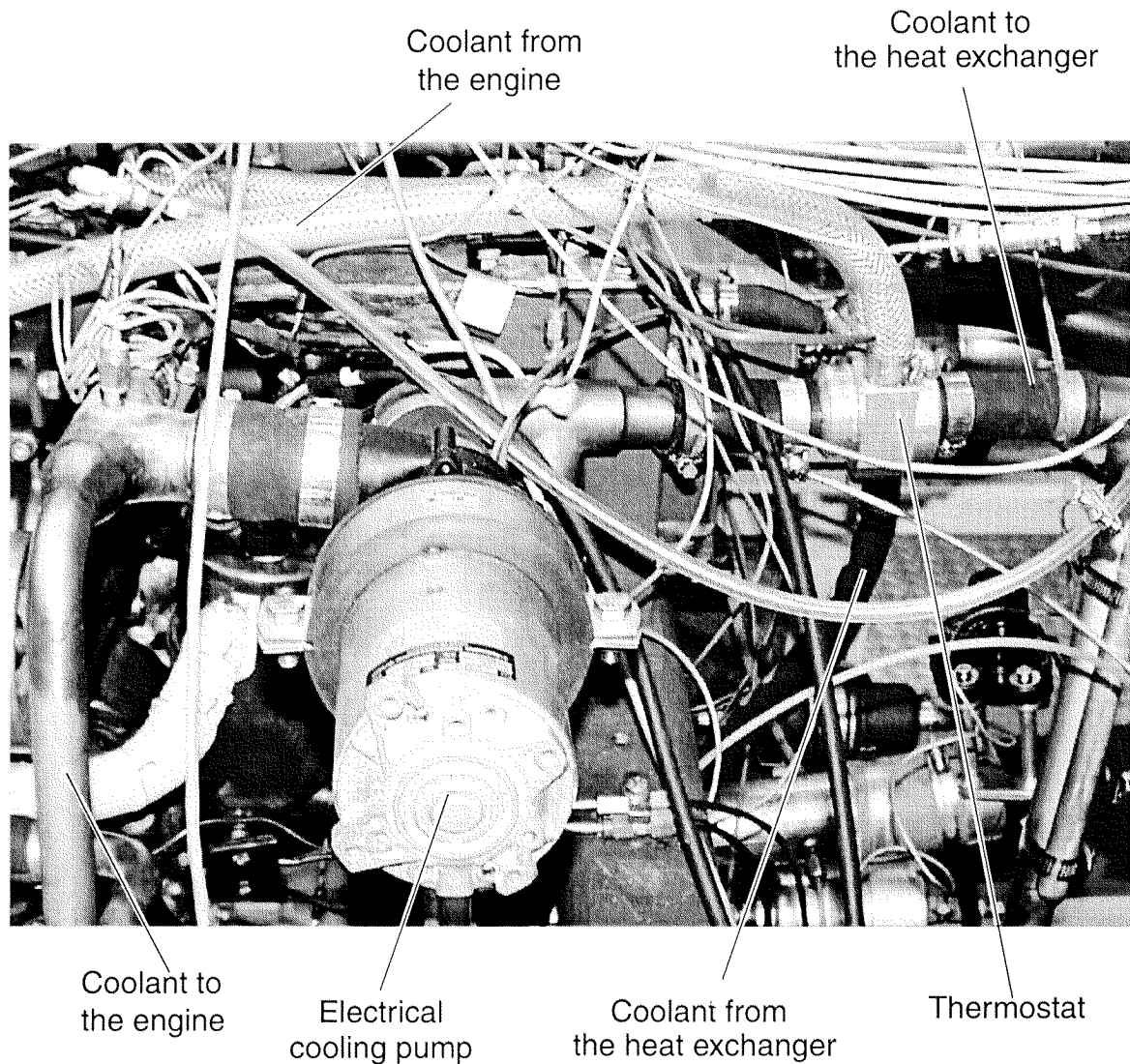


**Figure 4-3:** Conventional cooling system configuration on the test bench

Instead of a coolant-to-air radiator a coolant-to-water heat exchanger is used on the test bench. The mass of air ramming the radiator in a vehicle is emulated by a controlled flow of cold water from a secondary cooling circuit to the heat exchanger. During the part-load measurements under stationary engine operating conditions the vehicle velocity estimated on the basis of engine speed and torque is constant. A constant water flow from the secondary cooling circuit is the consequence.

In the improved configuration of the cooling system the thermostat is substituted by an electrically operated valve, as visible in Fig. 4-4.

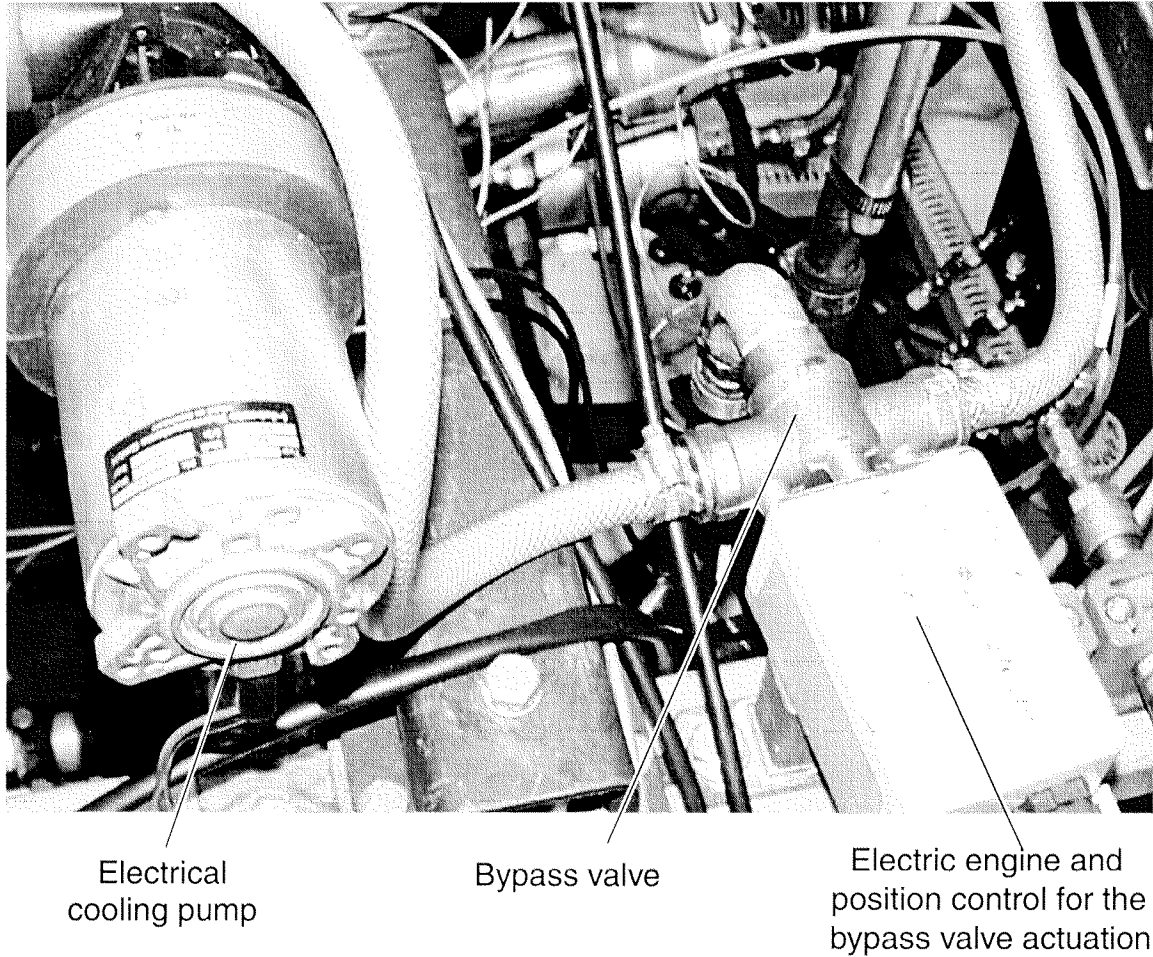


**Figure 4-4:** Improved cooling system configuration on the test bench

## 4.4 Emulation of vehicle and powertrain

In order to emulate the vehicle behaviour on the test bench, models describing the components not realized in hardware have to be developed. The main equations used for describing the vehicle and the powertrain are given in the following paragraphs. More information about the modelling of such a system can be found in [15], [65], and [66].

#### 4.4.1 Vehicle

The test cycle delivers the trajectories of desired vehicle speed as well as the gear to be driven. The torque resistance at the wheel resulting from the test cycle velocity profile is calculated taking into account three different components of resistance torque  $T_{wheel}$  ([35], [43]), namely torque due to rolling friction  $T_{rol}$ , air drag  $T_{air}$ , and vehicle inertia  $T_{\theta_v}$ :

$$T_{wheel} = T_{rol} + T_{air} + T_{\theta_v} = m_v \cdot k_{rol}(v) \cdot g \cdot r + \frac{1}{2} \cdot c_w \cdot A \cdot \rho_{air} \cdot v^2 \cdot r + \frac{\theta_v}{r} \cdot \frac{dv}{dt} \quad (4.1)$$

where  $\theta_v = m_v \cdot r^2$ .

The wheel angular velocity  $\omega_{wheel}$  is calculated as a function of the wheel radius  $r$  and of the instant vehicle velocity  $v$  prescribed by the driving cycle.

An overview of the vehicle parameters is given in Appendix A.

#### 4.4.2 Powertrain

Knowing the torque  $T_{wheel}$  and angular speed  $\omega_{wheel}$  on the wheel as well as the transmission efficiency  $\eta$  and the ratio  $i$ , defined as:

$$\eta = \frac{T_{wheel} \cdot \omega_{wheel}}{T_G \cdot \omega_G} \quad i = \frac{\omega_{wheel}}{\omega_G}, \quad (4.2)$$

the corresponding torque  $T_G$  and speed  $\omega_G$  at the clutch side of the gearbox can then be calculated. In the transmission the shift gearbox and the differential gear are included. The resulting torque is:

$$T_G = \frac{T_{wheel} \cdot i}{\eta(\omega_G, T_G, i_G)}. \quad (4.3)$$



where both global transmission ratio  $i$  and efficiency  $\eta$  result from the corresponding shift and differential gear values:

$$i = i_G \cdot i_{diff}, \quad \eta(\omega_G, T_G, i_G) = \eta_G(\omega_G, T_G, i_G) \cdot \eta_{diff}$$

The ratios for the different gears are given in Appendix A. More detailed data about the gear modelling can be found in [65].

Each energy transformation is characterized by its efficiency. The Willans approach correlates the provided and the delivered power for a defined energy transformation. It is often used to describe the efficiency of internal combustion engines, where for a defined engine operating speed, an affine correlation between provided and delivered power exists ([37]). The same approach can be used to describe the efficiency of the energy transformation that occurs in a mechanical transmission. In this case also the requested power result is directly proportional to the delivered power. For a defined gear transmission ratio  $i$  it is:

$$i \cdot T_{wheel} = e(i_G) \cdot T_G - i \cdot T_{wheel,0}(i_G, \omega_G), \quad (4.4)$$

as plotted in Fig. 4-5. The torque at the clutch side of the transmission is therefore:

$$T_G = \frac{i \cdot T_{wheel}}{e(i_G)} + T_{G,0}(i_G, \omega_G), \quad (4.5)$$

where  $T_{G,0}(i_G, \omega_G) = i \cdot T_{wheel,0}(i_G, \omega_G) / (e(i_G))$ .

Based on the model of the clutch the desired value of the torque to be delivered by the engine to drive the given cycle is then calculated. This value is the input of the driver model, while the output is the load pedal (throttle) position.

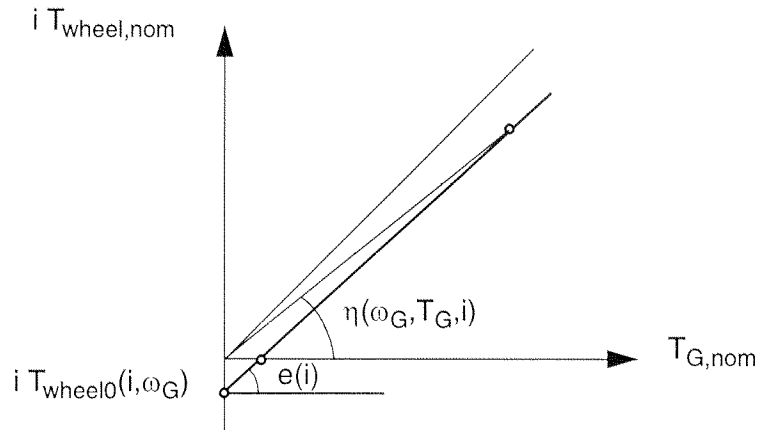


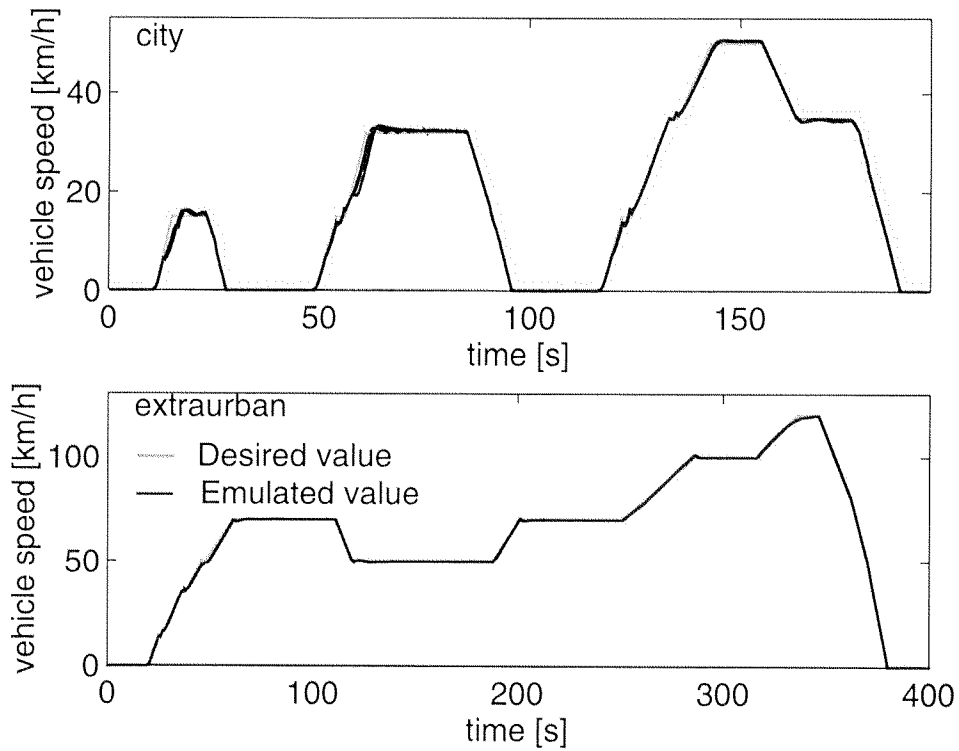
**Figure 4-5:** Willans representation of transmission efficiency

### 4.4.3 Results

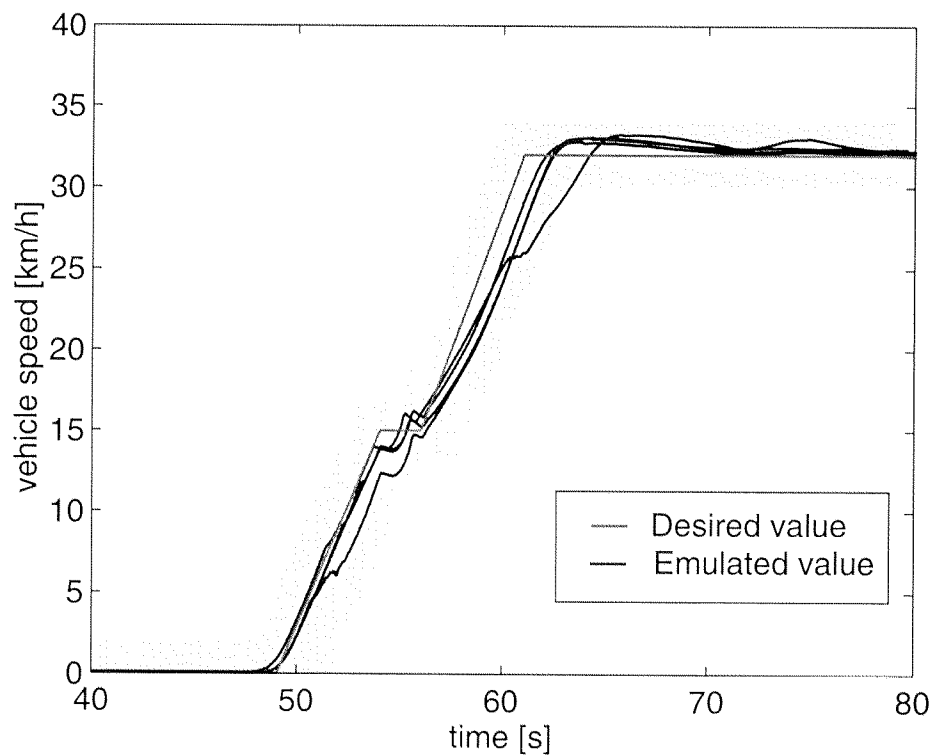
Fig. 4-6 shows the desired and emulated vehicle speeds. The emulated values relative to the four city cycles that characterize the MVEG test cycle are superimposed in the top frame in Fig. 4-6. A detail of the acceleration phase is shown in Fig. 4-7. The regulations provide for a velocity tolerance range, which is shown in both Figs. 4-6 and 4-7. As Fig. 4-6 clearly shows the emulated values always stay within this tolerance range.

Fig. 4-8 shows the engine torque for the measured cycles. A detailed view of the engine torque during the four city cycles of the test is shown in Fig. 4-9, while Figs. 4-10 and 4-11 show the engine speed.

Finally, Fig. 4-12 shows the fuel consumption data obtained by means of measurements under various operating conditions, namely cold and pre-warmed engine. The measurements show that driving the test cycle without pre-warming the engine causes an increase in fuel consumption of about 7%. For the conventional configuration of the cooling system considered this value represents the maximum potential achievable when an improvement of the cooling system is considered. The comparison between the fuel consumption achieved during the MVEG-A test cycle for a cold or a pre-warmed engine was made only for the conventional configuration of the cooling circuit.



**Figure 4-6:** Desired and emulated vehicle speed



**Figure 4-7:** Desired and emulated vehicle speed (detail from Fig. 4-6)

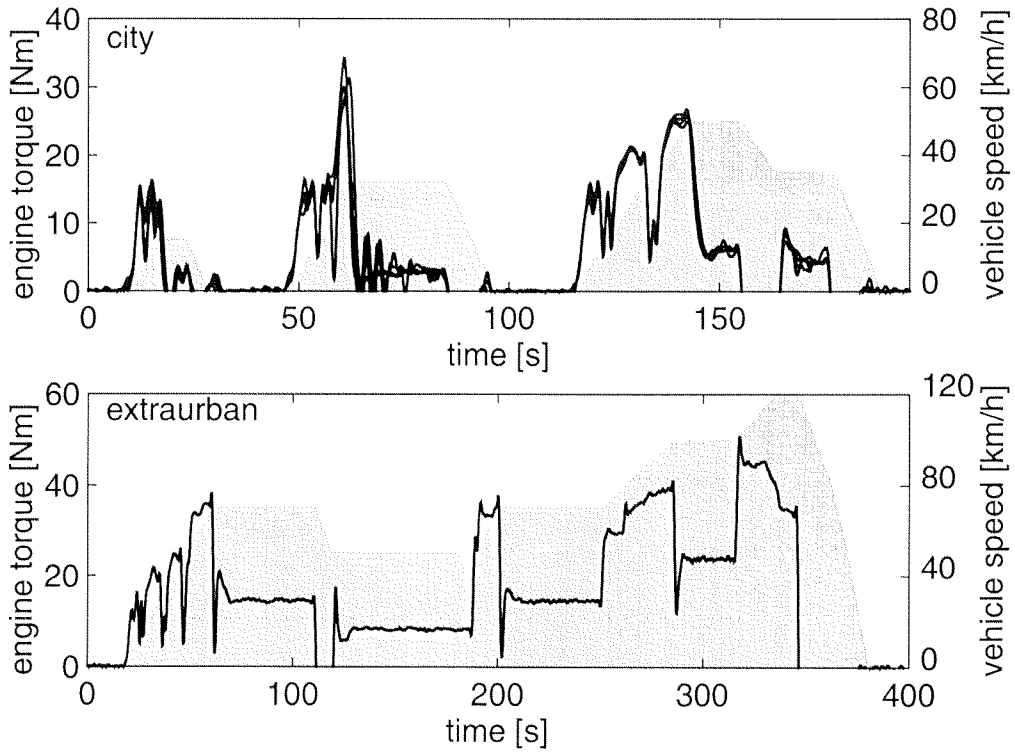


**Figure 4-8:** Measured engine torque

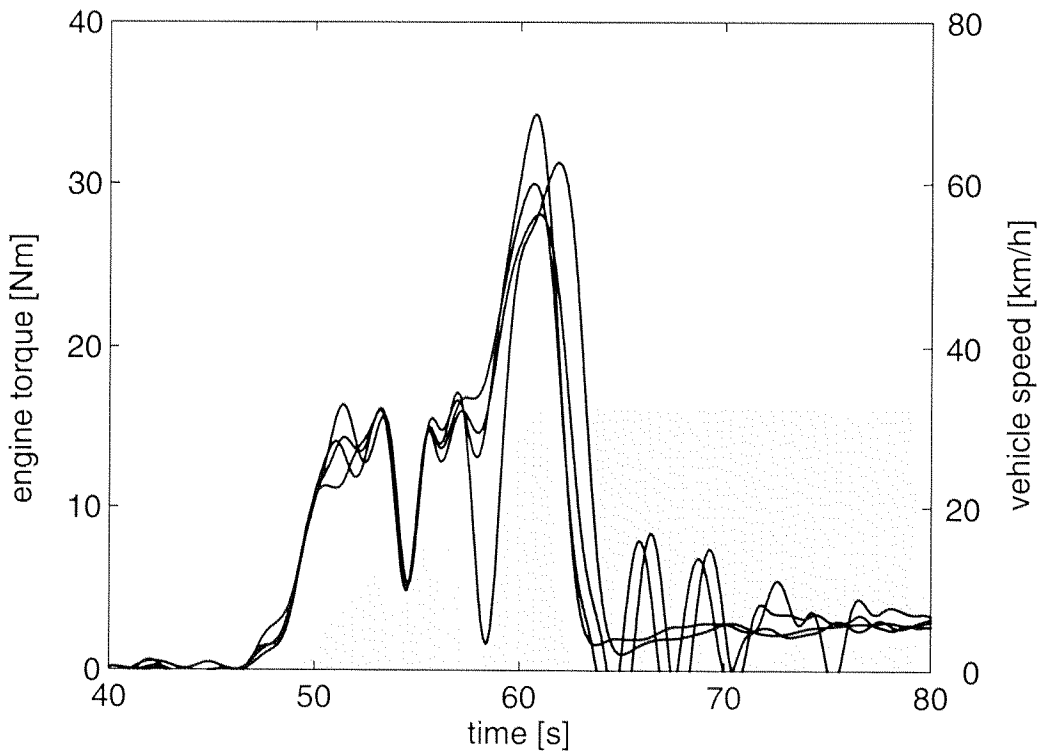


**Figure 4-9:** Measured engine torque (detail from Fig. 4-8)

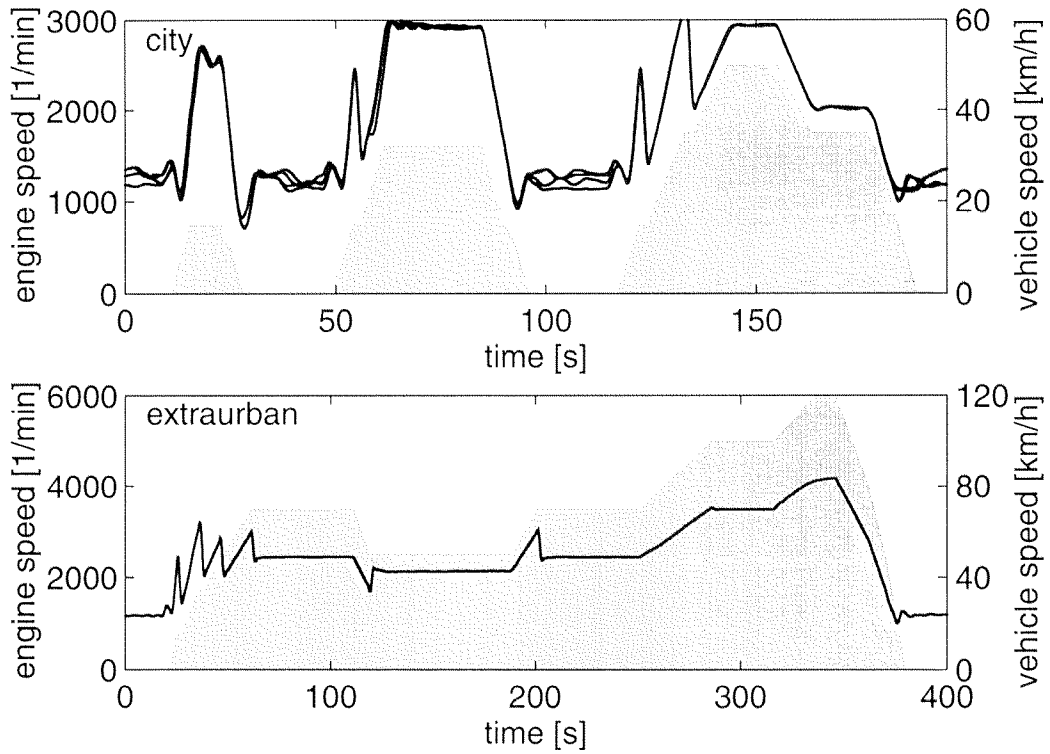


**Figure 4-10:** Measured engine speed

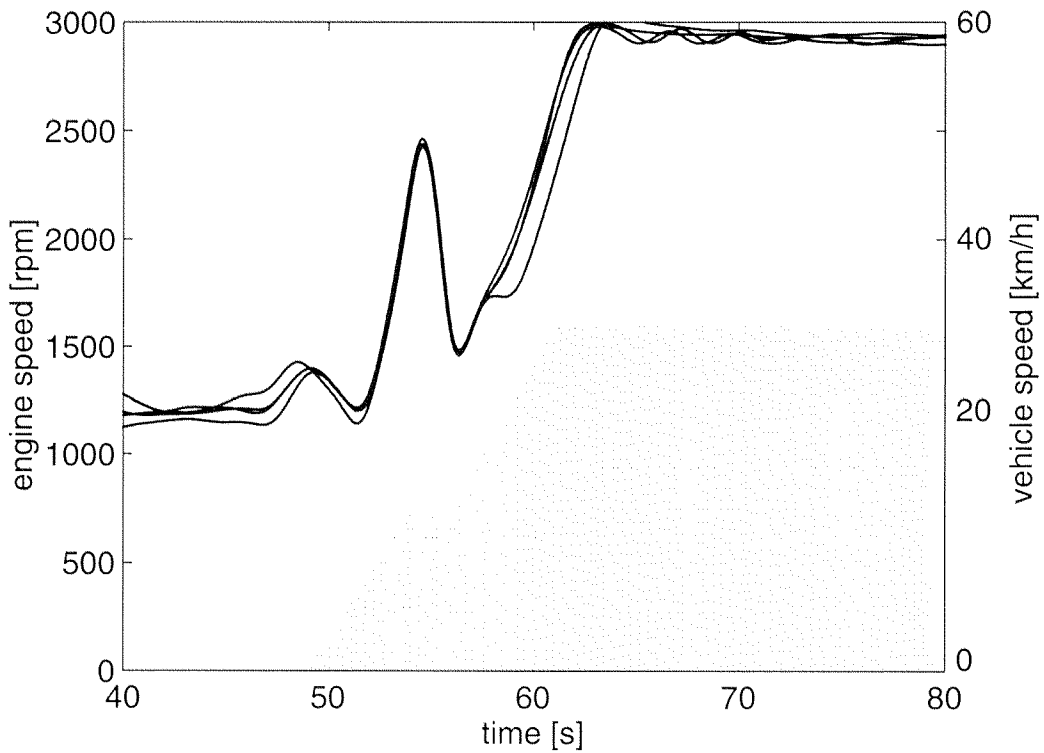


**Figure 4-11:** Measured engine speed (detail from Fig. 4-10)

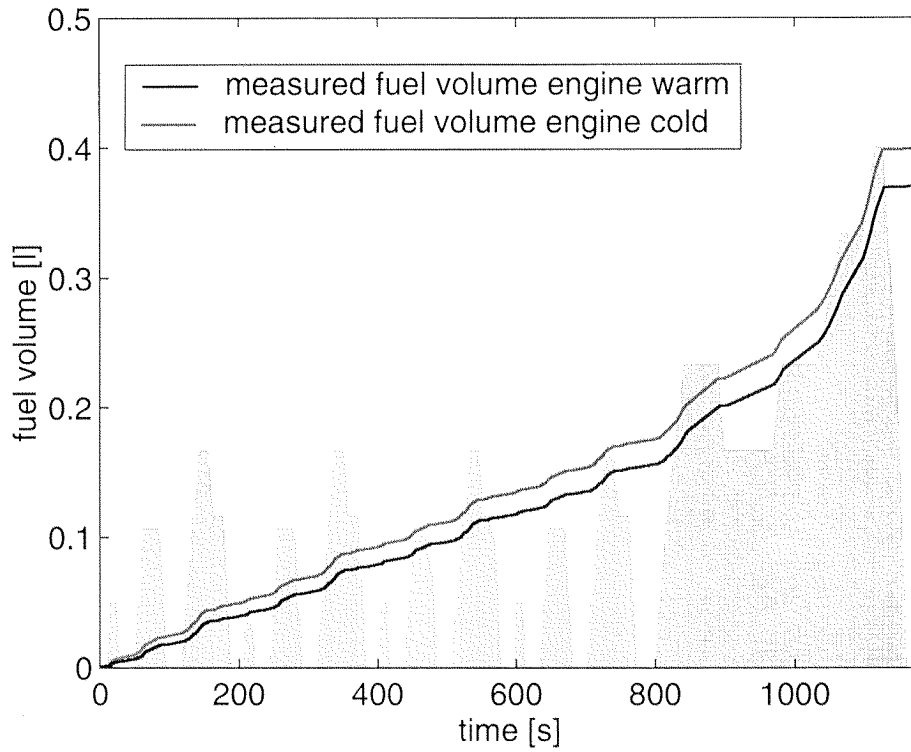


**Figure 4-12:** Measured fuel consumption (conventional configuration)

Seite Leer /  
Blank leaf

## **CHAPTER 5**

# **ENGINE THERMOMANAGEMENT BENEFITS**

Various measurements have been conducted in order to check the benefits in fuel economy of the proposed modifications in the cooling strategy. A particular focus has been given to engine cold-start and part-load operating conditions. Besides stationary measurements, experiments over predefined driving cycles have been performed. In this way it was possible to test the performance of the proposed configuration of the cooling system over a wide range of engine operating conditions.

### **5.1 Test bench settings**

The results presented in this chapter were obtained from various measurements conducted on a dynamic test bench. For all the measurements the same test bench and engine configuration were used.

For these tests the air-to-coolant radiator was substituted by a water-to-coolant heat exchanger. The water flow through the heat exchanger was chosen to be constant for all the operating points considered. Its value is equivalent to the air mass flow due to the wind that collides with the radiator when the vehicle moves at about 35 km/h.

For the measurements concerning the conventional as well as the improved configuration of the cooling system, the cooling pump used is electrically



actuated. When the conventional configuration is measured, the electrical pump conveys the same coolant mass flow as the corresponding mechanical pump (see Chapter 2.1.1). This permits a better comparison of the effective differences in the cooling pump energy demand for the two system configurations considered.

Almost all the accessories conventionally belt-driven by the engine are not implemented on the test bench. Namely no fan, generator, power steering pump, or air conditioning compressor are present on the test bench. Because of the absence of the alternator all the electrical accessories are supplied externally. This includes the engine electronics, ignition, injection, fuel feed pump, as well as the electrical coolant pump.

## 5.2 Engine cold start under stationary operating conditions

In Chapter 3 controllers for the coolant pump and for the bypass valve have been described. For the measurements of the improved cooling system the control structure includes both the feedback and the feedforward controller as explained in Section 3.6.

In a first step the performance of the cooling circuit is measured during engine cold start. In order to better isolate the effective influence of the modifications in the cooling strategy on the general system behaviour the stationary engine operating conditions are performed on the test bench. Three different engine operating points are considered, namely:

- Operating point OP1:  $n_{ICE} = 2500$  [rpm];  $bmep = 2$  [bar]
- Operating point OP2:  $n_{ICE} = 2500$  [rpm];  $bmep = 4$  [bar]
- Operating point OP3:  $n_{ICE} = 2500$  [rpm];  $bmep = 6$  [bar]

Fig. 1-6, pg. 10 shows that the heat flow removed by the coolant is almost constant for variations of the engine speed, while its variations due to changes in the engine load are greater. For this reason the measurements are carried out for different engine loads at constant engine speed.

### 5.2.1 Coolant temperature

A comparison between the temperature traces of the coolant leaving the engine for the conventional and the improved configuration of the cooling system for the three different engine operating points specified above is given in Fig. 5-1.

First, the temperature trace for the operating point  $n_{ICE} = 2500$  [rpm] and  $b MEP = 2$  [bar] is discussed. At start, the temperature slope is the same for the two configurations considered: indeed, the rapidity with which the coolant temperature rises results from the balance between the heat developed during combustion and the thermal capacity of the different parts of the engine (engine block as well as oil and coolant). Heat is removed from the system only by means of irradiation or of exhaust gas transport. In both configurations, in fact, the bypass valve is completely open, which means that the radiator is completely bypassed and no heat is removed from the system by the coolant. The fact that the coolant mass flow is massively different for the two systems considered has no direct influence on the coolant temperature slope as long as the radiator is fully bypassed. Indeed, since the mass of coolant contained in the bypassed cooling circuit is the same for the two system configurations, the influence of the coolant (or its thermal capacity) remains the same.

In the case of the conventional cooling system, the thermostat begins to open as soon as the coolant in which it is immersed reaches its activation temperature. In this case, the coolant temperature slope decreases until steady-state operating conditions are obtained. The steady-state temperature is clearly lower than the temperature desired. On the contrary, when the improved thermomanagement is active, the coolant temperature slope stays constant at the maximum value possible for the engine operating point considered until the desired temperature of the coolant leaving the engine  $T_{eng, out, DES} = 90$  °C is reached. The coolant temperature then remains stable due to the implementation of the feedforward controller.

An analysis of the two other engine operating points measured shows that the coolant temperature slope at start varies with the delivered torque since at those operating points more heat is produced during combustion while the engine thermal capacity remains the same.

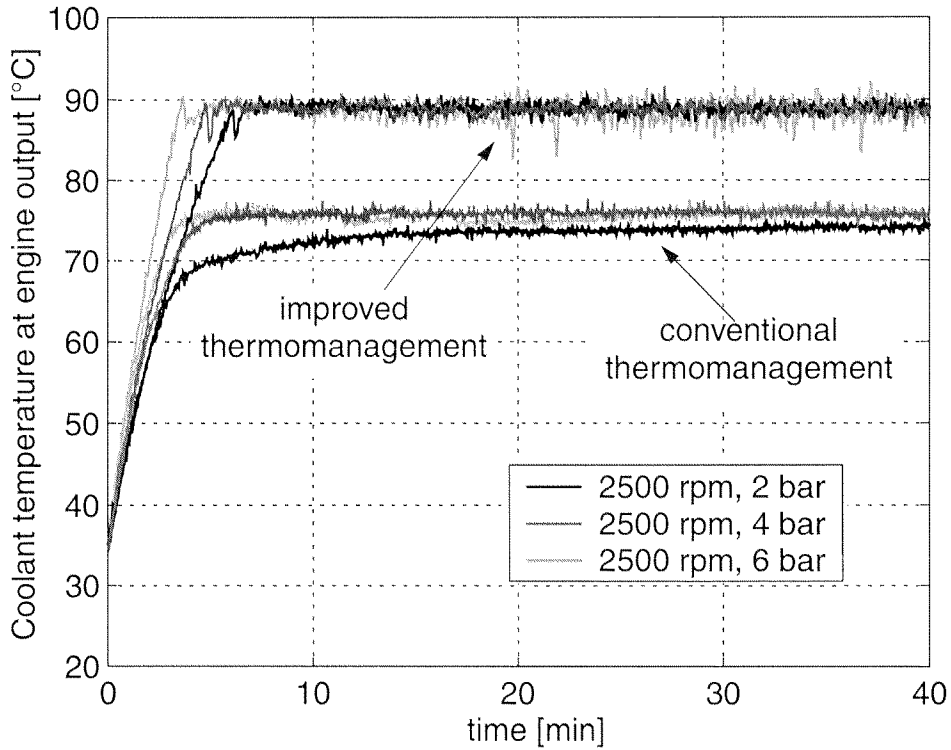


**Figure 5-1:** Coolant temperature at cold start

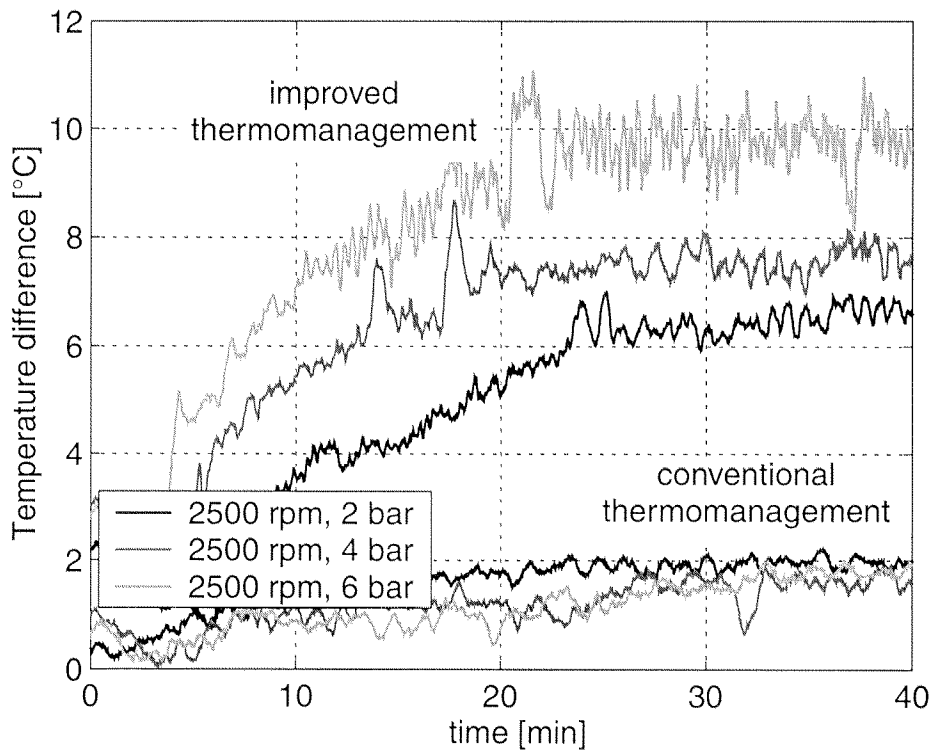


**Figure 5-2:** Coolant temperature difference  $T_{eng,out} - T_{eng,in}$  at cold start

The improved configuration of the cooling system permits to raise significantly the coolant temperature in thermal stationary conditions for all the operating points considered. The coolant temperature slope is the maximum possible for the operating point considered since the radiator is bypassed until the desired coolant temperature is reached. Because of the good performance of the controller designed the coolant temperature does not overshoot or have any limit cycles.

The temperature differences over the engine  $T_{eng, out} - T_{eng, in}$  for the various measurements are plotted in Fig. 5-2. The results show that the temperature difference over the engine not only is larger when the improved configuration of the cooling system is considered, but also that this value increases with increasing engine load. The heat to be removed by the coolant is:

$$\dot{Q}_c^* = c_{pc} \cdot \dot{m}_c^* \cdot \Delta T_{eng}.$$

In the proposed thermomanagement concept the coolant mass flow is reduced to a minimum in order to guarantee a temperature difference over the engine  $\Delta T_{eng}$  of 15 °C. Nevertheless, for the engine operating points considered, the coolant mass flow calculated is lower than the minimum flow measurable. Therefore, for the three operating points considered, if the coolant mass flow is set to the minimum value measurable, the temperature difference over the engine is lower than 15 °C and remains proportional to the engine load.

### 5.2.2 Oil temperature

One of the goals of improving the engine thermomanagement is the reduction of engine internal friction losses. This target can generally be reached by increasing the oil and the engine component temperatures. As a direct consequence, the oil viscosity drops causing a reduction in the engine losses, as visible in eq. (2.19).

Results from the measurements conducted on the test bench are presented in Fig. 5-3. The initial oil temperatures do not coincide for all the measurements taken. For one, the measurements are not conducted on a temperature conditioned test bench. It is therefore not possible to always provide the identical initial thermal conditions. In addition, since the measurements are performed over a period of time of several weeks, changes in the ambient temperature are inevitable. However, these differences do not affect the overall results.

In order to still establish a homogeneity in the comparison criteria for all the test, all the measured values are compared starting at the time at which the coolant temperature is 35 °C. The trajectories of the values of interest for the two configurations analysed are compared during the next 40 minutes. Over this period of time, both systems reach steady-state operating conditions for all the values considered. With this criterion, the start value of the oil temperature for the different measurements considered is not constant, as evident in Fig. 5-3. Nevertheless, the maximum variation in the oil temperature at the beginning of the measurements is lower than 10 °C. Various measurements of the same engine operating point (three to five) have proven that the value of the start condition does not affect the steady-state oil temperature.

The measurements show that by means of the improved engine thermomanagement it is possible to raise the temperature of the lubricating oil considerably ( $\Delta T_{oil} \cong 15$  °C for all the measured engine operating points in Fig. 5-3). For any chosen configuration of the cooling system the oil temperature strongly varies as a function of the engine operating point, although the coolant temperature remains almost constant.

### 5.2.3 Fuel consumption

The reduction in fuel consumption achievable with the proposed configuration of the engine thermomanagement is the central point of this thesis work. Fig. 5-4 shows the fuel mass flows obtained from the conventional and the proposed configuration of the cooling system when the engine is operated with constant speed  $n_{ICE} = 2500$  [rpm] and with a constant mean effective pressure  $b_{mep} = 2$  [bar].

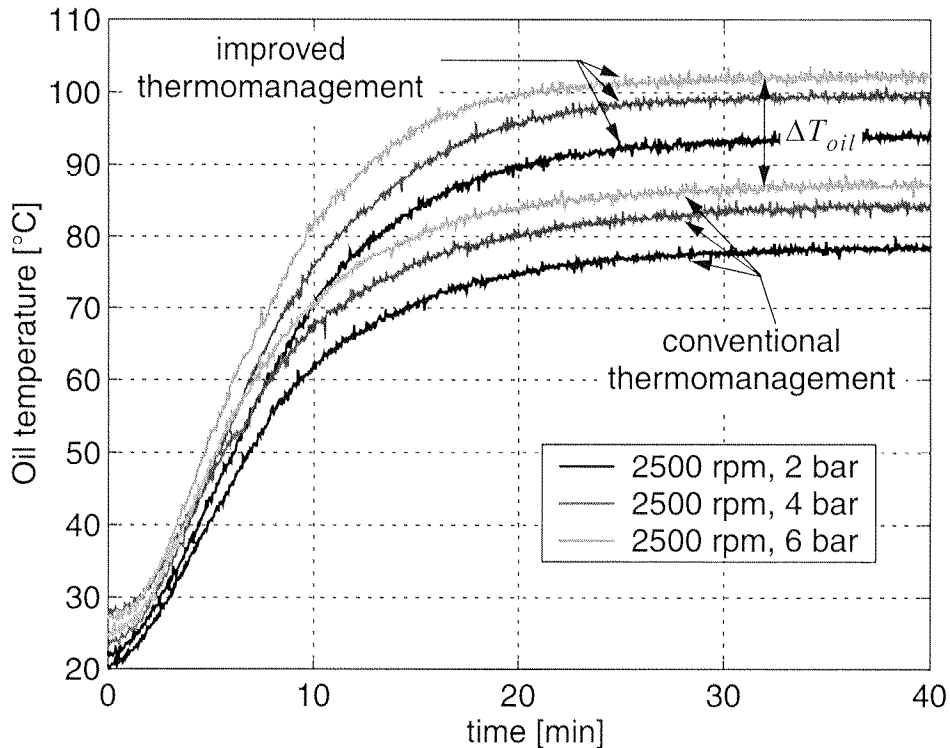


**Figure 5-3:** Oil temperature at cold start (various operating points)

In the first part of the tests the engine thermal conditions, namely coolant and oil temperature, almost coincide (cf. Figs. 5-1 and 5-3). For each of the operating points initially considered the differences between the fuel consumption obtained for the two different system configurations studied thus are insignificant, as shown in Fig. 5-4. Only when coolant and especially oil temperatures diverge (a few minutes after the tests start) the fuel mass flow of the improved cooling system is lower than the one of the conventional system. The slight increase in fuel consumption at about 4 minutes after start is due to Exhaust Gas Recirculation (EGR). This reproducible phenomenon is caused by the particular configuration of the exhaust tract and by the pressure wave supercharger. Since a comparison between two configurations of the cooling systems is analysed here, a reproducible increase of the fuel consumption over a limited period of time does not affect the validity of the results.

The reduction in fuel consumption visible here is only due to the different engine thermal conditions. Indeed, since the coolant pump in both cases is electrically driven and since the electrical power is supplied externally and not

produced by the internal combustion engine by means of an alternator, differences in the coolant pump energy supply are not included in the fuel consumption.

When engine cold start is considered, the fuel consumption is higher than in steady-state *warm* operating conditions, as Fig. 5-4 shows. The following aspects contribute to the additional fuel consumption:

- worse indicated efficiency  $\eta_{ig}$  because of incomplete combustion and higher heat losses over the cylinder walls
- decreased air-to-fuel ratio  $\lambda_{A/F}$  (enrichment during cold start)
- increased mechanical friction  $mp_{if}$  due to higher oil viscosity.

The fuel mass flow is therefore:

$$\dot{m}_f^* \propto \frac{1}{\eta_{ig}} \cdot mip_g \cdot n_{ICE} \cdot \frac{1}{f(\lambda_{A/F})}, \quad (5.1)$$

with  $mip_g = mep + mp_{if} + mp_{gexch}$ .

The following considerations help to explain the variation in fuel consumption for different engine operating temperatures. Eq. (5.1) can be formulated for two different engine thermal conditions, namely *cold* and *warm* for the conventional and for the improved configuration of the cooling system, respectively. The fuel mass flow variations between *cold* and *warm* engine depending on variations of the influence parameters of eq. (5.1) can therefore be expressed as follows, where the index 0 indicates the warm steady-state conditions (eq. (2.17), pg. 32):

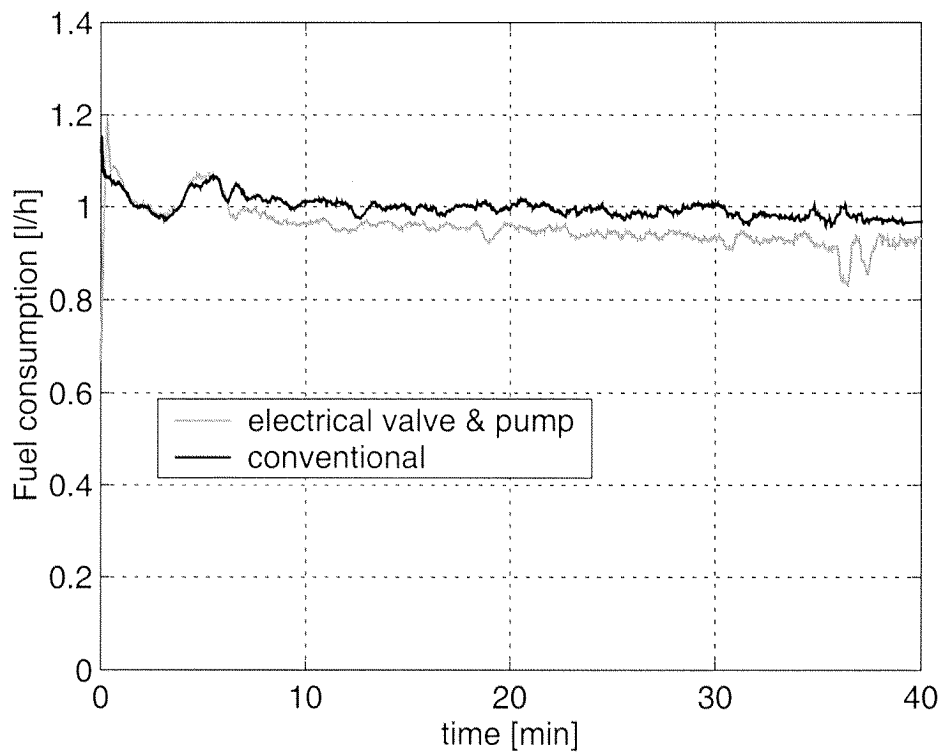


**Figure 5-4:** Fuel mass flow during cold start (2500 rpm, 2 bar)

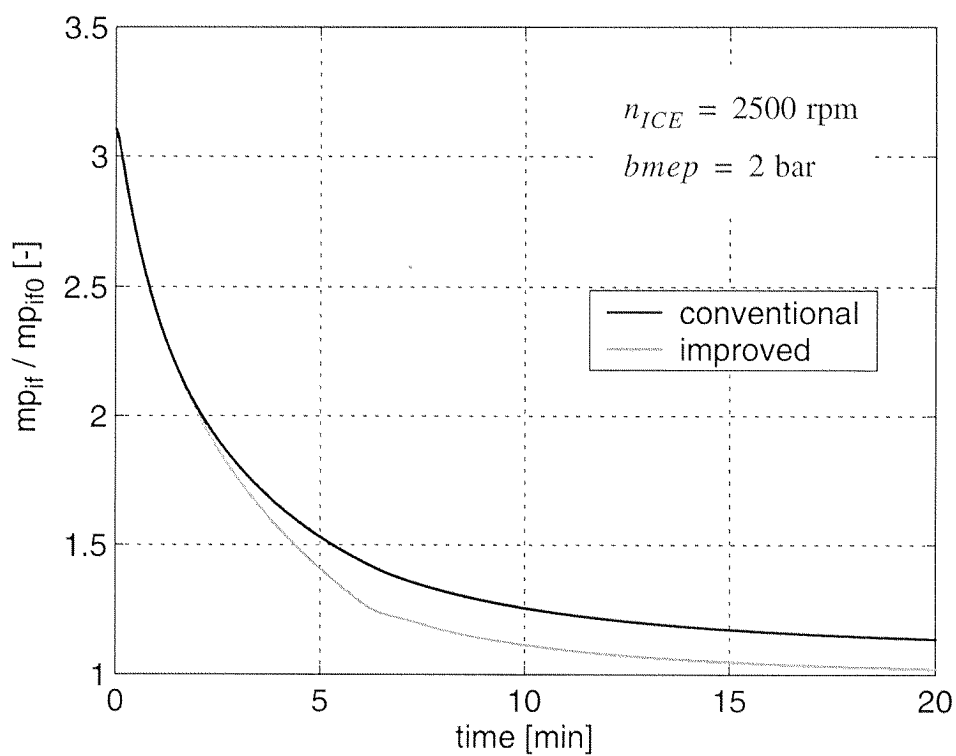


**Figure 5-5:** Relative mean pressure from internal friction at engine cold start



$$\Delta \dot{m}_f^* \propto n_{ICE} \cdot \left[ mep \cdot \left( \frac{1}{\eta_{ig} \cdot f(\lambda_{A/F})} - \frac{1}{\eta_{ig0} \cdot f(\lambda_{A/F0})} \right) \right. \\ \left. + \frac{mp_{if}}{\eta_{ig} \cdot f(\lambda_{A/F})} - \frac{mp_{if0}}{\eta_{ig0} \cdot f(\lambda_{A/F0})} + \frac{mp_{gexch}}{\eta_{ig} \cdot f(\lambda_{A/F})} \right. \\ \left. - \frac{mp_{gexch0}}{\eta_{ig0} \cdot f(\lambda_{A/F0})} \right] \quad (5.2)$$

Eq. (5.2) can be simplified considering that, as measured, the air-to-fuel ratio is quite rapidly brought to the steady-state value by the air/fuel ratio controller ( $f(\lambda_{A/F}) \cong const$ ), that the cylinder wall temperature a few minutes after start reaches values near its steady-state conditions ([42]), and that after a few cycles the combustion proceeds regularly ( $\eta_{ig} = const$ ). Since the engine is operated at constant load, the first part of eq. (5.2) is zero. Considering that the mean pressure for the gas exchanges  $mp_{gexch}$  is proportional to the difference between the ambient pressure  $p_{amb} \approx 1$  and the pressure in the intake manifold  $p_m \approx 0.06 \cdot mip_g + 0.2$ , we obtain:

$$mp_{gexch} \approx 0.8 - 0.06 \cdot (mep - mp_{if}), \quad (5.3)$$

$$mp_{gexch} - mp_{gexch0} \approx 0.06 \cdot (mp_{if} - mp_{if0}), \quad (5.4)$$

since the engine is assumed to deliver constant torque over the whole engine cold start process. As evident from eq. (5.4), the effects of variations in the work for the gas exchanges ( $mp_{gexch} - mp_{gexch0}$ ) can be neglected if compared with the effect of the work for internal friction ( $mp_{if} - mp_{if0}$ ). Neglecting the effect of variations in the work for the gas exchanges in eq. (5.2), the variation in the fuel consumption between warm and cold engine is therefore affected only by the internal friction term:

$$\Delta \dot{m}_f^* \propto mp_{if0} \cdot \left( \frac{mp_{if}}{mp_{if0}} - 1 \right). \quad (5.5)$$

The correlation between the mean pressure due to internal friction in cold and warm engine conditions has already been expressed in eq. (2.19), pg. 33 as a function of the oil and coolant temperatures ([24], [42]). The mean pressure needed to overcome internal friction has been calculated based on eq. (2.19) for the conventional and the improved engine thermomanagement during cold start at constant  $n_{ICE} = 2500$  [rpm] and constant  $b MEP = 2$  [bar]. The correlation between this value in cold and warm (steady-state) engine conditions is shown in Fig. 5-5 above. Clearly, the internal friction not only drops with the progress of engine warm-up, but the effect of higher coolant and oil temperatures on the system is shown as well when the engine works in steady-state operating conditions.

Thirty minutes after engine start the engine reaches its thermal stationary conditions, as the coolant and oil temperature trajectories in Figs. 5-1 and 5-3 evidence. When the average fuel flow under thermal stationary operating conditions during a defined interval of time is considered (here 10 minutes), the effect of the different coolant and engine component temperatures on fuel consumption can be clearly seen. The fuel consumption values for each of the stationary operating points considered for the conventional and the improved configuration of the cooling system are summarised in Table 5-1.

The benefits in terms of fuel consumption obtained with the improved configuration of the cooling system can be compared when tests of defined duration are compared. For this purpose cold-start tests lasting 40 minutes have been performed for all three engine operating points analysed and for both configurations of the cooling system. The integral fuel consumption data over the duration of these tests are plotted in Fig. 5-6. For each configuration of the cooling system and engine operating conditions various cold-start tests have been performed and the mean value of the integral fuel consumption 40 minutes after start has been calculated. Based on these measurements the fuel consumption reduction data obtained for each operating point are shown on the right margin of Fig. 5-6.

The oil temperature for both configurations considered depends on the engine load, as visible in Fig. 5-6. Nevertheless, the correlation of the oil temperature with the entity of the internal friction and, as a consequence, of the fuel consumption are not linear, as eq. (2.19), pg. 33 expresses. An improve-

**Table 5-1:** Stationary engine operating conditions [30...40min]

Engine operating point	System config.	Coolant temp. [°C]	Oil temp. [°C]	Mean fuel consumpt. [l/h]	Fuel consumpt. reduction
2500 rpm 2 bar	Convent.	74	78	1.005	7.4%
	Improved	89	94	0.93	
2500 rpm 4 bar	Convent.	75	84	1.39	3.6%
	Improved	89	99	1.34	
2500 rpm 6 bar	Convent.	75	87	1.93	3.1%
	Improved	89	102	1.87	

ment of the oil temperature and a decrease of the engine internal friction is therefore more effective for low engine loads than for higher ones, as the results on the right margin of Fig. 5-6 show.

#### 5.2.4 Water pump energy demand

The proposed configuration of the coolant systems is designed such as to guarantee that only the minimum coolant mass flow needed to maintain a temperature difference over the engine of 15 °C is pumped through the system. On the other hand, in the conventional configuration of the cooling system, the mass flow is only proportional to the engine speed and large enough to guarantee a sufficient heat removal at full load. When the two different configurations are compared the coolant mass flow as well as the cooling pump energy demand are considerably different, especially when part-load operating conditions are considered. The cooling pump energy demands for the cold start measurements performed are shown in Fig. 5-7. The correlation between the quantity of coolant flowing in the cooling circuit and the energy demand of the considered pump is shown in Fig. 2-2, pg. 19.

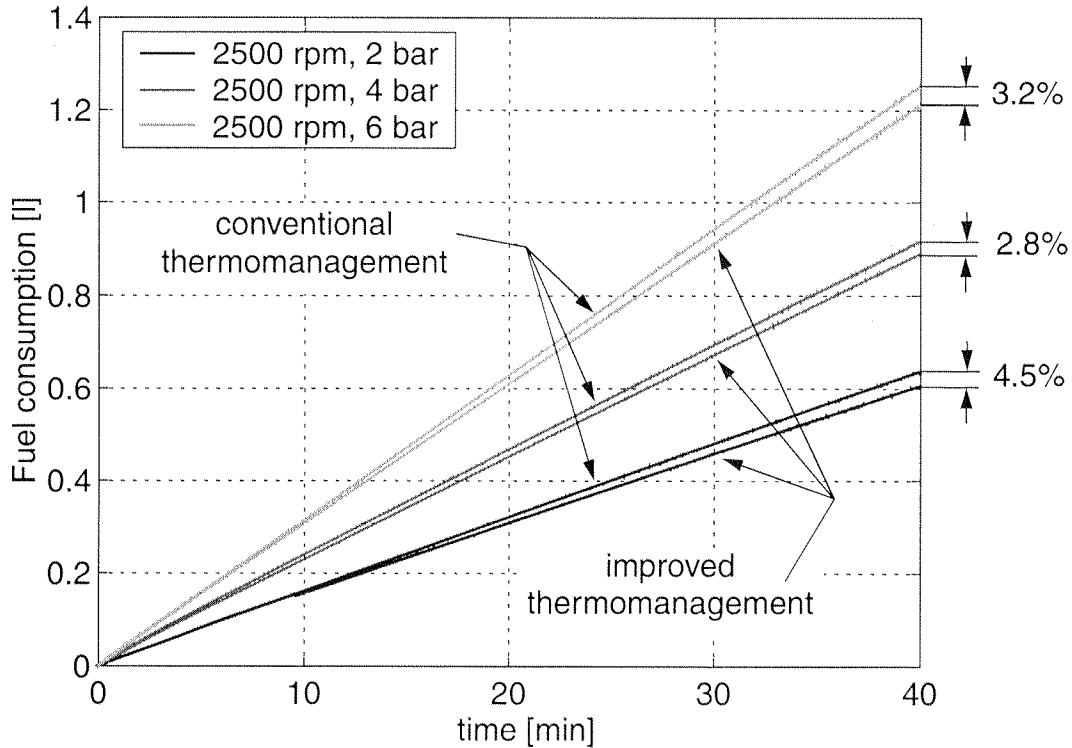


**Figure 5-6:** Global fuel consumption at cold start for various operating points

Since in all the test bench measurements the electricity needed for driving the cooling pump is provided by an external source rather than by an alternator belt-driven by the internal combustion engine, the energy demand of the pump is not included in the fuel consumption data shown in Figs. 5-4 and 5-6.

Nevertheless, when the total energy demand of the engine is analysed, the efficiency of the energy supply to the cooling pump has to be considered as well. Although the energy demand of the conventionally mechanically driven cooling pump is higher, the fact that the pump is belt-driven by the engine permits efficiencies higher than 90% in the energy transfer from the engine to the cooling pump. On the other hand, when an electrical pump is used, transmission efficiencies lower than 60% are typical due to the fact that the alternator first has to transform mechanical into electrical energy.

For most of its lifetime a vehicle typically is required to operate at mild ambient temperatures under part-load conditions only, as for example in urban traffic. Except for critical thermal conditions, e. g. while driving uphill at full-

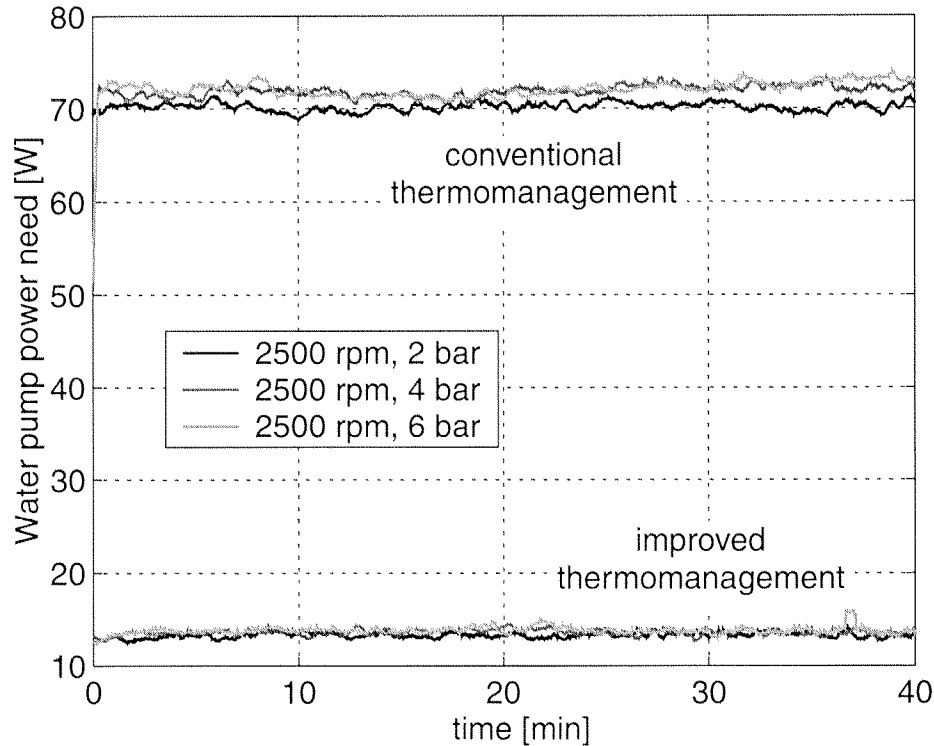


**Figure 5-7:** Power demand of the water pump at cold start

load uphill, the energy demand on the combustion engine from the electrical cooling pump is significantly lower for the proposed configuration of the cooling system than for the conventional one.

When the energy needed for the cooling pump supply is obtained by recuperation of kinetic energy during braking phases, the advantages of an electrical cooling pump are even more evident. In this case, whenever the vehicle slows down, the energy needed for driving the electrical cooling pump would otherwise be dissipated as heat.

### 5.3 MVEG-A test cycle

The cold-start measurements at constant engine speed and load discussed above best show the effects of modifications in the thermomanagement on coolant and oil temperatures as well as on the fuel and global energy consumption. Nevertheless, the validation of the suggested strategy in real or at

least standardized operating condition gives a better estimation of the effective fuel consumption reduction achievable. The two configurations of the cooling system have been tested while emulating the European MEVG-A driving cycle. In both cases *engine cold start* conditions are considered.

The air-to-coolant radiator is substituted with a water-to-coolant heat exchanger. During all the tests the valve that controls the water flow to the heat exchanger maintains a constant position. The water flow through the water-to-coolant exchanger is therefore constant. For the system this is equivalent to a radiator being exposed to a constant air flow. A constant vehicle speed is therefore simulated, which is a sufficient approximation of reality.

Fig. 5-8 shows the coolant and oil temperatures during the MVEG-A test cycle for the two configurations of the cooling system considered. Due to the absence of a conditioned test bench it is not possible to exactly reproduce the initial thermal conditions from one test to another. However, these temperature differences of the coolant and the oil between the two tests performed are so small as to not substantially affect the results. During the first test minutes the coolant temperature is almost the same in both tests. In the conventional configuration of the cooling system the situation changes when the thermostat first reaches its activation temperature. The course of the coolant temperature makes it evident how the delays between the coolant temperature variation and the progressive phase change of the wax (which determines the valve opening position) act on the system. Indeed, the coolant temperature increases with high gradients when the engine load increases, while it drops abruptly when the engine idles.

In contrast, when the improved configuration of the cooling system is considered the coolant temperature increases steadily until the desired temperature of 90 °C is first reached. In this phase the temperature gradient is proportional to the heat developed during combustion since the radiator is completely bypassed and no heat is removed from the system by the coolant (cf. Fig. 1-6, pg. 10).

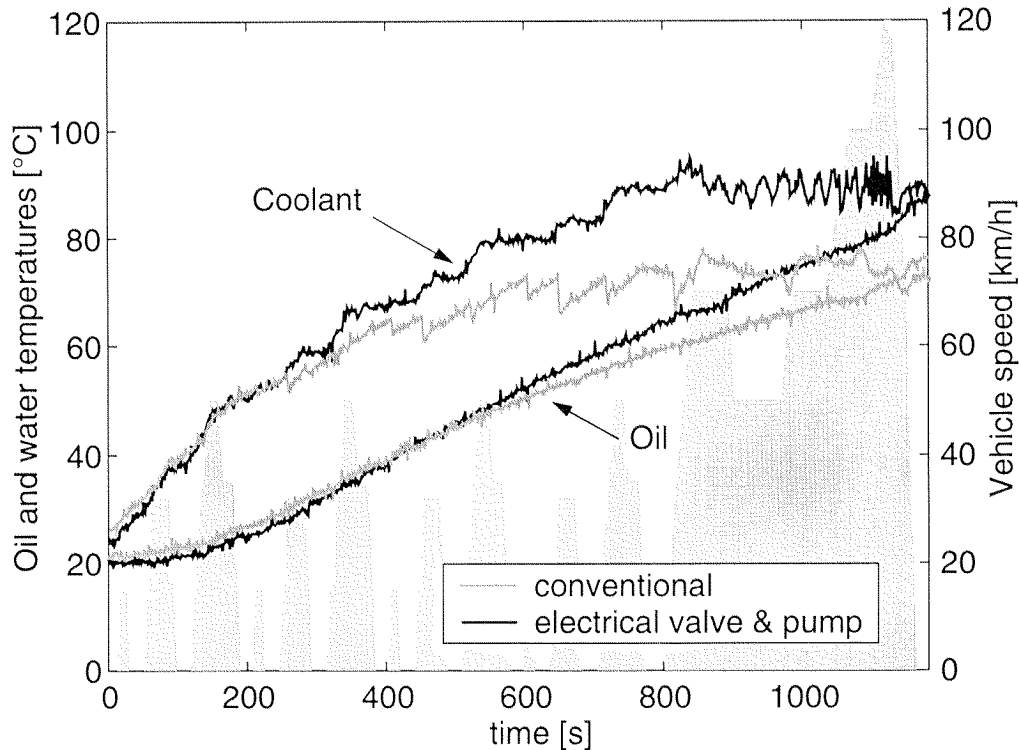


**Figure 5-8:** Coolant and oil temperatures during cold MEVG-A cycle

In essence, the modification of the cooling strategy permits to raise the coolant temperature and to reach the desired level in the shortest time possible. Analogous considerations are valid for the oil temperature course as plotted Fig. 5-8.

Extending the results of these tests to the global thermal efficiency of the two systems it is interesting to compare the coolant temperature difference over the engine during the whole cycle as plotted in Fig. 5-9 and the pump energy demand as plotted in Fig. 5-10.

In the conventional configuration of the cooling system the need of removing more heat from the system during thermally demanding engine operating conditions is characterised by high mass flows and a low temperature difference over the engine. On the other hand, when the improved cooling system is applied to the engine the coolant mass flow is maintained at a minimum until the maximal temperature difference over the engine is reached. Only in this case the coolant mass flow is increased. The reduction in the energy demand

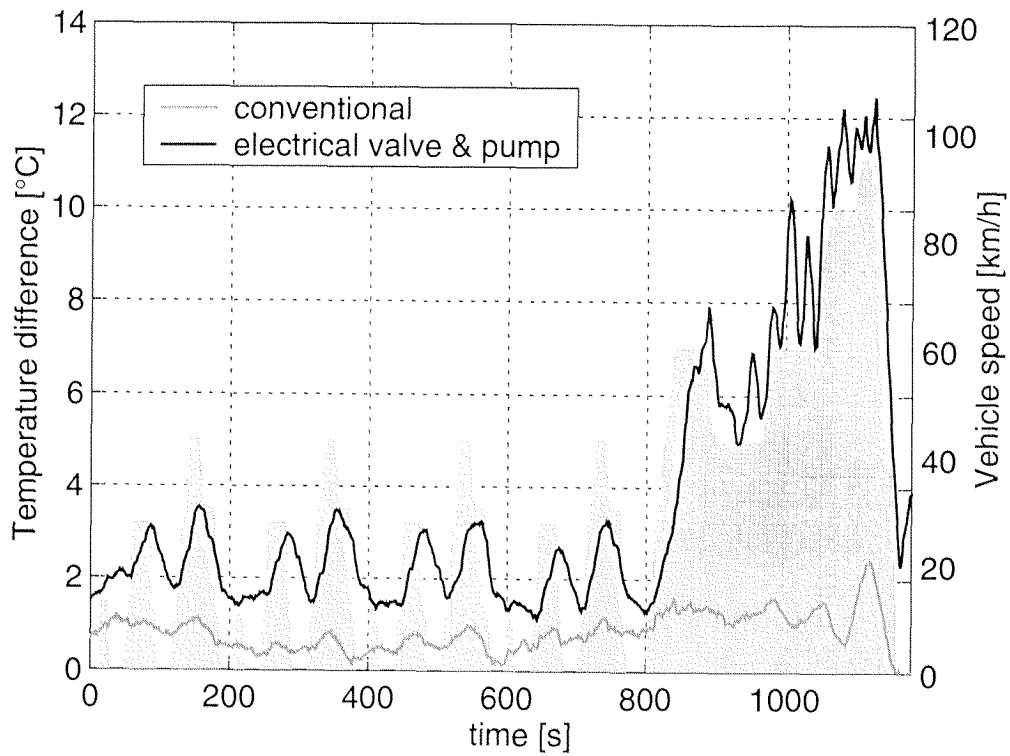


**Figure 5-9:** Coolant temperature difference over the engine

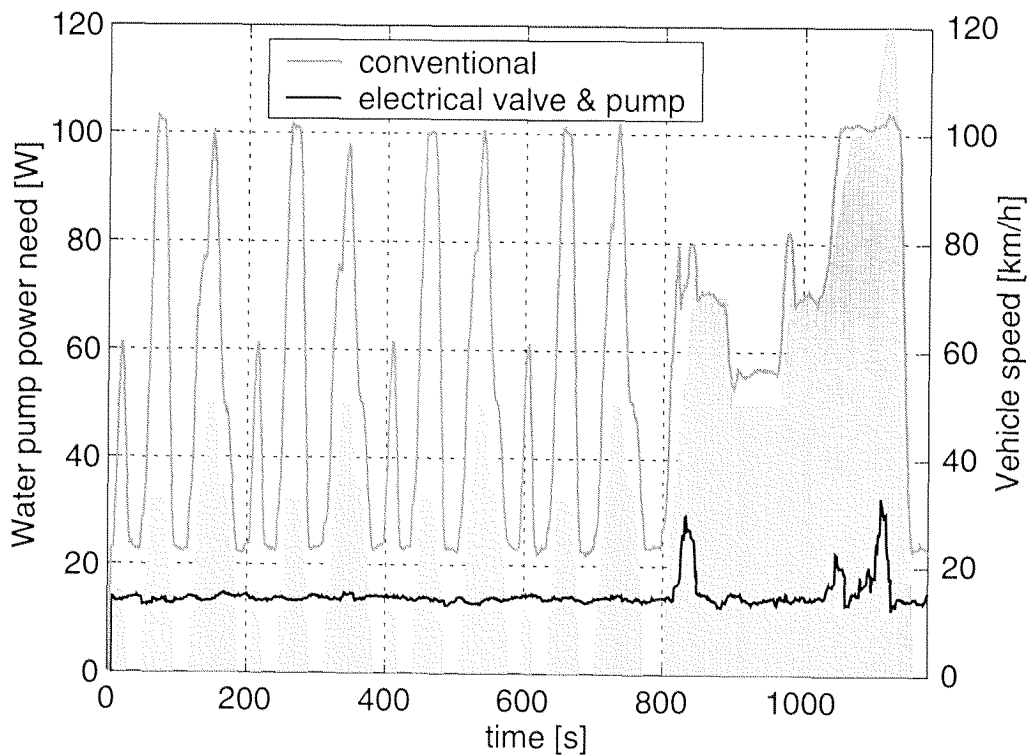


**Figure 5-10:** Water pump power demand during cold MVEG-A cycle



for the cooling pump can be clearly seen in Fig. 5-10. Again, as with the engine cold start at a constant engine operating point described above, the reduction in the pump energy demand obtained with the proposed configuration of the cooling system does not affect the global fuel consumption since the cooling pump is driven externally.

Finally, Fig. 5-11 shows the global fuel consumptions for the two configurations considered. A fuel consumption reduction of 3% over the whole cycle was measured. Once more, the integral fuel consumption of the two different configurations tested starts to diverge significantly when oil and coolant temperatures differs.

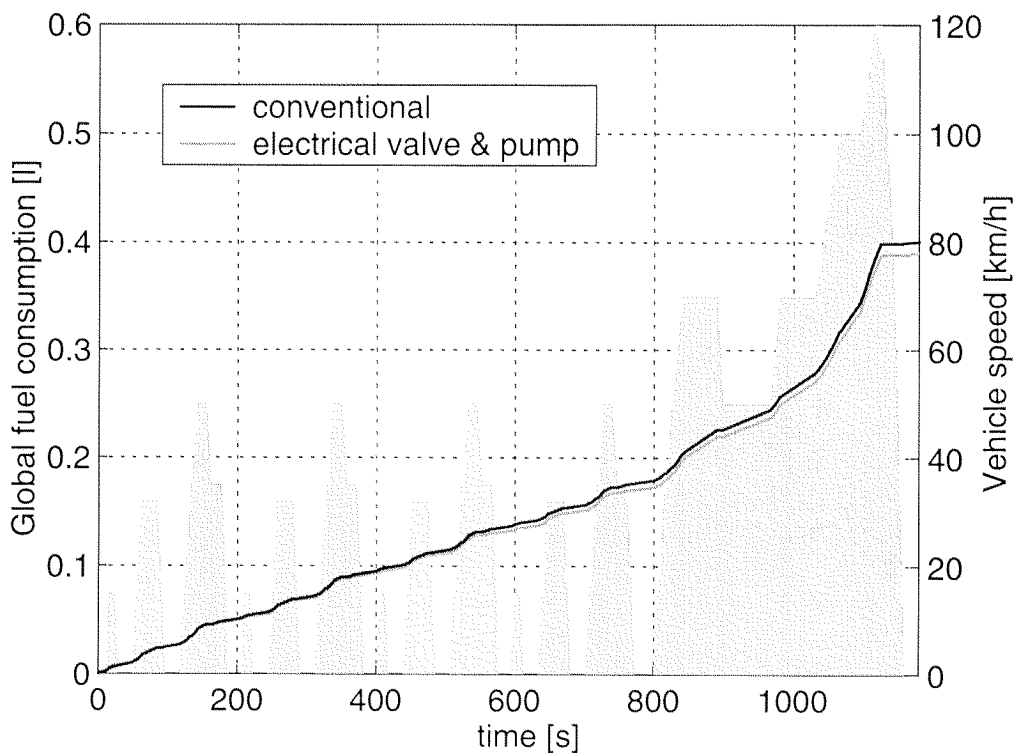


**Figure 5-11:** Global fuel consumption during cold MVEG-A cycle

## 5.4 Error estimation

All the measurements taken are used to compare the influence of different cooling system configurations on the fuel consumption. The accuracy and the precision of the measurements taken are therefore quite important. For each test three to five different measurements were taken.

In the following the error typical of measurements of the integral fuel consumption is defined. The term  $\Delta FC$  designates the difference in fuel consumption over a defined period of time (e.g. 40 minutes as plotted in Fig. 5-6) for the conventional and the improved configuration of the cooling system:

$$\Delta FC(t) = (FC_{conv}(t) - FC_{impr}(t)), \quad (5.6)$$

In order to guarantee the validity of the results the measurement error for each measurement must be considerably smaller than the reduction in fuel consumption obtained:

$$\max(\text{error}(FC_{conv}(t), FC_{impr}(t))) \ll \Delta FC(t). \quad (5.7)$$

Considering the integral fuel consumption over a defined period of time, there may be three different sources of systematic and random measurements errors:

- engine torque  $\varepsilon_T$ ,
- engine speed  $\varepsilon_n$ ,
- fuel flow  $\varepsilon_{FC}$ .

Appendix C contains the error definition, its calculation for these measurements, as well as the results for each operating point.

The relative error of the integral fuel consumption results from the sum of each of these errors:

$$\varepsilon = \varepsilon_T + \varepsilon_n + \varepsilon_{FC}. \quad (5.8)$$

For eq. (5.8) the relative errors  $\varepsilon_T$ ,  $\varepsilon_n$ ,  $\varepsilon_{FC}$  of each measured value are consistent, which yields a conservative estimation of the relative error in the measurement of integral fuel consumption. Table 5-2 lists the estimations of the integral fuel consumption for different engine operating points as obtained during cold start experiments.

**Table 5-2:** Results from different measurements and error estimation

Engine operating point	System configuration	Integral fuel consumption after 40 min [l]	Relative error [%]	Confidence interval [l]
2500 rpm 2 bar	Conventional	0.640	1.2	$\pm 0.0038$
	Improved	0.611	0.94	$\pm 0.0029$
2500 rpm 4 bar	Conventional	0.915	0.78	$\pm 0.0036$
	Improved	0.889	0.71	$\pm 0.0032$
2500 rpm 6 bar	Conventional	1.252	0.52	$\pm 0.0032$
	Improved	1.211	0.44	$\pm 0.0027$

For all the measurements of integral fuel consumption the confidence error amounts to ca. 10% of the fuel consumption reduction obtained for the two different configurations of the cooling systems. According to eq. (5.7), it is therefore demonstrated that the fuel consumption measurements are precise enough for a valid comparison between the two configurations of the cooling system.

## CHAPTER 6

### CONCLUSIONS AND OUTLOOK

The engine cold start experiments performed for stationary engine operating conditions as well as for the standard European Test Cycle MVEG-A have shown that by improving engine thermomanagement the fuel consumption can be reduced substantially. The measurements particularly focus on part-load engine operating conditions, namely the conditions for which the conventional configurations of the cooling system are not ideally suited. Indeed, they are designed to guarantee an adequate heat removal under critical thermal conditions, normally reached only at engine full-load operation and during 3 to 5% of the global vehicle lifetime ([1], [49], [50]).

The proposed configuration of the cooling system in the first place yields a more flexible cooling system and shortens the system time constants. Both targets are obtained by actively controlling the temperature of the coolant that leaves the engine. In addition, the possibility of independently limiting the temperature of the coolant entering the engine opens up new perspectives. In conventional applications only the first of these two temperature levels is controlled by a proportional controller (the solid-to-liquid wax actuator) characterized by a considerable time constant (ca. 30 seconds). Since this system configuration must guarantee that even under high thermal loads the coolant temperature difference over the engine does not exceed limits critical for the thermal stress of engine components and since it must reduce the eventuality of temperature overshoots, conservative operating strategies are needed. This causes engine overcooling at part-load operating conditions and at engine cold start.

The realization of a combined feedback and feedforward control structure permits to improve system response time as well as robustness. The feedforward control structure includes a model based estimator for the engine block as well as for the cylinder wall temperature for both the electrical bypass valve and the cooling pump. This leads to almost negligible temperature overshoots at engine cold start as well as to just a small temperature limit cycle or none at all during stationary operating conditions.

The reduction in fuel consumption measured on the test bench at cold start under stationary engine operating conditions varies between 2.8 and 4.5% of the value obtained with an engine of the conventional design. The fact that the reduction in fuel consumption obtained for engine cold start during the MVEG-A test cycle also amounts to 3% of the consumption obtained with a conventional configuration of the cooling circuit is significant as well. Better yet, those results can be extended to other test cycles. Indeed, as Figs. 5-1 and 5-3 for stationary engine operating conditions and Fig. 5-8, pg. 110 for the MVEG-A test cycle clearly show, the effective engine operating point only marginally affects the trajectories of coolant and oil temperatures during engine cold start.

At stationary engine operating conditions alone, the reduction in fuel consumption is even more evident, especially for very low engine loads. As displayed in Table 5-1, pg. 106 the reduction then varies between 3.1% and 7.4%. Compared to such complex measures as vehicle mass reduction or internal engine improvements to reduce fuel consumption, the low cost as well as the simplicity and flexibility of implementing the solution proposed here is very convincing.

The results obtained can be also extrapolated to larger SI engines of different sizes. Since for small SI engines as the one considered in the present work the ratio of coolant heat flow over the brake power is higher than for SI engines with larger displacements ([41], Ch. 12), the percentage in the reduction of fuel consumption due to variations of the coolant temperature might therefore diminish for larger SI engines.

The proposed configuration of the cooling system permits to considerably reduce the coolant mass flow and therefore the energy needed by the pump. For the experiments conducted in both configurations of the cooling system the power to the cooling pump is externally supplied. This implies that the reduction in the energy need of the pump is not reflected in the global fuel consumption. In conventional configurations the cooling pump is directly belt-driven by the engine, with efficiencies of around 95%. This value is much higher than the 60 to 80% achievable with an electrical cooling pump, where the alternator first has to transform the energy from the engine from mechanical to electrical. However, the global energy needed by the electrical cooling pump still is considerably lower than that required by the mechanical pump. At part-load operation, the required energy can be reduced by a factor of six.

The advantage of operating the cooling pump as well as other auxiliaries electrically is evident when the possibility of recuperating vehicle kinetic energy during the braking phases is considered. Indeed, the recuperated energy can be used for supplying the auxiliary devices. Furthermore, the possibility of integrating air conditioning system, catalyst heating devices, secondary heaters, and other devices in the thermomanagement enables the development of new strategies aiming at the reduction of fuel consumption and emission.

Seite Leer /  
Blank leaf

## Appendix A

### EMULATION PARAMETERS

#### A.1 MVEG-A test cycle

The European Directive 70/220/ECE prescribes a test cycle known as MVEG-A cycle ([68]) or NEDC. For a vehicle with a manual shift gear box, the gear ranges are prescribed. The velocity profile as well as the prescribed gears are shown in Fig. A-1.

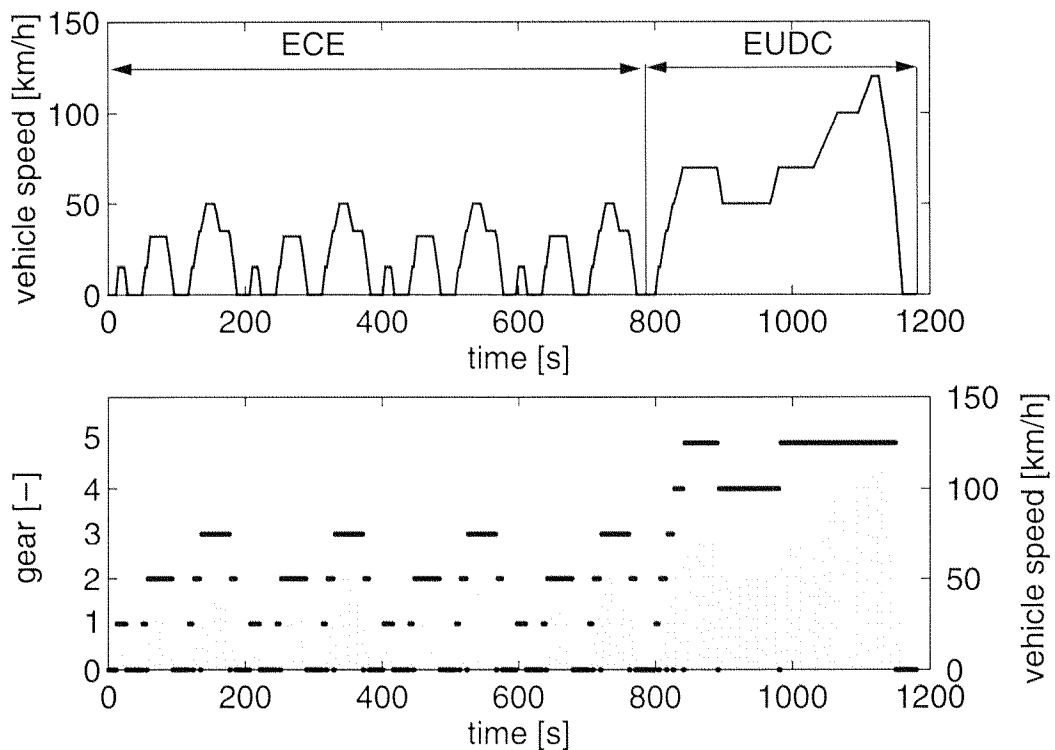


**Figure A-1:** Prescribed velocity and gears during MVEG-A test cycle



The cycle is also known as EC, ECE, EEC or EU test cycle. It consists of an urban part, known as ECE, and an extraurban part, also denominated EUDC. The whole cycle lasts 1180 seconds for a global course of 11.007 km at a mean velocity of 33.6 km/h.

## A.2 Vehicle parameters

Parameter	Symbol	Value	Unit
Vehicle mass	$m_v$	800	[kg]
Vehicle front surface	$A$	2.0	[m <sup>2</sup> ]
Wheel radius	$r$	0.25	[m]
Aerodynamic coefficient	$c_w$	0.25	[-]
Velocity-dependent roll coefficient	$k_{rol,v}$	$9.9 \cdot 10^{-5}$	[m <sup>-2</sup> /s <sup>-2</sup> ]
Roll coefficient	$k_{rol}$	$\frac{k_{rol,v} \cdot v^2 + 0.9}{100}$	[-]
1st gear ratio	$i_{G1}$	0.268	[-]
2nd gear ratio	$i_{G2}$	0.488	[-]
3rd gear ratio	$i_{G3}$	0.758	[-]
4th gear ratio	$i_{G4}$	1.031	[-]
5th gear ratio	$i_{G5}$	1.266	[-]
Differential gear ratio	$i_{diff}$	0.241	[-]

### A.3 Engine parameters

Parameter	Symbol	Value	Unit
Stroke	$H$	0.054	[m]
Cylinder diameter	$D_{in}$	0.065	[m]
Number of cylinders	$z_c$	2	[-]
Inertia	$\theta_{ICE}$	0.05	[kgm <sup>2</sup> ]
Fuel consumption at idle	$FC_{idle}$	$7.3 \cdot 10^{-5}$	[kg/s]
Idling speed	$n_{ICE, idle}$	880	[rpm]
Volume of coolant in the tubes connecting engine and bypass valve	$V_{1-2}$	0.23	[l]
Volume of coolant in the tubes connecting bypass valve and radiator	$V_{3-5}$	0.7	[l]
Volume of coolant in the tubes connecting bypass valve and mixing point	$V_{3-4}$	0.09	[l]
Volume of coolant in the tubes connecting mixing point and engine	$V_{4-6}$	0.46	[l]

Seite Leer /  
Blank leaf

## Appendix B

### THERMAL MODEL OF THE ENGINE

This appendix contains a description of the model and of the coefficients used for the design of the feedforward controller as described in Chapter 3.

#### B.1 Equations describing the model

The following eqs. (B.1) to (B.3) describe the third-order system obtained in Chapter 6.

$$\begin{aligned} \frac{dT_{eng, out}}{dt} = & \frac{\dot{Q}_{w, c}^* - \dot{Q}_{c, eb}^* - \dot{Q}_c^*}{c_{pc} \cdot m_c} = \\ & \frac{1}{c_{pc} \cdot m_c} \cdot [a_1 \cdot (T_w - T_{eng, m}) \\ & - a_2 \cdot (T_{eng, m} - T_{eb}) - a_3 \cdot (T_{eng, out} - T_{eng, in})], \end{aligned} \quad (B.1)$$

$$\begin{aligned} \frac{dT_w}{dt} = & \frac{\dot{Q}_{g, w}^* - \dot{Q}_{w, c}^*}{c_{pw} \cdot m_w} = \\ & \frac{1}{c_{pw} \cdot m_w} \cdot [\dot{Q}_{g, w}^*(T_{ICE}, n_{ICE}) - a_1 \cdot (T_w - T_{eng, m})], \end{aligned} \quad (B.2)$$

$$\frac{dT_{eb}}{dt} = \frac{\dot{Q}_{c,eb}^* + \dot{Q}_{if}^* - \dot{Q}_{irr}^* + \dot{Q}_{ex,eb}^*}{c_{peb} \cdot m_{eb} + c_{poil} \cdot m_{oil}} = \quad (B.3)$$

$$\frac{1}{c_{peb} \cdot m_{eb} + c_{poil} \cdot m_{oil}} \cdot \left[ a_2 \cdot (T_{eng,m} - T_{eb}) + \tilde{z}_2(T_{ICE}, n_{ICE}) \right.$$

$$+ c_1 \cdot T_{eb} + c_2 \cdot T_{eb}^2 + c_3 \cdot T_{eb}^3 + d_1 \cdot T_{eng,in} + d_2 \cdot T_{eng,in}^2$$

$$\left. + d_3 \cdot T_{eng,in}^3 + d_4 \cdot T_{eng,in}^4 \right].$$

The coefficients  $a_1, a_2, a_3$  listed in eqs. (B.4) to (B.6) only depend on the engine geometry and are therefore valid for all the engine operating points considered:

$$a_1 = z_c \cdot \frac{2 \cdot \lambda_w \cdot A_w \cdot \alpha}{2 \cdot \lambda_w + \alpha \cdot d}, \quad (B.4)$$

$$a_2 = z_c \cdot \alpha \cdot A_{eb}, \quad (B.5)$$

$$a_3 = c_{pc} \cdot \dot{m}_c^*. \quad (B.6)$$

## B.2 Coefficients

The coefficients listed below depend on the engine operating point as well as on the engine geometry. Based on the equations listed below, maps for each parameter can be processed.

From the model of the system described in Chapter 3 it results:

$$\tilde{z}_1 = \dot{Q}_{g,w}^*(n_{ICE}, bmep) \quad (B.7)$$

$$\begin{aligned} \tilde{z}_2 = & 87680 \cdot V_d \cdot n_{ICE} + D^{-0.5} \cdot V_d \cdot n_{ICE} \cdot (214263 \cdot \Pi_v \\ & + 1058 \cdot H \cdot \Pi_v \cdot \omega_{ICE} + 9928 \cdot bmep) + A_{eb,irr} \cdot \alpha_{irr} \cdot T_{amb} \\ & + A_{eb,irr} \cdot \varepsilon \cdot \sigma \cdot T_{amb}^4 + A_{ex,eb} \cdot \alpha_{ex,eb} \cdot T_{ex} \end{aligned} \quad (B.8)$$

$$\begin{aligned} b_1 = & -370 \cdot V_d \cdot n_{ICE} + D^{-0.5} \cdot V_d \cdot n_{ICE} \cdot (-905 \cdot \Pi_v \\ & - 4.5 \cdot H \cdot \Pi_v \cdot n_{ICE} - 41 \cdot bmep) - A_{eb,irr} \cdot \alpha_{irr} \\ & + A_{ex,eb} \cdot \alpha_{ex,eb} \end{aligned} \quad (B.9)$$

$$\begin{aligned} b_2 = & V_d \cdot n_{ICE} + D^{-0.5} \cdot V_d \cdot n_{ICE} \cdot (2.5 \cdot \Pi_v + 0.01 \cdot H \cdot \Pi_v \cdot n \\ & + 0.1 \cdot bmep) \end{aligned} \quad (B.10)$$

$$\begin{aligned} b_3 = & -1 \cdot 10^{-3} \cdot V_d \cdot n_{ICE} + D^{-0.5} \cdot V_d \cdot n_{ICE} \cdot (-2 \cdot 10^{-3} \cdot \Pi_v \\ & - 1 \cdot 10^{-5} \cdot H \cdot \Pi_v \cdot n_{ICE} - 1 \cdot 10^{-4} \cdot bmep) \end{aligned} \quad (B.11)$$

$$b_4 = A_{eb,irr} \cdot \varepsilon \cdot \sigma \quad (B.12)$$

$$\begin{aligned} c_1 = & 350.5 \cdot V_d \cdot n_{ICE} + D^{-0.5} \cdot V_d \cdot n_{ICE} \cdot (-856 \cdot \Pi_v \\ & - 4.2 \cdot H \cdot \Pi_v \cdot n_{ICE} - 39.7 \cdot bmep) \end{aligned} \quad (B.13)$$

$$\begin{aligned} c_2 = & -V_d \cdot n_{ICE} + D^{-0.5} \cdot V_d \cdot n_{ICE} \cdot (2.4 \cdot \Pi_v \\ & + 0.01 \cdot H \cdot \Pi_v \cdot n_{ICE} + 0.1 \cdot bmep) \end{aligned} \quad (B.14)$$

$$\begin{aligned} c_3 = & -1 \cdot 10^{-3} \cdot V_d \cdot n_{ICE} + D^{-0.5} \cdot V_d \cdot n_{ICE} \cdot (-2 \cdot 10^{-3} \cdot \Pi_v \\ & - 1 \cdot 10^{-5} \cdot H \cdot \Pi_v \cdot n_{ICE} - 1 \cdot 10^{-4} \cdot bmep) \end{aligned} \quad (B.15)$$

The geometry of the engine used in this thesis work is known. Thus the coefficients defined above for the specific engine tested can be expressed by the following equations:

$$\begin{aligned} \tilde{z}_2 = & 4754 + (784 + 0.2 \cdot \omega_{ICE} + 13.9 \cdot bmep) \cdot \omega_{ICE} \\ & + 1.5 \cdot T_{ex, gas} \end{aligned} \quad (\text{B.16})$$

$$c_1 = (-2884 + 0.0008 \cdot \omega_{ICE} - 0.056 \cdot bmep) \cdot \omega_{ICE} \quad (\text{B.17})$$

$$c_2 = (0.0088 + 2.2 \cdot 10^{-6} \cdot \omega_{ICE} + 0.0001 \cdot bmep) \cdot \omega_{ICE} \quad (\text{B.18})$$

$$\begin{aligned} c_3 = & (-8.33 \cdot 10^{-6} - 2.13 \cdot 10^{-9} \cdot \omega_{ICE} \\ & - 1.5 \cdot 10^{-7} \cdot bmep) \cdot \omega_{ICE} \end{aligned} \quad (\text{B.19})$$

$$b_1 = 17.5 + (-3.3 - 0.0008 \cdot \omega_{ICE} - 0.06 \cdot bmep) \cdot \omega_{ICE} \quad (\text{B.20})$$

$$b_2 = (0.009 + 2.32 \cdot 10^{-6} \cdot \omega_{ICE} + 0.00016 \cdot bmep) \cdot \omega_{ICE} \quad (\text{B.21})$$

$$\begin{aligned} b_3 = & \omega_{ICE} \cdot (-8.33 \cdot 10^{-6} - 2.13 \cdot 10^{-9} \cdot \omega_{ICE} \\ & - 1.5 \cdot 10^{-7} \cdot bmep) \end{aligned} \quad (\text{B.22})$$

$$b_4 = 2.13 \cdot 10^{-8} \quad (\text{B.23})$$

# Appendix C

## ERROR ESTIMATION

The estimation of the measurement errors is of fundamental importance for the evaluation of any experimental results. This appendix thus contains a brief overview of the error estimation relative to the measurements conducted.

First, the terminology is defined. A general configuration of an ideal measurement system is plotted in Fig. C-1 ([55]). Given a (P) dimensional vector of values to be measured, a sensor system first transforms these inputs. The units of the (P) dimensional output of the sensor system  $y_S(t)$  normally differ from those of the input values  $y(t)$ . A reconstruction system containing the inverse function of the sensor system is thus needed in order to obtain the correct physical units of the measured values  $y_M(t)$ . The system is defined as ideal since:

$$\hat{y}(t) = D_M \cdot y(t) = D_R \cdot D_S \cdot y(t) = D_S^{-1} \cdot D_S \cdot y(t) = y(t) \quad (\text{C.1})$$

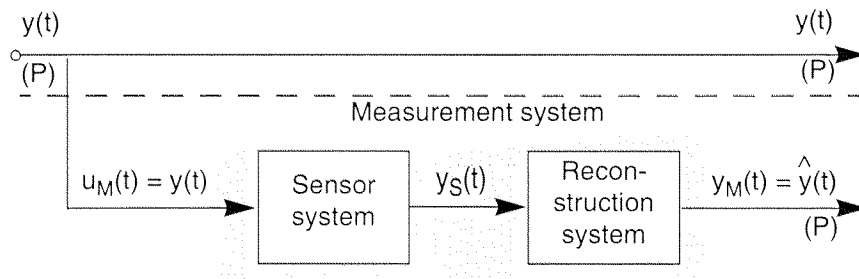


**Figure C-1:** Ideal measurement system

Nevertheless, real systems are characterized by errors. In the following, only time independent errors caused by an undesired dynamic behaviour of the



measurement system are considered. This kind of error disappears when, as here, stationary operating conditions are analysed.

There are systematic and random errors. Under identical measurement conditions the systematic errors always produce the same measured values. Since they are reproducible they can be measured and compensated during calibration procedures. On the other hand, random errors are not reproducible, and the values measured can vary between one measurement and another. Assuming that various measurements have been taken, random errors can be characterized by means of statistical instruments ([12], [55]). Based on the  $n$  measurements taken the mean value  $\mu_{y_M}$  and the standard deviation  $\sigma_{y_M}$  can be derived:

$$\sigma_{y_M} = \sqrt{\frac{\sum_{i=1}^n (y_M - \mu_{y_M})^2}{n-1}}. \quad (\text{C.2})$$

Since the standard deviation is independent of the distribution of the measurement results, it can be used to characterize the random error:

$$e_{y_M} = \sigma_{y_M}. \quad (\text{C.3})$$

Generally stated, the value to be measured and the measured value are proportional:

$$\hat{y}_M = k_M \cdot y \quad (\text{C.4})$$

For all the measured variables considered in this work  $k_M = 1$ . Indeed, the values obtained from the measurements have the same units as the value to be measured.

Usually, a measurement system is first calibrated in order to define the standard deviation and the distribution of the measurements. In this case the value to be measured  $y_1$  remains constant. When only random errors are present, the measured value is not constant, but varies in a confidence range whose amplitude depends on the confidence limit chosen:

$$y_M = y_1 \pm t_\sigma \cdot \sigma_{y_M}. \quad (\text{C.5})$$

The value of  $t_\sigma$  depends on the confidence limit chosen and on the kind of distribution obtained during the measurements. The distribution of the measured value for calibration purposes is shown in Fig. C-2 (a), where  $t_\sigma = 1$ .

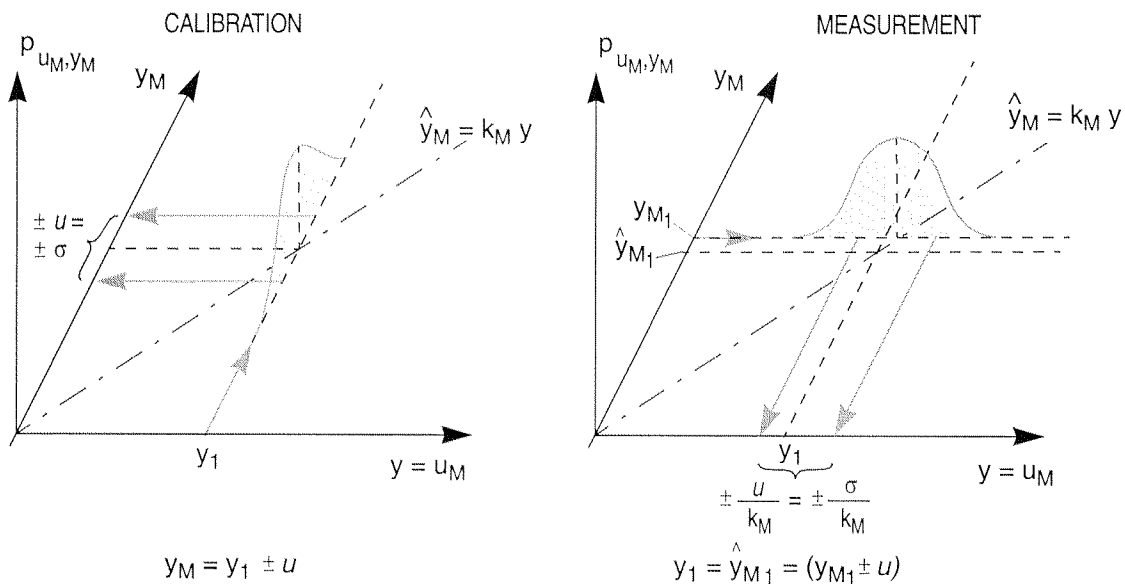


**Figure C-2:** Confidence interval for calibration (a) or measurements (b)

Once the system is calibrated for random errors either a single measurement or various measurements can be conducted. The difference between the two cases is explained below.

From a single measurement  $y_{M1}$  the original value  $y_1$  cannot be determined unambiguously. Nevertheless, when more measurements are taken, given that the standard deviation and the distribution of the measured values are known,

the estimated value  $y_{M_1}$  corresponding to the original value  $y_1$  can be found with a defined confidence level within the confidence interval  $u_{y, \sigma}$  centred on the measured value  $y_{M_1}$  :

$$\hat{y}_{M_1} = y_{M_1} \pm t_{\sigma} \cdot \sigma_{y_M} = y_{M_1} \pm u_{y, \sigma}, \quad (\text{C.6})$$

as shown in Fig. C-2 (b) for  $t_{\sigma} = 1$ .

With an increasing number of measurements within the same system configuration the mean value  $\mu_{y_M}$  with increasing precision estimates the correct value  $\hat{y}_M$  that corresponds to the original value  $y$ . The confidence interval thus decreases as the number of measurements  $n$  increases, as follows ([20], [55]):

$$u_{\mu, \sigma} = t_{\sigma} \cdot \frac{\sigma_y}{\sqrt{n}}, \quad (\text{C.7})$$

making the estimation of the correct value more and more precise:

$$\hat{y}_M = \mu_{y_M} \pm u_{\mu, \sigma}. \quad (\text{C.8})$$

From the confidence interval and the mean value the relative error of the measurements can be calculated as well:

$$\varepsilon_y = \frac{2 \cdot |u_{\mu, \sigma}|}{\mu_{y_M}} \cdot 100. \quad (\text{C.9})$$

In the following an error estimation analysis is conducted on the conventional and on the improved configuration of the cooling system for each of the engine operating points considered in Section 5.2 for engine cold start. The aim of the experiments is the definition of the integral fuel consumption over the first 40 minutes from engine cold start, as plotted in Fig. 5-6. In this case, considering the experimental setup, three different sources of systematic and random errors can be located:

- engine torque
- engine speed
- fuel flow

Both engine speed and torque are controlled to be constant. Therefore during an engine cold-start experiment numerous engine speed and torque measurements of the same engine operating point are obtained. For the error estimation engine speed and torque are measured every 60 seconds. For three cold-start measurements over 40 minutes,  $n = 120$  measurements are obtained. Table C-1 presents the confidence interval and relative error of engine speed and torque measurements for the two different configurations of the cooling system and for the first of the engine operating points considered (2500 rpm, 2 bar) for a normal distribution and a confidence level  $P = 95.5\%$  (i. e.  $t_{\sigma} = 1.98$ , [55]).

For the determination of the error encountered in the measurements of fuel flow a different approach is needed. Indeed, it would be wrong to assume that variations in the fuel consumption measured are only caused by random errors in the measurement system since the non-stationary engine thermal conditions as well as EGR phenomena affect the effective fuel consumption. For this reason a moving average over time was considered for the fuel mass flow. Indeed, the fuel mass flow over three time intervals of 10 minutes each is analysed. As Table C-1 shows for the lowest engine load measured, the mean value of the fuel flow diminishes with increasing time from cold start due to the fact that the engine reaches more and more favourable thermal conditions (see Fig. 5-3). In each of the three intervals considered the mean value, as well as the standard deviation and the confidence interval are calculated. The resulting relative error is displayed in the last column in Table C-1.

Engine cold start under stationary operating conditions was performed for two further engine operating points (Chapter 5.2). The results in terms of relative error for torque, speed, and fuel flow measurements are calculated for these engine operating points as well. The results are displayed in Tables C-2 and C-3. It can be observed that the relative error in the engine torque diminishes with increasing engine torques, in accordance with the specifications provided by the test bench producer.

**Table C-1:** Partial random error (cold start at 2500 rpm, 2 bar)

Configu- ration	Variable	Mean value	Standard deviation	Confid. interval	Relative error
Convent.	Engine torque	5.79 [Nm]	0.1426 [Nm]	$\pm 0.0255$ [Nm]	0.88 [%]
	Engine speed	2491 [rpm]	3.0918 [rpm]	$\pm 0.5520$ [rpm]	0.04 [%]
	Fuel cons. [30...40min]	1.005 [l/h]	0.0056 [l/h]	$\pm 0.0014$ [l/h]	0.28 [%]
	Fuel cons. [20...30min]	1.012 [l/h]	0.0075 [l/h]	$\pm 0.0019$ [l/h]	0.37 [%]
	Fuel cons. [10...20min]	1.013 [l/h]	0.0083 [l/h]	$\pm 0.0021$ [l/h]	0.41 [%]
Improved	Engine torque	5.82 [Nm]	0.1004 [Nm]	$\pm 0.0180$ [Nm]	0.62 [%]
	Engine speed	2492 [rpm]	4.5861 [rpm]	$\pm 0.8188$ [rpm]	0.07 [%]
	Fuel cons. [30...40min]	0.93 [l/h]	0.0046 [l/h]	$\pm 0.0016$ [l/h]	0.25 [%]
	Fuel cons. [20...30min]	0.95 [l/h]	0.0070 [l/h]	$\pm 0.0018$ [l/h]	0.37 [%]
	Fuel cons. [10...20min]	0.96 [l/h]	0.0086 [l/h]	$\pm 0.0021$ [l/h]	0.45 [%]

**Table C-2:** Partial random error (cold start at 2500 rpm, 4 bar)

Configu- ration	Variable	Mean value	Standard deviation	Confid. interval	Relative error
Convent.	Engine torque	11.54 [Nm]	0.086 [Nm]	$\pm 0.0265$ [Nm]	0.46 [%]
	Engine speed	2491 [rpm]	1.0486 [rpm]	$\pm 1.2519$ [rpm]	0.10 [%]
	Fuel cons. [30...40min]	1.39 [l/h]	0.0061 [l/h]	$\pm 0.0015$ [l/h]	0.22 [%]
	Fuel cons. [20...30min]	1.42 [l/h]	0.0084 [l/h]	$\pm 0.0021$ [l/h]	0.29 [%]
	Fuel cons. [10...20min]	1.44 [l/h]	0.0092 [l/h]	$\pm 0.0023$ [l/h]	0.32 [%]
Improved	Engine torque	11.52 [Nm]	0.0907 [Nm]	$\pm 0.0280$ [Nm]	0.49 [%]
	Engine speed	2490 [rpm]	2.6670 [rpm]	$\pm 0.824$ [rpm]	0.07 [%]
	Fuel cons. [30...40min]	1.34 [l/h]	0.0041 [l/h]	$\pm 0.0010$ [l/h]	0.15 [%]
	Fuel cons. [20...30min]	1.36 [l/h]	0.006 [l/h]	$\pm 0.0015$ [l/h]	0.22 [%]
	Fuel cons. [10...20min]	1.37 [l/h]	0.0073 [l/h]	$\pm 0.0019$ [l/h]	0.27 [%]

**Table C-3:** Partial random error (cold start at 2500 rpm, 6 bar)

Configu- ration	Variable	Mean value	Standard deviation	Confid. interval	Relative error
Convent.	Engine torque	17.26 [Nm]	0.0828 §[Nm]	± 0.0254 [Nm]	0.29 [%]
	Engine speed	2490 [rpm]	3.7609 [rpm]	± 1.1630 [rpm]	0.09 [%]
	Fuel cons. [30...40min]	1.93 [l/h]	0.0054 [l/h]	± 0.0013 [l/h]	0.14 [%]
	Fuel cons. [20...30min]	1.96 [l/h]	0.0113 [l/h]	± 0.0028 [l/h]	0.29 [%]
	Fuel cons. [10...20min]	1.98 [l/h]	0.0127 [l/h]	± 0.0032 [l/h]	0.32 [%]
Improved	Engine torque	17.24 [Nm]	0.0359 [Nm]	± 0.0111 [Nm]	0.13 [%]
	Engine speed	2489 [rpm]	3.6362 [rpm]	± 0.932 [rpm]	0.07 [%]
	Fuel cons. [30...40min]	1.87 [l/h]	0.0090 [l/h]	± 0.0022 [l/h]	0.24 [%]
	Fuel cons. [20...30min]	1.88 [l/h]	0.0109 [l/h]	± 0.0027 [l/h]	0.29 [%]
	Fuel cons. [10...20min]	1.89 [l/h]	0.0132 [l/h]	± 0.0033 [l/h]	0.35 [%]

The aim of the measurement is to compare the integral fuel consumption data during cold start for the two different cooling system configurations at each of the engine operating points considered. Relative errors in the integral fuel consumption are the sums of the relative errors of engine speed  $\varepsilon_n$  and torque  $\varepsilon_T$  as well as of the fuel volume flow  $\varepsilon_{FC}$ :

$$\varepsilon = \varepsilon_T + \varepsilon_n + \varepsilon_{FC} \quad (\text{C.10})$$

Summing up the errors of eq. (C.10) yields a conservative estimate of the total error.

**Table C-4:** Results from different measurements

Engine operating point	System configuration	Integral fuel consumption after 40 min [l]	Relative error [%]	Confidence interval [l]
2500 rpm 2 bar	Conventional	0.640	1.2	$\pm 0.0038$
	Improved	0.611	0.94	$\pm 0.0029$
2500 rpm 4 bar	Conventional	0.915	0.78	$\pm 0.0036$
	Improved	0.889	0.71	$\pm 0.0032$
2500 rpm 6 bar	Conventional	1.252	0.52	$\pm 0.0032$
	Improved	1.211	0.44	$\pm 0.0027$

Once the relative error for the integral fuel consumption is known, the relative confidence interval is calculated. The corresponding error of the fuel flow measurements during the last time period ([30 ... 40min]) was considered. Indeed, the larger relative error and standard deviation of measurements taken before the engine reaches its thermal stationary condition (see tables C-1, C-2,



and C-3) are due to physical phenomena (changing thermal conditions as well as light EGR phenomena related to the pressure-wave supercharging device).

The resulting values of relative error for the integral fuel consumption are listed in Table C-4.

For all the measurements of integral fuel consumption the confidence error amounts to ca. 10% of the fuel consumption reduction obtained for the two different configurations of the cooling systems. According to eq. (5.7), it is therefore demonstrated that the fuel consumption measurements are sufficient precise for a valid comparison between different configurations of the cooling system.

## REFERENCES

- [1] A. C. Alkides, R. M. Cole: The Effect of Coolant Temperatures on the Performance and Emissions of a Single Cylinder Drived-Chamber Diesel Engine, *SAE International Congress, SAE Paper 841053*, Detroit, 1984.
- [2] A. Amstutz: *Geregelte Abgasrückführung zur Senkung der Stickoxid- und Partikelemissionen beim Dieselmotor mit Comprex-Aufladung*, Diss. ETH Nr. 9421, Switzerland, 1991.
- [3] N. S. Ap, N. C. Golm: New Concept of Engine Cooling System (New-cool), *SAE International Congress, SAE Paper 911775*, Detroit, 1991.
- [4] O. Arici, J. H. Johnson, A. J. Kulkarni: The Vehicle Engine Cooling System Simulation. Part 1 - Model Development, *SAE International Congress, SAE Paper 1999-01-0240*, Detroit, 1999.
- [5] W. F. Ball, N. S. Jackson, A. D. Pilley, B. C. Porter: The Friction of a 1.6 Litre Automotive Engine - Gasoline and Diesel, *SAE International Congress, SAE Paper 860418*, Detroit, 1986.
- [6] N. C. Barford: *Experimental Measurements*, Wiley, New York, 1985.
- [7] R. Bauer, W. Brox, A. Fischer, R. Hofmann, H. Lamberger, J. Städler: BMW V8-Motoren: Steigerung von Umweltverträglichkeit und Kundennutzen, *MTZ Motortechnische Zeitschrift*, Vol. 57, pp. 86-92, 1996.
- [8] A. Beard, G. J. Smith: A Method of Calculating the Heat Dissipation from Radiators to Cool Vehicle Engines, *SAE International Congress, SAE Paper 710208*, Detroit, 1971.

- [9] H. Bednarek, U. Tacke: Heat Management - a Technique for Resolving the Conflicting Aims Between Fuel Consumption and Comfort, VDI Berichte 1505, pp. 83-107, VDI-Verlag, Düsseldorf, 1999.
- [10] K. Bolenz: Development and Influence of the Power Demand of Accessory Parts, *3rd Aachener Kolloquium Fahrzeug- und Motorentechnik*, Aachen, 1991.
- [11] K. Braun: *Optimale Regelung der Betriebstemperatur eines Ottomotors*, Diplomarbeit am Institut für Mess- und Regeltechnik, ETH Zurich, Switzerland, 1983.
- [12] P. J. Brown, W. A. Fuller: *Statistical Analysis of Measurement Error Models and Applications*, American Mathematical Society, Providence, 1989.
- [13] D. J. Butchers: Emerging trends in automotive power semiconductor systems, *SAE International Congress, SAE Paper 1999-01-0160*, Detroit, 1999.
- [14] M. J. Clough: Precision Cooling of a Four Valve per Cylinder Engine, *SAE International Congress, SAE Paper 931123*, Detroit, 1993.
- [15] E. Cortona, L. Guzzella, A. Amstutz: Analysis of Different Concepts for Braking Energy Recuperation, *Control and Diagnostics in Automotive Applications, Paper 98A5005*, Detroit, 1998.
- [16] E. Cortona, C. H. Onder: Engine Thermal Management with Electrical Cooling Pump, *SAE International Congress, SAE Paper 2000-01-0965*, Detroit, 2000.
- [17] S. M. Cotran, T. D. Lain, C. M. Feng: Engine and Starting System Computer Simulation, *SAE Transactions*, Vol. 99, pp. 1615-1624, 1992.

- [18] H. Couëtouse, D. Gentile: Cooling System Control in Automotive Engines, *SAE International Congress, SAE Paper 920798*, Detroit, 1992.
- [19] G. E. Cozzone: Effect of Coolant Type on Engine Operating Temperatures, *SAE International Congress, SAE Paper 1999-01-0135*, Detroit, 1999.
- [20] R. H. Dieck: *Measurement Uncertainty: Methods and Applications*, American Technical Publisher, Hitchin, 1997.
- [21] Ph. Dietrich, M. Eberle: Das ETH Hybrid III Antriebskonzept, *VDI Berichte 1225*, VDI-Verlag, 1995.
- [22] Dubbel: *Taschenbuch für den Maschinenbau*, Springer Verlag, 1987.
- [23] G. P. Dyer: Analysis of energy consumption for various power assisted steering systems, *SAE International Congress, SAE Paper 970379*, Detroit, 1997.
- [24] M. K. Eberle: *Thermodynamik des Verbrennungsmotors, Skript Vorlesungs Nr. 30-251, ETH Zürich Abt. Maschinenbau*, 1990.
- [25] W. Eichsieder, G. Raab, J. Hager, M. Raup: Use of Simulation Tools with Integrated Coolant Flow Analysis for the Cooling System Design, *SAE International Congress, SAE Paper 971815*, Detroit, 1997.
- [26] G. Einaudi, W. Mortara: Engine Cooling Electronic System, *SAE International Congress, SAE Paper 885085*, Detroit, 1988.
- [27] K. Elsbett, L. Elsbett, G. Elsbett, M. Behrens: The Duothermic Combustion for D. I. Diesel Engines, *SAE International Congress, SAE Paper 860310*, Detroit, 1986.
- [28] K. Elsbett, L. Elsbett, G. Elsbett, M. Behrens: Elsbett Reduced Cooling for DI Engines Without Water or Air, *SAE International Congress, SAE Paper 870027*, Detroit, 1987.

- [29] K. Elsbett, L. Elsbett, G. Elsbett, M. Behrens: New Development in DI Diesel Engine Technology, *SAE International Congress, SAE Paper 890134*, Detroit, 1989.
- [30] T. Esch, T. Saupe, E. Fahl, F. Koch : Verbrauchseinsparung durch bedarfsgerechten Antrieb der Nebenaggregate, *MTZ Motortechnische Zeitschrift*, Vol. 55, pp. 416-431, 1994.
- [31] J. W. Evans, J. T. Light: Expanding the Limits on Engines Imposed by Circulating Liquid Engine Cooling Systems, *SAE International Congress, SAE Paper 861428*, Detroit, 1986.
- [32] I. C. Finlay, D. Harris, D. J. Boam: Factors Influencing Combustion Chamber Wall Temperature in a Liquid-cooled, Automotive, Spark-ignition Engine, *Proc. Inst. Mech. Engrs.*, Vol. 199, pp. 207-215, 1985.
- [33] G. F. Franklin, J. D. Powell, A. Emami-Naeini: *Feedback Control of Dynamic Systems*, Addison-Wesley, 1994.
- [34] H. P. Geering: *Regelungstechnik*, Springer, Berlin, 1996.
- [35] T. Gillespie: *Fundamentals of Vehicle Dynamics*, Society of Automotive Engineering, Detroit, 1992.
- [36] I. Gorille: Leistungsbedarf und Antrieb von Nebenaggregaten, 2. *Aachener Kolloquium Fahrzeug- und Motorentechnik*, Aachen, 1989.
- [37] A. B. Greene, G. G. Lucas: *The Testing of Internal Combustion Engines*, English University Press Ltd. 1969.
- [38] L. Guzzella, R. Martin: The SAVE Engine Concept, *MTZ Motortechnische Zeitschrift*, Vol. 10, pp. 644-657, 1998.
- [39] G. Gyarmathy: How does the Comprex® pressure-wave supercharger work, *SAE International Congress, SAE Paper 830234*, Detroit, 1983.

- [40] Y. Harigaya, F. Toda, M. Suzuki: Local Heat Transfer on a Combustion Chamber Wall of a Spark-Ignition Engine, *SAE International Congress, SAE Paper 931130*, Detroit, 1993.
- [41] J. B. Heywood: *Internal Combustion Engine Fundamentals*, McGraw-Hill Book Company, 1988.
- [42] J. Inhelder: *Internal Combustion Engine Verbrauchs- und Schadstoff-optimiertes Ottomotoraufladekonzept*, Diss. ETH Nr. 11948, Switzerland, 1996.
- [43] F. Jauch: *Optimierung des Antriebsstranges von Kraftfahrzeugen durch Fahrsimulation*, Diss. Universität Stuttgart, Germany, 1989.
- [44] T. Kabozuka, N. Ogawa, Y. Hirano, Y. Hasashi: The Development of Engine Evaporative Cooling System, *SAE International Congress, SAE Paper 870033*, Detroit, 1987.
- [45] E. W. Kaiser, W. G. Rotschild, G. A. Lavoie: The Effect of Fuel and Operating Variables on Hydrocarbon Species Distribution in the Exhaust from a Multicylinder Engine, *Combustion Science and Technology*, Vol. 32, pp. 245-265, 1983.
- [46] E. W. Kaiser, W. G. Rotschild, G. A. Lavoie: Storage and Partial Oxidation of Unburned Hydrocarbons in Spark-Ignition Engines - Effect of Compression Ratio and Spark Timing, *Combustion Science and Technology*, Vol. 36, pp. 171-189, 1984.
- [47] J. Kern, P. Ambros: Concepts for a Controlled Optimized Vehicle Engine Cooling System, *SAE International Congress, SAE Paper 971816*, Detroit, 1997.
- [48] F. W. Koch, F. G. Haubner: Cooling System Development and Optimization for DI Engines, *SAE International Congress, SAE Paper 2000-01-0283*, Detroit, 2000.

- [49] W. Krause, K. H. Spies: Dynamic Control of the Coolant Temperature for a Reduction of Fuel Consumption and Hydrocarbon Emission, *SAE International Congress, SAE Paper 960271*, Detroit, 1996.
- [50] F. Metzler, U. Hesse, G. Rocklage, M. Schmitt: Thermomanagement, *SAE International Congress, SAE Paper 1999-01-0238*, Detroit, 1999.
- [51] R. Müller, J. Niklas, K. Scheuer: The Braking System Layout of Electric Vehicles - Example BMW E1, *SAE International Congress, SAE Paper 930508*, Detroit, 1993.
- [52] V. A. Nelson, J. D. Robichaux: A Model to Simulate the Behavior Automotive Thermostat, *SAE International Congress, SAE Paper 971814*, Detroit, 1997.
- [53] K. J. Patton, R. G. Nietschke, J. B. Heywood : Development and Evaluation of a Friction Model for Spark-Ignition Engines, *SAE International Congress, SAE paper 890836*, Detroit, 1989.
- [54] M. Pretscher, N. S. Ap: Nucleate Boiling Engine Cooling System - Vehicle Study, *SAE International Congress, SAE Paper 931132*, Detroit, 1993.
- [55] K. H. Ruhm: Fehlerhafte Messsysteme, unsichere Resultate, *SGA Lernmodul Nr. 12*, Baden, 1998.
- [56] S. G. Russ, E. W. Kaiser, W. O. Siegi, D. H. Podsiadlik, K. M. Barrett: Compression Ratio and Coolant Temperature Effects on HC Emissions from a Spark-Ignition Engine, *SAE International Congress, SAE paper 950163*, Detroit, 1995.
- [57] E. Shafai: *Fahrzeugemulation an einem dynamischen Verbrennungsmotor-Prüfstand*, Diss. ETH Nr. 9080, Switzerland, 1990.

- [58] P. J. Shayler, S. J. Christian, T. Ma: A Model for the Investigation of Temperature, Heat Flow and Friction Characteristics During Engine Warm-Up, *SAE International Congress, SAE paper 931153*, Detroit, 1993.
- [59] Y. Shibata, H. Shimonosono, Y. Yamai: New Design of Cooling System with Computer Simulation and Engine Compartment Simulator, *SAE International Congress, SAE Paper 931075*, Detroit, 1993.
- [60] Y. Shimizu, T. Kawai: Development of electric power steering, *SAE International Congress, SAE paper 910014*, Detroit, 1991.
- [61] M. Schmidt, B. Lenzen: Entwicklung und Erprobung von Verfahren zum verbesserten Einsatz der Nebenaggregate an Diesel- und Ottomotoren bei stationärem und instationärem Betrieb, *FVV-Vorhaben Nr. 622*, Heft 491, 1997.
- [62] T. Schmitz: Modellbildung und Simulation der Antriebsdynamik von Personenwagen, *VDI Berichte 224*, VDI-Verlag, Düsseldorf, 1994.
- [63] R. Schöttle, D. Schramm: Zukünftige Energiebordnetze im Kraftfahrzeug, *VDI Jahressbuch 1997*, 1997.
- [64] J. Schramm, S. C. Sorenson: Effects of Lubricating Oil on Hydrocarbon Emissions in a SI Engine, *SAE International Congress, SAE paper 890622*, Detroit, 1989.
- [65] P. Soltic: Part-Load Optimized SI Engine Systems, Diss. ETH Nr. 13942, Switzerland, 2000.
- [66] P. Soltic, L. Guzzella: Optimum SI Engine Based Powertrain System for Lightweight Passenger Cars, *SAE International Congress, SAE paper 2000-01-0827*, Detroit, 2000.
- [67] N. Sunayama: Heat Transfer/Thermal Analysis for Cylinder Head, *SAE International Congress, SAE paper 910301*, Detroit, 1991.



- [68] D. A. System: *Emission Standards for Passenger Cars Worldwide*, Delphi Technical Centre Luxembourg, 1988.
- [69] D. Taraza, N. Henein, W. Bryzik: Friction Losses in Multi-Cylinder Diesel Engines, *SAE International Congress, SAE paper 2000-01-0921*, Detroit, 2000.
- [70] R. Valentine, P. Pinewski: Advanced motor control electronics, *SAE International Congress, SAE paper 961693*, Detroit, 1996.
- [71] O. Vogel: *Load Control of SI Engines Using Secondary Valves*, Diss. ETH Nr. 13633, Zurich, 2000.
- [72] B. Voss: Wirkungsgradverbesserung von Fahrzeugantrieben durch eine bedarfsorientierte Auslegung der Nebenaggregate und ihrer Antriebe, *VDI Berichte 159*, VDI-Verlag, Düsseldorf, 1991.
- [73] Y. Watanabe, H. Ishikawa, M. Miyahara: An Application Study of Evaporative Cooling to Heavy Duty Diesel Engines, *SAE International Congress, SAE Paper 870023*, Detroit, 1987.
- [74] H. P. Willumeit, P. Steinberg: Der Wärmeübergang im Verbrennungsmotor, *MTZ Motortechnische Zeitschrift*, Vol 47, 1986.
- [75] H. P. Willumeit, P. Steinberg, H. Oetting, B. Scheibner, W. Lee: New Temperature Control Criteria for More Efficient Gasoline Engines, *SAE International Congress, SAE Paper 841292*, Detroit, 1984.
- [76] Z. Xu, J. H. Johnson, E. C. Chiang: A Simulation Study of a Computer Controlled Cooling System for a Diesel Powered Truck, *SAE International Congress, SAE Paper 841711*, Detroit, 1984.
- [77] J. Yang: Coolant Pump Throttling - A Simple Method to Improve the Control over SI Engine Cooling System, *SAE International Congress, SAE paper 961813*, Detroit, 1996.

- [78] K. P. Zeyen, T. Pels: ISAD - A Computer Controlled Integrated Starter - Alternator - Damper - System, *SAE International Congress*, *SAE paper 972660*, Detroit, 1997.

Seite Leer /  
Blank leaf

## CURRICULUM VITAE

Name: Cortona Kanne  
First name: Elena  
Date of birth: 28 April 1970  
Place of birth: Ivrea, Italy

### Education

1976-1981 Primary school, Ivrea, Italy  
1981-1984 Secondary school, Ivrea, Italy  
1984-1989 High school 'Liceo Classico C. Botta', Ivrea, Italy  
1989-1995 Studies in mechanical engineering ("Dott. Ing. Mech.")  
Politecnico di Torino, Italy  
1995 Diploma thesis in mechanical engineering at the  
RWTH Aachen, Germany  
1995 Diploma in mechanical engineering  
Politecnico di Torino, Italy  
1996-2000 Doctoral student and research assistant at the  
Engine Systems Lab, Institute of Energy Technology,  
Swiss Federal Institute of Technology (ETH), Zurich,  
Switzerland